

APPENDIX 2.10.4

TABLE OF CONTENTS

	<u>Page</u>
2.10.4 NUHOMS®-MP197 CASK LEAD SLUMP ANALYSIS	2.10.4-1
2.10.4.1 Introduction	2.10.4-1
2.10.4.2 Finite Element Model.....	2.10.4-1
2.10.4.3 FEA Results.....	2.10.4-6
2.10.4.4 Conclusions	2.10.4-6
2.10.4.5 References	2.10.4-7

LIST OF FIGURES

2.10.4-1	NUHOMS®-MP197 cask 2-Dimensional Finite Element Model with Lid End Drop Boundary Conditions
2.10.4-2	NUHOMS®-MP197 cask 2-Dimensional Finite Element Model with Bottom End Drop Boundary Conditions
2.10.4-3	Displacement Pattern – Lid End Drop, Hot Environment Load Case
2.10.4-4	Displacement Pattern – Lid End Drop, Cold Environment Load Case
2.10.4-5	Displacement Pattern – Bottom End Drop, Hot Environment Load Case
2.10.4-6	Displacement Pattern – Bottom End Drop, Cold Environment Load Case

APPENDIX 2.10.4

NUHOMS[®]-MP197 CASK LEAD SLUMP ANALYSIS

2.10.4.1 Introduction

The purpose of this analysis is to determine the amount of lead slump that occurs in the NUHOMS[®]-MP197 cask during a hypothetical accident condition end drop. The load cases considered in this calculation are hypothetical accident condition lid and bottom end drops. The impact loads are combined with thermal loads corresponding to a 100° F ambient environment and a -20° F ambient environment.

During a hypothetical accident condition end drop, permanent deformation of the lead gamma shield may occur. The lead gamma shield is supported by friction between the lead and cask shells, in addition to bearing at the end of the lead column.

A nonlinear finite element analysis is performed in order to quantify the amount of lead slump generated during an end drop event. A 2-dimensional axisymmetric ANSYS [1] finite element model is constructed for this purpose. The results of the finite element analysis provide both stresses and displacements generated during the end drop event. The displacement results are used in this section to determine the maximum size of the axial gap that develops between the lead gamma shield column and the structural shell of the cask. The effect of this cavity size on the shielding ability of the transport package is evaluated in Chapter 7. Both stress and displacement distributions computed by the finite element analysis are used to perform a buckling evaluation of inner containment shell of the NUHOMS[®]-MP197 cask in Appendix 2.10.5.

2.10.4.2 Finite Element Model

2.10.4.2.1 Approach

A 2-dimensional axisymmetric ANSYS [1] finite element model, constructed primarily from PLANE42 elements, is used in this analysis. LINK1 elements are used to model the lid and RAM port cover bolts. Pre-load stresses of 87 ksi. and 25 ksi. are applied to the lid and RAM port cover bolts respectively. Gap elements are used to model the interaction between the lead gamma shield and the cask inner and outer shells. The coefficient of sliding friction for lead on mild steel varies from 0.3 for lubricated surfaces to 0.95 for dry surfaces [7]. A lower bound coefficient of static friction of 0.25 is conservatively used for the buckling analysis.

In order to determine the amount of lead slump settling, an elastic plastic analysis is required. The material properties of the lid, bottom, inner shell, and outer shell of the transport cask are modeled with bilinear stress-strain curves, while the lead material is modeled with a multilinear stress-strain curve.

The neutron shield, shield shell, trunnions and bearing block are not included in the model. The effect of the unmodeled weight is accounted for by increasing the density of the outer shell in the neutron shield region. The modified density of the outer shell in this region is computed in the following way.

The weight of the section of the outer shell, W_{os} , that will be given an increased density is,

$$W_{os} = \pi \{ [41.00 \text{ in. (outer shell o.r.)}]^2 - [38.5 \text{ in. (outer shell i.r.)}]^2 \} \times 144.0 \text{ in. (section length)} \times 0.29 \text{ (density)} = 26,075 \text{ lb.}$$

The weight of the entire FEM prior to density modification, W_m , is 128,050 lb. (Section 2.2). The actual calculated weight of the transport cask, W_{tc} , is 150,027 lb. (Section 2.2). However, a conservative weight of 150,320 lb. is used. Therefore, the modified density used in this analysis, ρ_m , is

$$\rho_m = \frac{W_{os} + (W_{tc} - W_m)}{\pi(41.00^2 - 38.50^2) \times 144} = \frac{26,075 + (150,320 - 128,050)}{\pi(41.00^2 - 38.50^2) \times 144} = 0.538 \text{ lb.in.}^{-3}$$

2.10.4.2.2 Material Properties

The maximum temperature of the transport cask during transport in the 100° F ambient environment is 302° F (Chapter 3, Table 3-1). Properties of NUHOMS®-MP197 cask materials are taken at 300° F for both hot and cold environment cases, which is conservative. The transport cask material properties are as follows.

Outer Shell (SA-240 Type 316) @ 300° F. [1] [2] [3]

$$E = 27.0 \times 10^6 \text{ psi.}$$

$$S_y = 23.4 \text{ ksi.}$$

$$S_u = 72.9 \text{ ksi.}$$

$$\alpha_{70^\circ\text{F}} = 8.5 \times 10^{-6} \text{ in./in. } ^\circ\text{F}^{-1}$$

$$\alpha_{300^\circ\text{F}} = 9.2 \times 10^{-6} \text{ in./in. } ^\circ\text{F}^{-1}$$

$$\nu = 0.3$$

$$\rho = 0.29$$

$$\text{Elongation, } e = 40\%$$

$$\epsilon @ S_y = 23,400 / 27.0 \times 10^6 = 0.000867 \text{ in. in.}^{-1}$$

$$\text{Tangent Modulus, } E_T = (72,900 - 23,400) / (0.40 - 0.000867) = 124,020 \text{ psi.}$$

Lid Material (SA-693 Type 630, Condition H1100) @ 300° F. [1] [2] [3]

$$E = 27.2 \times 10^6 \text{ psi.}$$

$$S_y = 101.8 \text{ ksi.}$$

$$S_u = 140.0 \text{ ksi.}$$

$$\alpha_{70^\circ\text{F}} = 5.89 \times 10^{-6} \text{ in./in. } ^\circ\text{F}^{-1}$$

$$\alpha_{300^\circ\text{F}} = 5.90 \times 10^{-6} \text{ in./in. } ^\circ\text{F}^{-1}$$

$$\nu = 0.3$$

$$\rho = 0.29$$

$$\text{Elongation, } e = 14\%$$

$$\varepsilon @ S_y = 101,800 / 27.2 \times 10^6 = 0.003743 \text{ in. in}^{-1}$$

$$\text{Tangent Modulus, } E_T = (140,000 - 101,800) / (0.14 - 0.003743) = 280,353 \text{ psi.}$$

Lead (B-29) @ 300° F. [4] [5] [6]

$$E = 2.06 \times 10^6 \text{ psi.}$$

$$\nu = 0.45$$

$$\rho = 0.41$$

$$\alpha_{70^\circ\text{F}} = 16.07 \times 10^{-6} \text{ in./in. } ^\circ\text{F}^{-1}$$

$$\alpha_{300^\circ\text{F}} = 17.34 \times 10^{-6} \text{ in./in. } ^\circ\text{F}^{-1}$$

Multi-linear Stress/Strain Curve:

Strain	Stress
0.000485	1000
0.030	1,700
0.100	2,380
0.300	2,720
0.500	3,060

Inner Shell, Flange, Bottom, RAM Closure Plate (SA-240 Type XM-19 or SA-182 Type FXM-19) @ 300° F. [1] [2] [3]

$$E = 27.0 \times 10^6 \text{ psi.}$$

$$S_y = 43.3 \text{ ksi.}$$

$$S_u = 94.2 \text{ ksi.}$$

$$\alpha_{70^\circ\text{F}} = 8.2 \times 10^{-6} \text{ in./in. } ^\circ\text{F}^{-1}$$

$$\alpha_{300^\circ\text{F}} = 8.8 \times 10^{-6} \text{ in./in. } ^\circ\text{F}^{-1}$$

$$\nu = 0.3$$

$$\rho = 0.29$$

$$\text{Elongation, } e = 35\%$$

$$\varepsilon @ S_y = 43,300 / 27.0 \times 10^6 = 0.001604 \text{ in. in}^{-1}$$

$$\text{Tangent Modulus, } E_T = (94,200 - 43,300) / (0.35 - 0.001604) = 146,100 \text{ psi.}$$

2.10.4.2.3 Boundary Conditions

Lid End Drop Boundary Conditions

The weights of the transport cask internals and bottom impact limiter are accounted for by applying equivalent pressures. The actual weights of the transport cask internals and bottom impact limiter, including the thermal shield, are 88,390 lb. and 14,085 lb. respectively (Section 2.2). The weights of the transport cask internals and bottom impact limiter, used in this analysis, are conservatively increased to 88,500 lb. and 14,200 lb. respectively. The pressure equivalent to the weight of the internals, P_i , is,

$$P_i = 88,500 / [\pi \times 34.00^2 \text{ (cavity inner radius)}] = 24.3689 \text{ psi.}$$

The pressure equivalent to the weight of the bottom impact limiter, including the thermal shield, P_{bil} , is,

$$P_{bil} = 14,200 / [\pi \times 40.50^2 \text{ (cask outer radius)}] = 2.7577 \text{ psi.}$$

The reaction pressure at the top end of the cask in the lid region is made equivalent to the weight of the lid plus the weight of the internals. The reaction pressure at the top end of the cask in the flange region is made equivalent to the weight of the entire model plus the weight of the bottom impact limiter minus the weight of the lid. The reaction pressure at the lid, R_l , is,

$$R_l = \frac{88,500 + \pi(34^2)(4.50)(0.29)}{\pi(34^2)} = 25.67 \text{ psi.}$$

The reaction pressure at the flange, R_f , is,

$$R_f = \frac{150,320 + 14,200 - \pi(34^2)(4.50)(0.29)}{\pi[(37.34^2 - 34.00^2) + (40.50^2 - 37.65^2)]} = 110.32 \text{ psi.}$$

These reaction pressures are applied to the finite element model and then adjusted slightly for each load case in order to balance the reaction forces at the boundary conditions.

Symmetry displacement boundary conditions are applied along the y-axis of the 2-dimensional axisymmetric model. A single node along the y-axis of the model at the bottom (non-impact) end of the cask is held in the axial direction. An inertial load of 100gs in the negative y-direction is also applied to the model. A plot of the finite element model and boundary conditions for the lid end drop load case is provided in Figure 2.10.4-1.

Bottom End Drop Boundary Conditions

The weights of the transport cask internals and top impact limiter are also accounted for by applying equivalent pressures. The actual weight of the top impact limiter is 13,782 lb. The weight of the top impact limiter used in this analysis is conservatively increased to 13,900 lb. The pressure equivalent to the weight of the internals, P_i , is,

$$P_i = 88,500 / [\pi \times (34.00^2 - 8.75^2) \text{ (cavity inner radius)}] = 26.10 \text{ psi.}$$

The pressure equivalent to the weight of the top impact limiter, P_{il} , is,

$$P_{il} = \frac{13,900}{\pi[37.34^2 + (40.50^2 - 37.65^2)]} = 2.74 \text{ psi.}$$

The reaction pressure at the bottom end of the cask in the central region is made equivalent to the weight of the bottom plus the weight of the internals. The reaction pressure at the bottom end of the cask in the outer region is made equivalent to the weight of the entire model plus the weight of the top impact limiter minus the weight of the bottom. The reaction pressure in the center region, R_c , is,

$$R_c = \frac{88,500 + \pi(34^2)(6.50)(0.29)}{\pi(34^2)} = 26.25 \text{ psi.}$$

The reaction pressure at the outer edge, R_o , is,

$$R_o = \frac{150,320 + 13,900 - \pi(34^2)(6.50)(0.29)}{\pi(40.50^2 - 34.00^2)} = 103.45 \text{ psi.}$$

These reaction pressures are applied to the finite element model and then adjusted slightly for each load case in order to balance the reaction forces at the boundary conditions.

Symmetry displacement boundary conditions are applied along the y-axis of the 2-dimensional axisymmetric model. A single node along the y-axis of the model at the lid (non-impact) end of the cask is held in the axial direction. An inertial load of 100gs in the positive y-direction is also applied to the model. A plot of the finite element model and boundary conditions for the bottom end drop load case is provided in Figure 2.10.4-2.

Thermal Loads

Two thermal load cases are applied to each drop orientation load case, yielding a total of four load combinations. The two temperature distributions applied correspond to the 100° F. and -20° F ambient temperature environments. The temperature distributions applied to the finite element model for both the 100° F hot environment condition and the -20° F cold environment condition are taken from Chapter 3.

2.10.4.3 FEA Results

In order to quantify the axial length of the cavity that develops as a result of lead slump, the difference between the maximum axial deflections of adjacent lead and structural shell nodes, at the load step corresponding to 75 gs, is determined. This difference is taken to be the maximum cavity length caused by lead slump.

The following table summarizes the axial gap between the lead and cavity after all four load combinations analyzed. Nodal displacement distributions for the four load combinations are shown Figures 2.10.4-3 through 2.10.4-6.

Load Combination	Gap
75g Lid End Drop, Hot Environment	0 in.
75g Lid End Drop, Cold Environment	0.235 in.
75g Bottom End Drop, Hot Environment	0 in.
75g Bottom End Drop, Cold Environment	0.107 in.

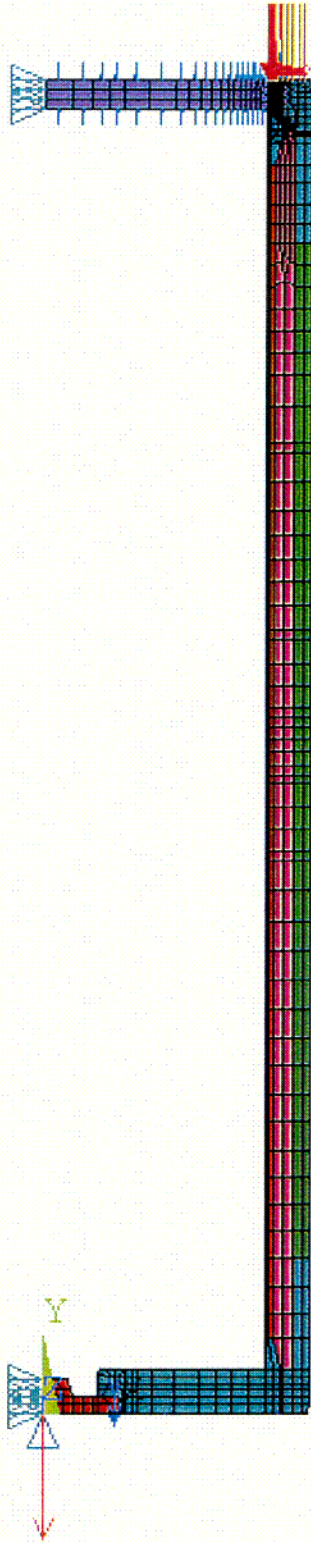
2.10.4.4 Conclusions

The table above shows that the maximum longitudinal gap, caused by lead slump, is 0.235 inches, and occurs during accident condition lid end drop, in the cold environment. The table above, as well as the displacement plots (Figures 2.10.4-3 through 2.10.4-6) also show that in the hot environment, differential thermal expansion between the lead shield and the structural shells precludes gap formation during both lid and end drops. The effect of the gap on the shielding ability of the NUHOMS®-MP197 cask is analyzed in Chapter 6.

2.10.4.5 References

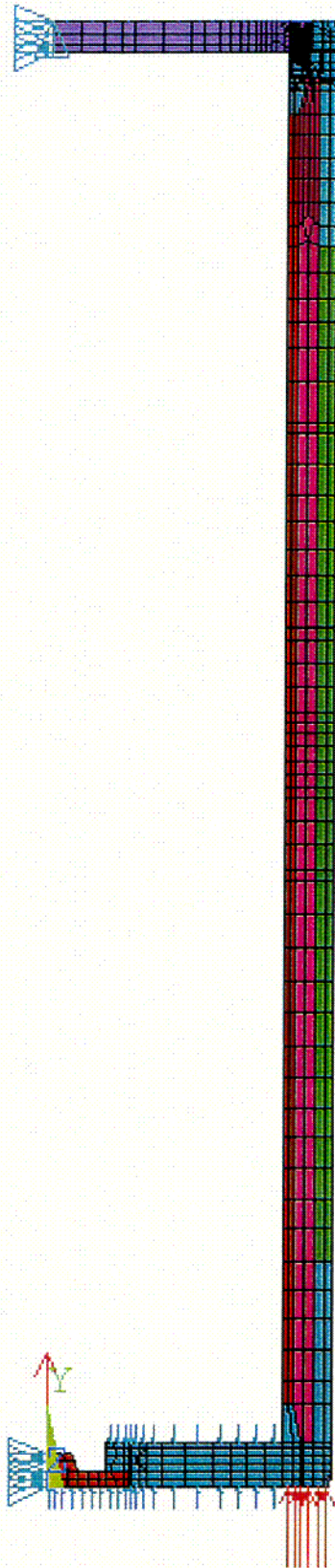
1. ANSYS User's Manual, Rev 5.6, 1998.
2. American Society of Mechanical Engineers, ASME Boiler and Pressure Vessel Code, Section II, Part D, 1998, including 1999 addenda.
3. American Society of Mechanical Engineers, ASME Boiler and Pressure Vessel Code, Section II, Part A, 1998, including 1999 addenda.
4. An Assessment of Stress-Strain Data Suitable for Finite-Element Elastic-Plastic Analysis of Shipping Containers, NUREG/CR-0481.
5. Cask Design Guide, ORNL-NSIC-68, February 1970.
6. A Survey of Strain Rate Effects for some Common Structural Materials Used in Radioactive Material Packaging and Transportation Systems, U.S. Energy Research and Development Administration, Battelle Columbus Laboratories, August 1976.
7. Baumeister & Marks, Standard Handbook for Mechanical Engineers, 7th Edition.

Figure 2.10.4-1
NUHOMS[®]-MP197 cask 2-Dimensional Finite Element Model
with Lid End Drop Boundary Conditions



201

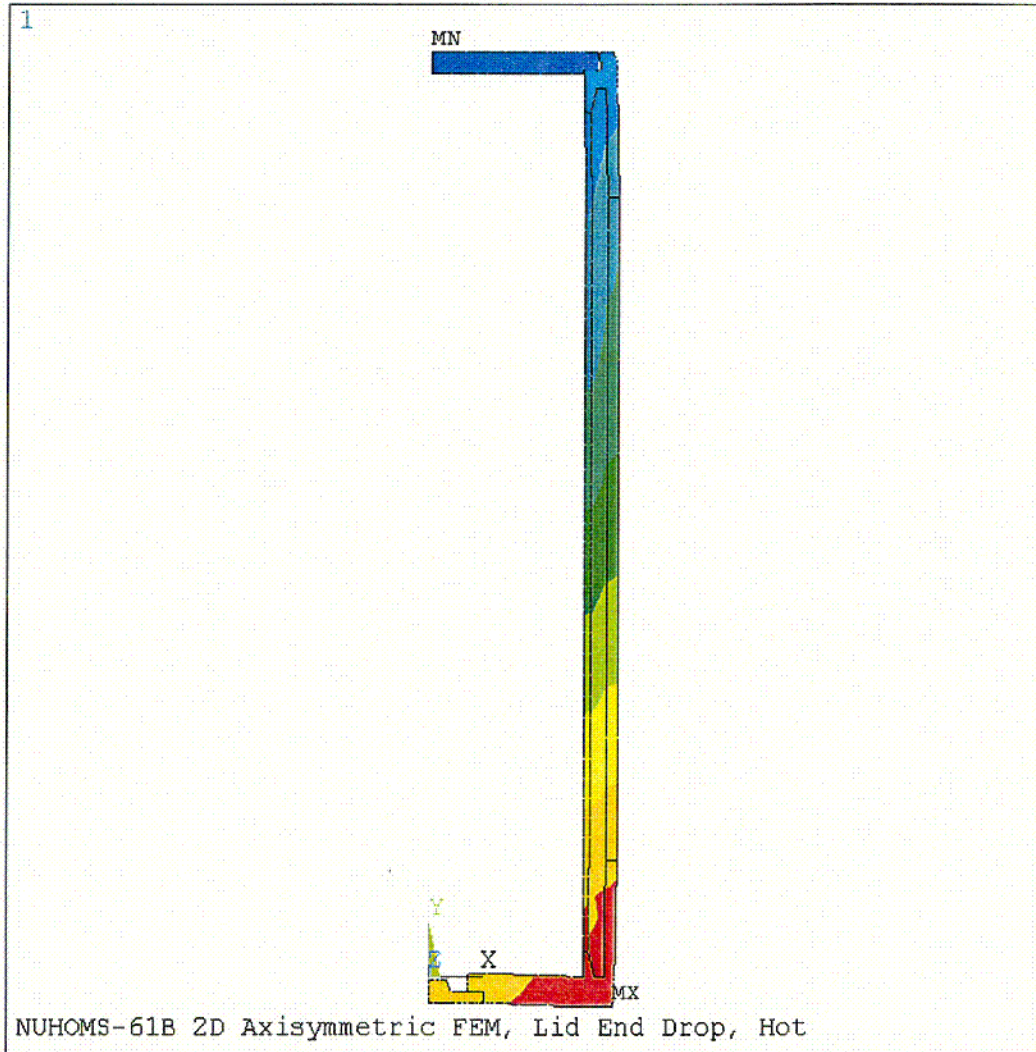
Figure 2.10.4-2
NUHOMS[®]-MP197 cask 2-Dimensional Finite Element Model
with Bottom End Drop Boundary Conditions



CO2

Rev. 0 4/01

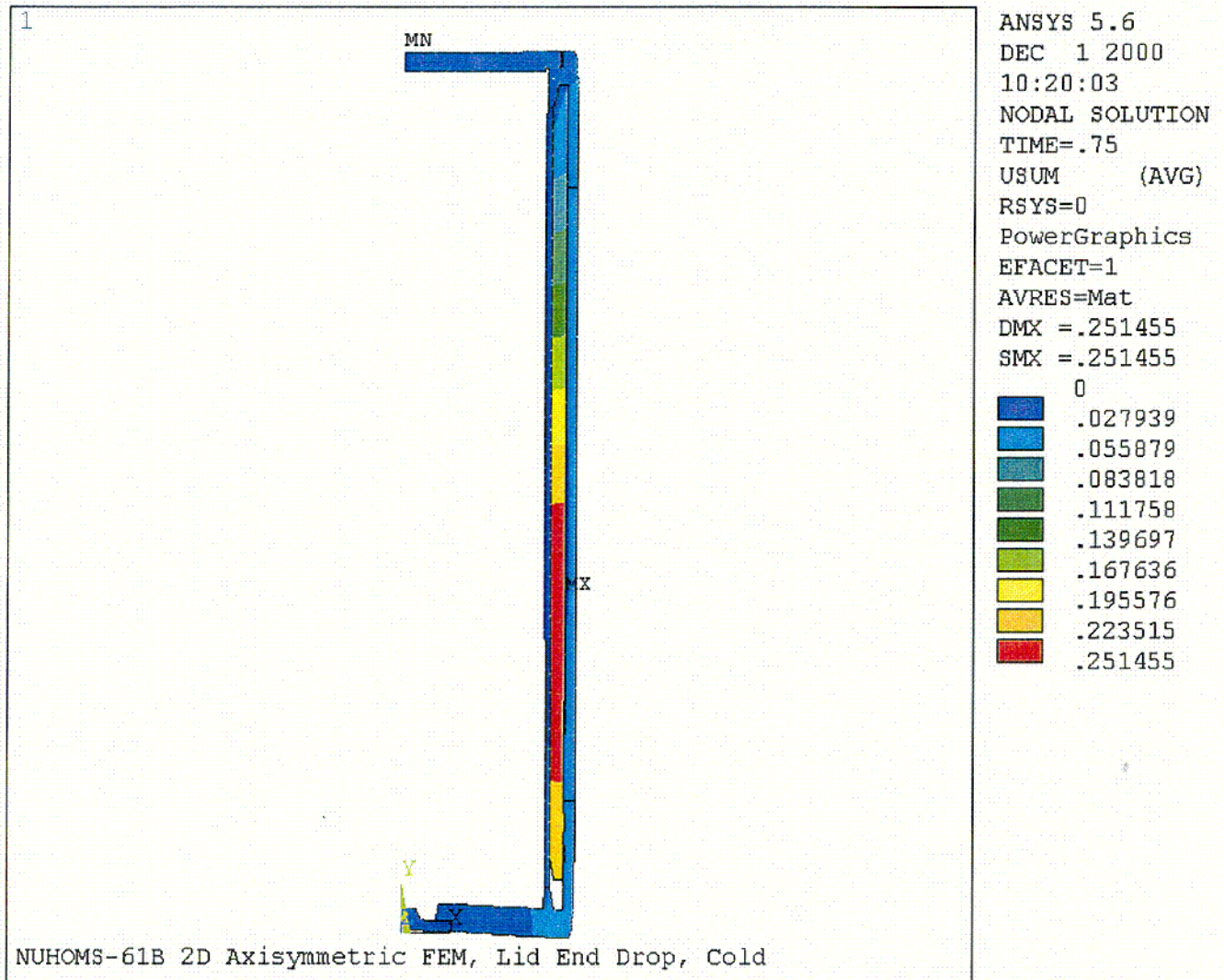
Figure 2.10.4-3
Displacement Pattern – Lid End Drop, Hot Environment Load Case



C03

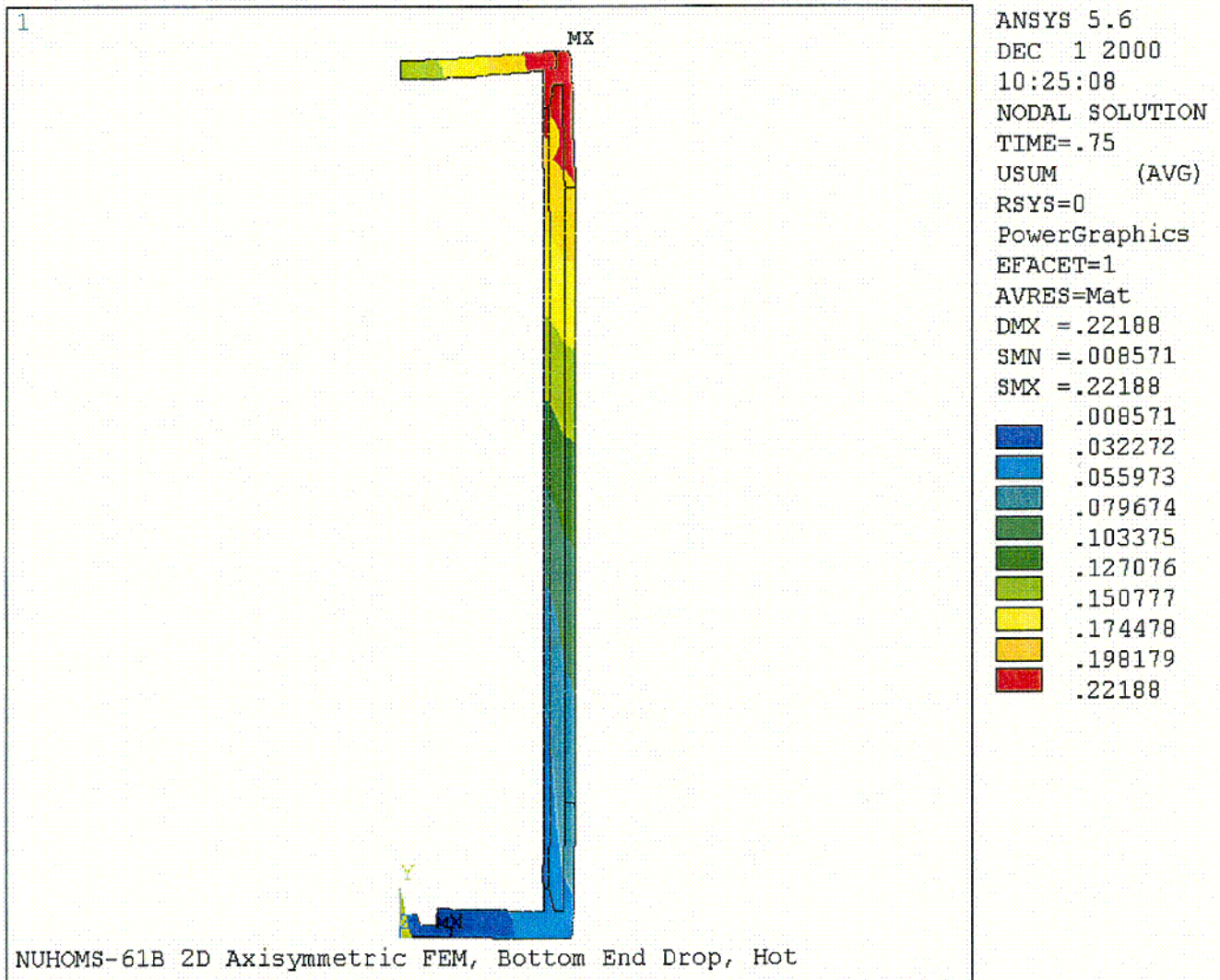
Rev. 0 4/01

Figure 2.10.4-4
Displacement Pattern – Lid End Drop, Cold Environment Load Case



CO4

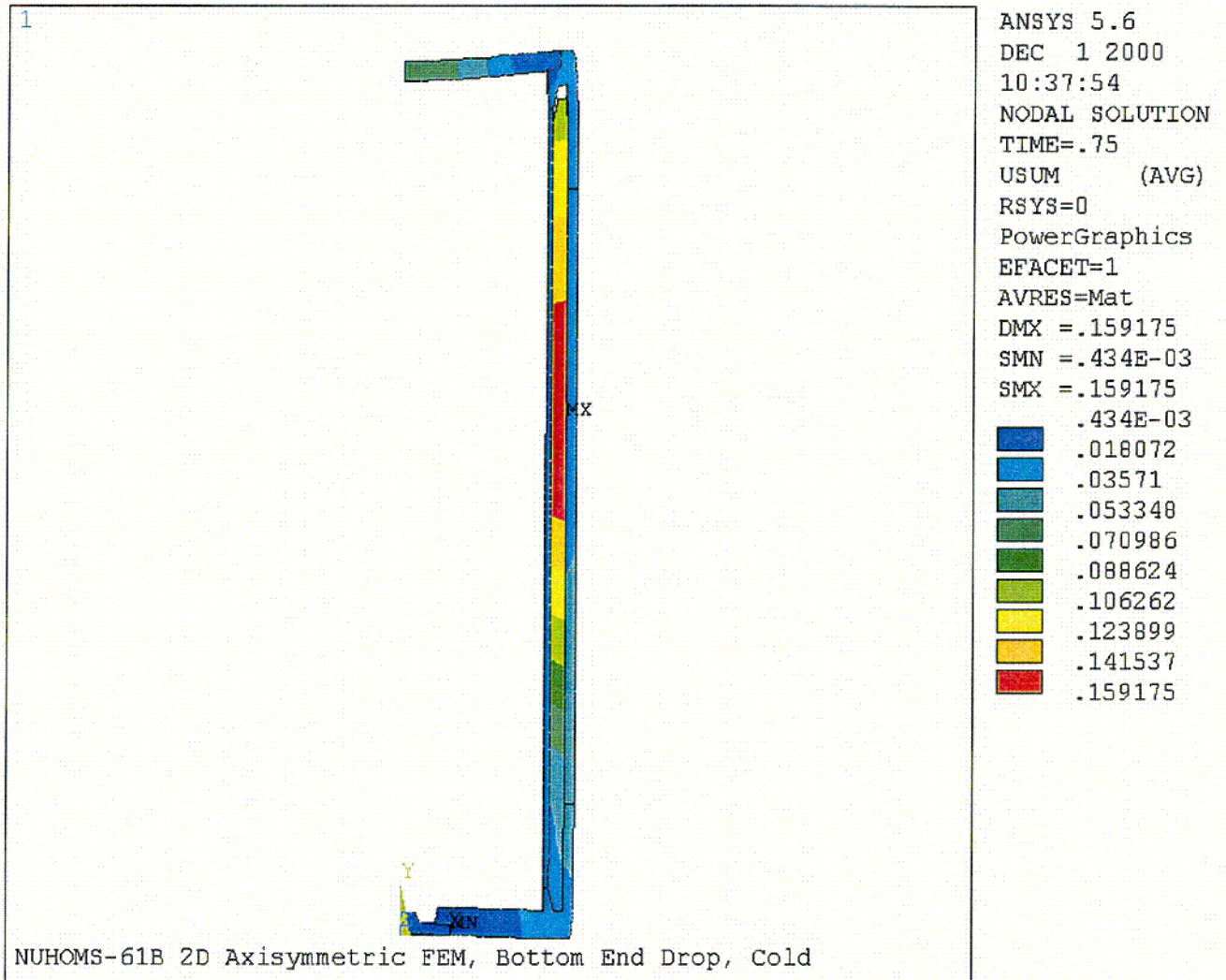
Figure 2.10.4-5
Displacement Pattern – Bottom End Drop, Hot Environment Load Case



C05

Rev. 0 4/01

Figure 2.10.4-6
Displacement Pattern – Bottom End Drop, Cold Environment Load Case



COE

APPENDIX 2.10.5

TABLE OF CONTENTS

	<u>Page</u>
2.10.5 NUHOMS[®]-MP197 CASK INNER CONTAINMENT BUCKLING ANALYSIS	2.10.5-1
2.10.5.1 Introduction	2.10.5-1
2.10.5.2 Material Properties	2.10.5-2
2.10.5.3 Allowable Buckling Stress Determination	2.10.5-4
2.10.5.4 Finite Element Model	2.10.5-10
2.10.5.5 FEA Results	2.10.5-13
2.10.5.6 Conclusions	2.10.5-16
2.10.5.7 References	2.10.5-17

LIST OF FIGURES

2.10.5-1	NUHOMS [®] -MP197 cask 2-Dimensional Finite Element Model with Lid End Drop Boundary Conditions
2.10.5-2	NUHOMS [®] -MP197 cask 2-Dimensional Finite Element Model with Bottom End Drop Boundary Conditions
2.10.5-3	Stress Intensity – Lid End Drop, Hot Environment
2.10.5-4	Stress Intensity – Lid End Drop, Cold Environment
2.10.5-5	Stress Intensity – Bottom End Drop, Hot Environment
2.10.5-6	Stress Intensity – Bottom End Drop, Cold Environment
2.10.5-7	Collapse Load Determination – Lid End Drop, Hot Environment
2.10.5-8	Collapse Load Determination – Lid End Drop, Cold Environment
2.10.5-9	Collapse Load Determination – Bottom End Drop, Hot Environment
2.10.5-10	Collapse Load Determination – Bottom End Drop, Cold Environment

APPENDIX 2.10.5

NUHOMS[®]-MP197 CASK INNER CONTAINMENT BUCKLING ANALYSIS

2.10.5.1 Introduction

The purpose of this analysis is to evaluate the structural adequacy of the NUHOMS[®]-MP197 cask inner shell with respect to buckling. The load cases considered in this calculation are hypothetical accident condition lid and bottom end drops. The impact loads are combined with thermal loads corresponding to a 100° F ambient environment and a -20° F ambient environment. The analysis is based on the methodology provided in ASME Code Case N-284-1 [1] and the Collapse Load Analysis described in ASME B&PV Code Appendix F [2].

During a hypothetical accident condition end drop, permanent deformation of the lead gamma shield may occur. The lead gamma shield is supported by friction between the lead and cask shells, in addition to bearing at the end of the lead column. During fabrication, a small gap may develop between the lead gamma shield and the cask structural shells due to differential thermal expansion of the dissimilar materials during cooling after the lead pour. The gap between the lead and cask shells reduces the stresses in the cask shells during the postulated end drop, while maximizing the amount of permanent deformation in the lead column (i.e. lead slump). Therefore, for the purpose of analysis, the lead is conservatively assumed to be initially in contact with both the cask inner and structural shells.

A nonlinear finite element analysis is performed in order to evaluate the buckling capacity of the inner shell of the transport cask. A 2-dimensional axisymmetric ANSYS [3] finite element model is constructed for this purpose. The results of the finite element analysis provide both stresses and displacements generated during the end drop event. The resulting stress distribution is compared with the allowable buckling stresses in both the hoop and the axial directions as dictated by ASME Code CASE N-284-1 [1]. The resulting deformation is used to perform a collapse load analysis described in ASME B&PV Code Appendix F [2].

2.10.5.2 Material Properties

The maximum temperature of the transport cask during transport in the 100° F ambient environment is 302° F (Chapter 3, Table 3-1). Properties of NUHOMS®-MP197 cask materials are taken at 300° F for both hot and cold environment cases, which is conservative. The transport cask material properties are as follows.

Outer Shell (SA-240 Type 316) @ 300° F. [4] [5] [6]

$$E = 27.0 \times 10^6 \text{ psi.}$$

$$S_y = 23.4 \text{ ksi.}$$

$$S_u = 72.9 \text{ ksi.}$$

$$\alpha_{70^\circ\text{F}} = 8.5 \times 10^{-6} \text{ in./in. } ^\circ\text{F}^{-1}$$

$$\alpha_{300^\circ\text{F}} = 9.2 \times 10^{-6} \text{ in./in. } ^\circ\text{F}^{-1}$$

$$\nu = 0.3$$

$$\rho = 0.29$$

$$\text{Elongation, } e = 40\%$$

$$\varepsilon @ S_y = 23,400 / 27.0 \times 10^6 = 0.000867 \text{ in. in}^{-1}.$$

$$\text{Tangent Modulus, } E_T = (72,900 - 23,400) / (0.40 - 0.000867) = 124,020 \text{ psi.}$$

Lid Material (SA-693 Type 630, Condition H1100) @ 300° F. [4] [5] [6]

$$E = 27.2 \times 10^6 \text{ psi.}$$

$$S_y = 101.8 \text{ ksi.}$$

$$S_u = 140.0 \text{ ksi.}$$

$$\alpha_{70^\circ\text{F}} = 5.89 \times 10^{-6} \text{ in./in. } ^\circ\text{F}^{-1}$$

$$\alpha_{300^\circ\text{F}} = 5.90 \times 10^{-6} \text{ in./in. } ^\circ\text{F}^{-1}$$

$$\nu = 0.3$$

$$\rho = 0.29$$

$$\text{Elongation, } e = 14\%$$

$$\varepsilon @ S_y = 101,800 / 27.2 \times 10^6 = 0.003743 \text{ in. in}^{-1}.$$

$$\text{Tangent Modulus, } E_T = (140,000 - 101,800) / (0.14 - 0.003743) = 280,353 \text{ psi.}$$

Lead (B-29) @ 300° F. [7] [8] [9]

$$E = 2.06 \times 10^6 \text{ psi.}$$

$$\nu = 0.45$$

$$\rho = 0.41$$

$$\alpha_{70^\circ\text{F}} = 16.07 \times 10^{-6} \text{ in./in. } ^\circ\text{F}^{-1}$$

$$\alpha_{300^\circ\text{F}} = 17.34 \times 10^{-6} \text{ in./in. } ^\circ\text{F}^{-1}$$

Multi-linear Stress/Strain Curve:

Strain	Stress
0.000485	1,000
0.030	1,700
0.100	2,380
0.300	2,720
0.500	3,060

Inner Shell, Flange, Bottom, RAM Closure Plate (SA-240 Type XM-19 or SA-182 Type FXM-19) @ 300° F. [4] [5] [6]

$$E = 27.0 \times 10^6 \text{ psi.}$$

$$S_y = 43.3 \text{ ksi.}$$

$$S_u = 94.2 \text{ ksi.}$$

$$\alpha_{70^\circ\text{F}} = 8.2 \times 10^{-6} \text{ in./in. } ^\circ\text{F}^{-1}$$

$$\alpha_{300^\circ\text{F}} = 8.8 \times 10^{-6} \text{ in./in. } ^\circ\text{F}^{-1}$$

$$\nu = 0.3$$

$$\rho = 0.29$$

$$\text{Elongation, } e = 35\%$$

$$\epsilon @ S_y = 43,300 / 27.0 \times 10^6 = 0.001604 \text{ in. in}^{-1}.$$

$$\text{Tangent Modulus, } E_T = (94,200 - 43,300) / (0.35 - 0.001604) = 146,100 \text{ psi.}$$

2.10.5.3 Allowable Buckling Stress Determination

The following analysis, based on ASME Code CASE N-284-1 [1], is used to determine the allowable axial and hoop buckling stresses.

2.10.5.3.1 Notation

The following notation is taken from Reference 1, Section –1200.

- Subscripts ϕ and θ = axial (meridional) and circumferential directions respectively.
- l_ϕ = distances between lines of support in the axial direction, use 193.50 in.
- R = shell mean radius = 68.00/2 in. (inner radius) + 1.25 in. (shell thickness) = 35.25 in.
- t = shell thickness, 1.25 in.
- t_ϕ, t_θ = thickness of elements of a stiffener, in. (defaults to t for unstiffened vessels).
- $M_\phi = \frac{l_\phi}{\sqrt{(R)(t)}}$
- $C_{\phi L}, C_\theta$ = elastic buckling coefficient under external pressure and axial compression respectively.
- $\sigma_{heL}, \sigma_{\phi eL}$ = local theoretical elastic instability stress in the hoop direction for cylinders under external pressure and axial compression respectively, psi.
- E = modulus of elasticity of the material at design temperature, 27.0×10^6 psi. @ 300° F [5].
- α_{eL} = capacity reduction factor to account for the difference between classical theory and predicted instability stresses for fabricated shells.
- σ_y = tabulated yield stress of material at design temperature, 43,300 psi. @ 300° F [5].
- σ_{xa}, σ_{ha} , allowable axial and hoop stresses for elastic buckling respectively, psi.
- σ_{xc}, σ_{hc} , allowable axial and hoop stresses for inelastic buckling respectively, psi.
- $\sigma_\phi, \sigma_\theta$ = calculated axial and hoop membrane stress components respectively, psi.
- FS = factor of Safety, 2 for normal conditions, 1.34 for accident conditions ([1], Section – 1400 (a)).
- K = the ratio of the axial membrane force per unit length to the hoop compressive membrane force per unit length, $\sigma_\phi t_\phi / \sigma_\theta t_\theta$

2.10.5.3.2 Allowable Hoop Stress Determination

The analytical method provided in ASME Code Case N-284-1 is used to determine the allowable buckling stress with respect to external pressure of the NUHOMS[®]-MP197 cask inner shell.

Since the vessel is assumed to be unstiffened, only the theoretical buckling calculation for unstiffened shells or local buckling between stiffeners of stiffened shells applies ([1], Section 1712.1). Reference 1, Section –1712.2, Stringer Buckling and General instability, does not apply since it analyzes the global buckling of a stiffened vessel.

Theoretical Buckling Value

Local Buckling, external pressure, with no end pressure ([1], Section –1712.1.1 (b) (1)):

$$M_{\phi} = \frac{l_{\phi}}{\sqrt{(R)(t)}} = \frac{193.50}{\sqrt{(35.25)(1.25)}} = 29.15 \text{ in.}$$

$$\frac{R}{t} = \frac{35.25}{1.25} = 28.2, \quad 1.65 \frac{R}{t} = 46.53$$

$$\Rightarrow 3.0 < M_{\phi} < 1.65 \frac{R}{t}$$

Therefore,

$$C_{\alpha} = \frac{0.92}{M_{\phi} - 1.17} = \frac{0.92}{29.15 - 1.17} = 0.0329$$

$$\Rightarrow \sigma_{\alpha L} = \sigma_{reL} = C_{\alpha} \frac{(E)(t)}{R} = 0.0329 \frac{(27.0 \times 10^6)(1.25)}{35.25} = 31,481 \text{ psi.}$$

Capacity Reduction Factor

From Reference 1, Section –1511 (b), for local buckling of cylindrical shells, stiffened or unstiffened under Hoop Compression,

$$\alpha_{\alpha L} = 0.8.$$

Plasticity Reduction Factor

The plasticity reduction factor is computed based on the formulae provided in Reference 1, Section -1611 (b) as follows.

$$\Delta = \frac{\alpha_{\theta L} \sigma_{\theta eL}}{\sigma_y} = \frac{(0.8)(31,481)}{43,300} = 0.582$$

Since $\Delta \leq 0.67$,

$$\eta_{\theta} = 1.$$

Allowable Buckling Stress

Elastic buckling interaction equations ([1], Section -1713.1.1 (b)) for normal conditions, hoop compression only:

$$\sigma_{ha} = \frac{(\alpha_{\theta L})(\sigma_{heL})}{FS} = \frac{(0.8)(31,481)}{2} = 12,593 \text{ psi.}$$

For accident conditions,

$$\sigma_r = 12,593 \text{ psi.} \times (2.0 \text{ normal condition F.S.} / 1.34 \text{ accident condition F.S.}) = 18,796 \text{ psi.}$$

Inelastic buckling interaction equations for hoop compression only ([1], Section -1713.2.1):

$$\sigma_{rc} = \eta_{\theta} \sigma_{ra} (1)(12,593) = 12,593 \text{ psi.}$$

For accident conditions,

$$\sigma_{rc} = 12,593 \text{ psi.} \times (2.0 \text{ normal condition F.S.} / 1.34 \text{ accident condition F.S.}) = 18,796 \text{ psi.}$$

2.10.5.3.3 Allowable Axial Stress Determination

The analytical method provided in ASME Code Case N-284-1 [1] is used to determine the NUHOMS[®]-MP197 cask allowable buckling axial stress.

Theoretical Buckling Value

Local Buckling ([1], Section -1712.1.1 (a)):

$$M_{\phi} = \frac{l_{\phi}}{\sqrt{(R)(t)}} = \frac{193.50}{\sqrt{(35.25)(1.25)}} = 29.15 \text{ in.}$$

$$\Rightarrow M_{\phi} \geq 1.73$$

Therefore,

$$C_{\phi} = 0.605$$

$$\Rightarrow \sigma_{\phi L} = C_{\phi} \frac{(E)(t)}{R} = 0.605 \frac{(27.0 \times 10^6)(1.25)}{35.25} = 579,255 \text{ psi.}$$

Capacity Reduction Factor

From reference 1, Section -1511 (a), for local buckling of cylindrical shells, stiffened or unstiffened under axial compression, $\alpha_{\phi L}$ is the larger of (1) and (2).

(1) Effect of R/t

$$\frac{R}{t} = \frac{35.25}{1.25} = 28.2$$

$$\Rightarrow \alpha_{\phi L} = \text{MIN} \left\{ \begin{array}{l} 1.52 - 0.473 \log_{10} \left(\frac{R}{t} \right) = 0.834 \\ \frac{300\sigma_y}{E} - 0.033 = 0.448 \end{array} \right\} = 0.448$$

(2) Effect of Length

$$M_{\phi} \geq 10 \Rightarrow \alpha_{\phi L} = 0.207$$

Therefore, $\alpha_{\phi L} = 0.448$.

Plasticity Reduction Factor

The plasticity reduction factor is computed based on the formulae provided in Reference 1, Section -1611 (a) as follows.

$$\Delta = \frac{\alpha_{\phi L} \sigma_{\phi e L}}{\sigma_y} = \frac{(0.448)(579,255)}{43,300} = 5.993$$

Since $1.6 < \Delta < 6.25$,

$$\eta_{\phi} = \frac{1.31}{1 + 1.15\Delta} = 0.1660.$$

Allowable Buckling Stress

Elastic buckling interaction equations ([1], Section -1713.1.1 (a)) for normal conditions, axial compression only:

$$\sigma_{xa} = \frac{(\alpha_{\phi L})(\sigma_{\phi e L})}{FS} = \frac{(0.448)(579,255)}{2} = 129,753 \text{ psi.}$$

For accident conditions,

$$\sigma_{xa} = 129,753 \text{ psi.} \times (2.0 \text{ normal condition F.S.} / 1.34 \text{ accident condition F.S.}) = 193,661 \text{ psi.}$$

Inelastic buckling interaction equations for axial compression only ([1], Section -1713.2.1):

$$\sigma_{xc} = \eta_{\theta} \sigma_{xa} = (0.1660)(129,753) = 21,539 \text{ psi.}$$

For accident conditions,

$$\sigma_{xc} = 21,539 \text{ psi.} \times (2.0 \text{ normal condition F.S.} / 1.34 \text{ accident condition F.S.}) = 32,148 \text{ psi.}$$

2.10.5.3.4 Summary of Allowable Buckling Stresses

The following table summarizes the allowable inelastic hoop and axial stresses for the transport cask inner shell for both normal conditions of transport and hypothetical accident conditions.

	Normal Conditions of Transport	Hypothetical Accident Conditions
Maximum Allowable Hoop Stress (psi.)	12,593	18,796
Maximum Allowable Axial Stress (psi.)	21,539	32,148

2.10.5.4 Finite Element Model

2.10.5.4.1 Approach

A 2-dimensional axisymmetric ANSYS [3] finite element model, constructed primarily from PLANE42 elements, is used in this analysis. LINK1 elements are used to model the lid and RAM port cover bolts. Pre-load stresses of 87 ksi. and 25 ksi. are applied to the lid and RAM port cover bolts respectively (Appendix 2.10.2). Gap elements are used to model the interaction between the lead gamma shield and the cask inner and outer shells. The coefficient of sliding friction for lead on mild steel varies from 0.3 for lubricated surfaces to 0.95 for dry surfaces [4]. A lower bound coefficient of static friction of 0.25 is conservatively used for the buckling analysis.

In order to perform a collapse load analysis, as per ASME B&PV Code Appendix F [2], an elastic plastic analysis is required. The material properties of the lid, bottom, inner shell, and outer shell of the transport cask are modeled with bilinear stress-strain curves, while the lead material is modeled with a multilinear stress-strain curve.

The neutron shield, shield shell, trunnions and bearing block are not included in the model. The effect of the unmodeled weight is accounted for by increasing the density of the outer shell in the neutron shield region. The modified density of the outer shell in this region is computed in the following way.

The weight of the section of the outer shell, W_{os} , that will be given an increased density is,

$$W_{os} = \pi \{ [41.00 \text{ in. (outer shell o.r.)}]^2 - [38.5 \text{ in. (outer shell i.r.)}]^2 \} \times 144.0 \text{ in. (section length)} \times 0.29 \text{ (density)} = 26,075 \text{ lb.}$$

The weight of the entire FEM prior to density modification, W_m , is 128,050 lb. (Section 2.2). The actual calculated weight of the transport cask, W_{tc} , is 150,027 lb. (Section 2.2). However, a conservative weight of 150,320 lb. is used. Therefore, the modified density used in this analysis, ρ_m , is

$$\rho_m = \frac{W_{os} + (W_{tc} - W_m)}{\pi(41.00^2 - 38.50^2) \times 144} = \frac{26,075 + (150,320 - 128,050)}{\pi(41.00^2 - 38.50^2) \times 144} = 0.538 \text{ lb.in.}^{-3}$$

2.10.5.4.2 Lid End Drop Boundary Conditions

The weights of the transport cask internals and bottom impact limiter are accounted for by applying equivalent pressures. The actual weights of the transport cask internals and bottom impact limiter, including the thermal shield, are 88,390 lb. and 14,085 lb. respectively. The weights of the transport cask internals and bottom impact limiter, used in this analysis, are conservatively increased to 88,500 lb. and 14,200 lb. respectively. The pressure equivalent to the weight of the internals, P_i , is,

$$P_i = 88,500 / [\pi \times 34.00^2 \text{ (cavity inner radius [2]) }] = 24.3689 \text{ psi.}$$

The pressure equivalent to the weight of the bottom impact limiter, including the thermal shield, P_{bil} , is,

$$P_{bil} = 14,200 / [\pi \times 40.50^2 \text{ (cask outer radius [2]) }] = 2.7577 \text{ psi.}$$

The reaction pressure at the top end of the cask in the lid region is made equivalent to the weight of the lid plus the weight of the internals. The reaction pressure at the top end of the cask in the flange region is made equivalent to the weight of the entire model plus the weight of the bottom impact limiter minus the weight of the lid. The reaction pressure at the lid, R_l , is,

$$R_l = \frac{88,500 + \pi(34^2)(4.50)(0.29)}{\pi(34^2)} = 25.67 \text{ psi.}$$

The reaction pressure at the flange, R_f , is,

$$R_f = \frac{150,320 + 14,200 - \pi(34^2)(4.50)(0.29)}{\pi[(37.34^2 - 34.00^2) + (40.50^2 - 37.65^2)]} = 110.32 \text{ psi.}$$

These reaction pressures are applied to the finite element model and then adjusted slightly for each load case in order to balance the reaction forces at the boundary conditions.

Symmetry displacement boundary conditions are applied along the y-axis of the 2-dimensional axisymmetric model. A single node along the y-axis of the model at the bottom (non-impact) end of the cask is held in the axial direction. An inertial load of 100gs in the negative y-direction is also applied to the model. A plot of the finite element model and boundary conditions for the lid end drop load case is provided in Figure 2.10.5-1.

2.10.5.4.3 Bottom End Drop Boundary Conditions

The weights of the transport cask internals and top impact limiter are also accounted for by applying equivalent pressures. The actual weight of the top impact limiter is 13,782 lb. The weight of the top impact limiter used in this analysis is conservatively increased to 13,900 lb. The pressure equivalent to the weight of the internals, P_i , is,

$$P_i = 88,500 / [\pi \times (34.00^2 - 8.75^2) \text{ (cavity inner radius) }] = 26.0973 \text{ psi.}$$

The pressure equivalent to the weight of the top impact limiter, P_{til} , is,

$$P_{til} = \frac{13,900}{\pi[37.34^2 + (40.50^2 - 37.65^2)]} = 2.7362 \text{ psi.}$$

The reaction pressure at the bottom end of the cask in the central region is made equivalent to the weight of the bottom plus the weight of the internals. The reaction pressure at the bottom end of the cask in the outer region is made equivalent to the weight of the entire model plus the weight of the top impact limiter minus the weight of the bottom. The reaction pressure in the center region, R_c , is,

$$R_c = \frac{88,500 + \pi(34^2)(6.50)(0.29)}{\pi(34^2)} = 26.25 \text{ psi.}$$

The reaction pressure at the outer edge, R_o , is,

$$R_o = \frac{150,320 + 13,900 - \pi(34^2)(6.50)(0.29)}{\pi(40.50^2 - 34.00^2)} = 103.45 \text{ psi.}$$

These reaction pressures are applied to the finite element model and then adjusted slightly for each load case in order to balance the reaction forces at the boundary conditions.

Symmetry displacement boundary conditions are applied along the y-axis of the 2-dimensional axisymmetric model. A single node along the y-axis of the model at the lid (non-impact) end of the cask is held in the axial direction. An inertial load of 100gs in the positive y-direction is also applied to the model. A plot of the finite element model and boundary conditions for the bottom end drop load case is provided in Figure 2.10.5-2.

2.10.5.4.4 Thermal Loads

Two thermal load cases are applied to each drop orientation load case, yielding a total of four load combinations. The two temperature distributions applied correspond to the 100° F. and -20° F ambient temperature environments. The temperature distributions applied to the finite element model for both the 100° F hot environment condition and the -20° F cold environment condition are taken from Chapter 3.

2.10.5.5 FEA Results

Stress intensities and displacement patterns for the four load combinations are shown Figures 2.10.5-3 through 2.10.5-6.

2.10.5.5.1 Collapse Load Determination

As per paragraph F-1340 [2], the acceptability of a component may be demonstrated by collapse load analysis. The allowable collapse load shall not exceed 100% of plastic analysis collapse load ([2], F-1341.3). The plastic analysis collapse load is defined as that determined by plastic analysis according to the criteria given in II-1430 ([2], F-1321.6(c)).

Using the methodology described in II-1430 ([2], F-1321.6(c)) (see Figures 2.10.5-7 through 2.10.5-10), the allowable collapse loads are determined. Since the load-displacement curve taken from ANSYS does not cross the line of slope ϕ , for all load combinations, up to the 100 g load step, the collapse load is determined to be >100 gs.

2.10.5.5.2 Maximum Axial and Hoop Stresses

The maximum axial and hoop stresses, in the inner shell, at the load step corresponding to 75 gs, is extracted from the ANSYS results files for all four load combinations. These stresses are compared to the allowable axial and hoop stresses computed above using the methodology provided in ASME Code Case N-284-1 [1].

2.10.5.5.3 Summary of Results

The following table summarizes the maximum allowable collapse load and the maximum calculated and allowable hoop and axial stresses generated in the inner shell for all four load combinations analyzed.

Load Combination	Collapse Load	Stress Category	Maximum Stress (psi.)	Allowable Buckling Stress (psi.)
75g Lid End Drop, Hot Environment	>100 gs	Axial Stress	24,756	32,148
		Hoop Stress	10,677	18,796
75g Lid End Drop, Cold Environment	> 100 gs	Axial Stress	17,808	32,148
		Hoop Stress	5,386	18,796
75g Bottom End Drop, Hot Environment	>100 gs	Axial Stress	26,603	32,148
		Hoop Stress	12,594	18,796
75g Bottom End Drop, Cold Environment	>100 gs	Axial Stress	22,645	32,148
		Hoop Stress	15,934	18,796

2.10.5.5.4 Elastic Buckling Stress Interaction Check

Code Case N-284, Section -1713.1 [1] details the methodology used to evaluate the combination of elastic axial and hoop stresses through the use of interaction equations. These relationships must be satisfied for all η_i .

Since the combination of the 30 foot end drop with the normal condition temperature load is considered an accident condition, a Factor of Safety (FS) of 1.34 is used ([1], Section -1400 (c)).

For all load combinations evaluated above, the calculated axial stress is greater than the calculated hoop stress. Therefore, for all load combinations, the ratio of axial to hoop stress, $K \geq 0.5$. Consequently, the following equation is considered.

$$0.5\sigma_{ha} \frac{t_{\theta}}{t_{\phi}} = (0.5)(18,796) \left(\frac{1.25}{1.25} \right) = 9,398 \text{ psi.}$$

An interaction check is required, since the calculated axial stress, σ_{ϕ} , is greater than the above expression for all load combinations.

Consequently, the following interaction equation must hold ([1], -17131.1 (b)).

$$\frac{\sigma_{\phi} - 0.5\sigma_{ha} \frac{t_{\theta}}{t_{\phi}}}{\sigma_{xa} - 0.5\sigma_{ha} \frac{t_{\theta}}{t_{\phi}}} + \left(\frac{\sigma_{\theta}}{\sigma_{ha}} \right)^2 \leq 1.0$$

The left hand side of this interaction equation is tabulated below for the four load combinations considered.

Load Combination	Interaction Check
Lid End Drop, Hot Environment	$0.406 \leq 1.0 \checkmark$
Lid End Drop, Cold Environment	$0.128 \leq 1.0 \checkmark$
Bottom End Drop, Hot Environment	$0.542 \leq 1.0 \checkmark$
Bottom End Drop, Cold Environment	$0.791 \leq 1.0 \checkmark$

The interaction inequality holds for all load combinations.

2.10.5.5.5 Inelastic Buckling Stress Interaction Check

Code Case N-284, Section –1713.2 [1] details the methodology used to evaluate the combination of inelastic axial and hoop stresses through the use of interaction equations. These relationships must be satisfied when any of the values of $\eta_i < 1$. However, no interaction equations are given for meridional (axial) plus hoop compression, because it is conservative to ignore interaction of the two stress components when buckling is inelastic [1].

2.10.5.6 Conclusions

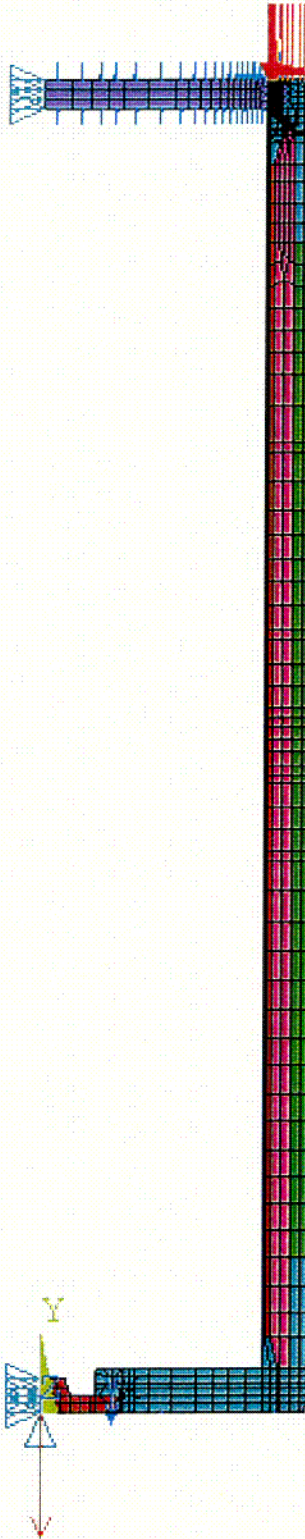
Based on the following results, the inner shell of the NUHOMS[®]-MP197 cask will not buckle during the accident condition end drop:

- The allowable collapse load, determined using the methodology described in ASME B&PV Code Appendix F [2], is greater than 100 gs, for all load combinations.
- The maximum calculated hoop and axial stresses in the inner shell, generated by the 75 g end drop, are less than the allowable axial and hoop stresses computed above using the methodology provided in ASME Code Case N-284-1 [1], for all load combinations.
- All interaction relations, provided in ASME Code Case N-284-1 [1], for combination of axial and hoop stresses are also satisfied.

2.10.5.7 References

1. Cases of ASME Boiler and Pressure Vessel Code, Case N-284-1, *Metal Containment Shell Buckling Design Methods*, Section III, Division 1, Class MC, 1998.
2. American Society of Mechanical Engineers, ASME Boiler and Pressure Vessel Code, Section III, along with appendices, 1998 including 1999 Addendum.
3. ANSYS User's Manual, Rev 5.6.
4. Baumeister & Marks, *Standard Handbook for Mechanical Engineers*, 7th Edition.
5. American Society of Mechanical Engineers, ASME Boiler and Pressure Vessel Code, Section II, Part D, 1998, including 1999 addenda.
6. American Society of Mechanical Engineers, ASME Boiler and Pressure Vessel Code, Section II, Part A, 1998, including 1999 addenda.
7. *An Assessment of Stress-Strain Data Suitable for Finite-Element Elastic-Plastic Analysis of Shipping Containers*, NUREG/CR-0481.
8. *Cask Design Guide*, ORNL-NSIC-68, February 1970.
9. *A Survey of Strain Rate Effects for some Common Structural Materials Used in Radioactive Material Packaging and Transportation Systems*, U.S. Energy Research and Development Administration, Battelle Columbus Laboratories, August 1976.

Figure 2.10.5-1
NUHOMS[®]-MP197 cask 2-Dimensional Finite Element Model
with Lid End Drop Boundary Conditions



007

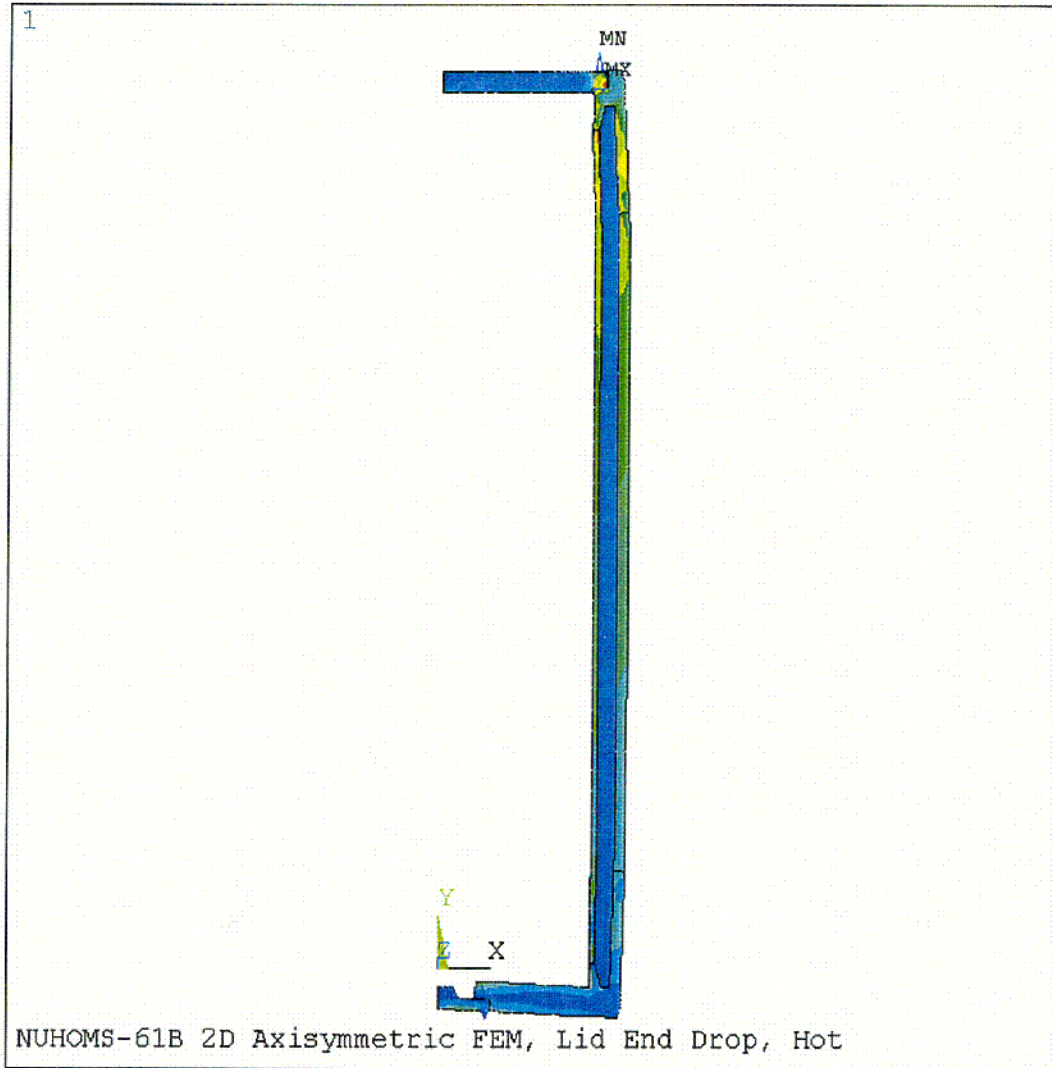
Rev. 0 4/01

Figure 2.10.5-2
NUHOMS®-MP197 cask 2-Dimensional Finite Element Model
with Bottom End Drop Boundary Conditions



008

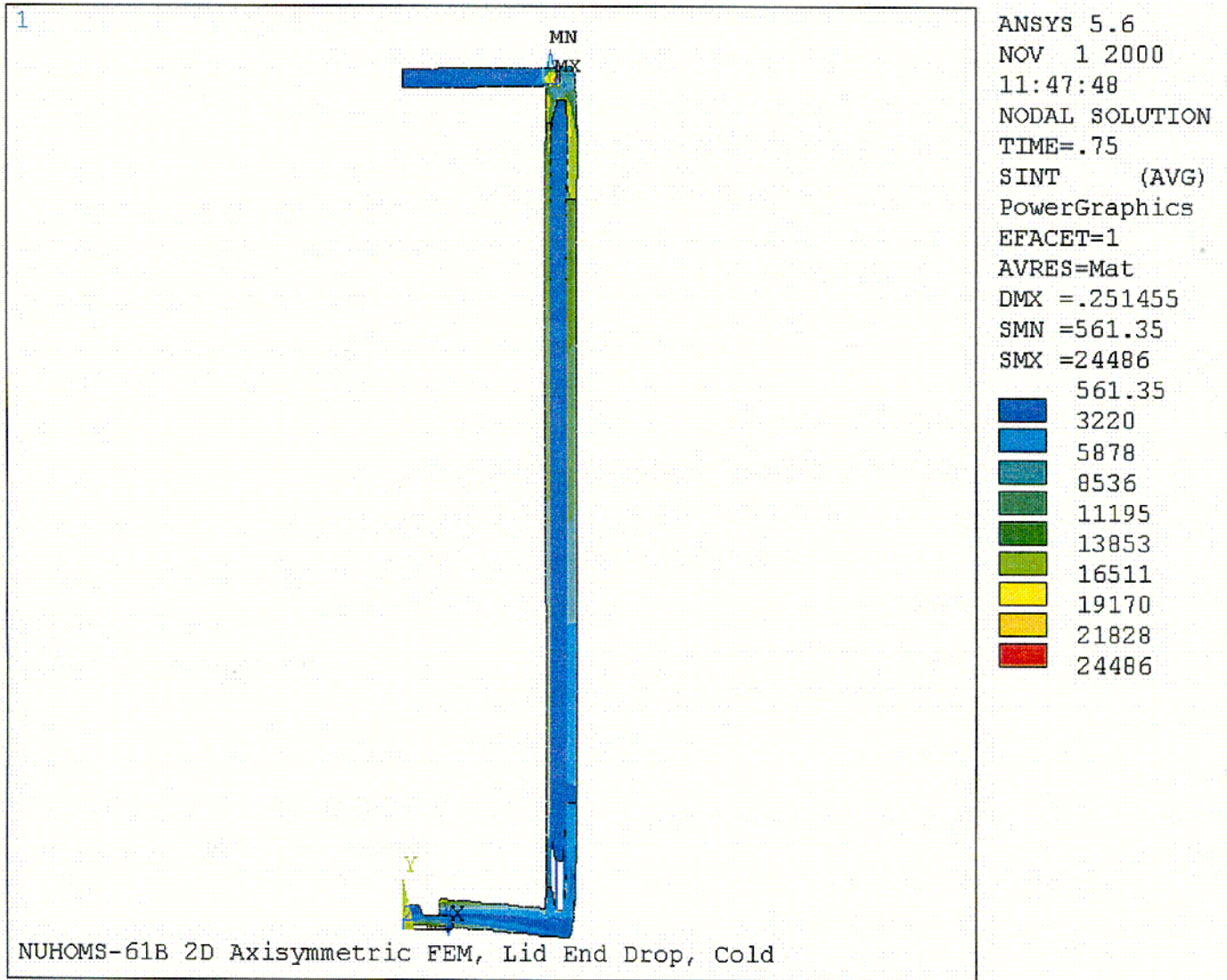
Figure 2.10.5-3
Stress Intensity – Lid End Drop, Hot Environment



ANSYS 5.6
NOV 1 2000
11:36:49
NODAL SOLUTION
TIME=.75
SINT (AVG)
PowerGraphics
EFACET=1
AVRES=Mat
DMX =.231137
SMN =292.792
SMX =24021
292.792
2929
5566
8202
10839
13475
16112
18748
21384
24021

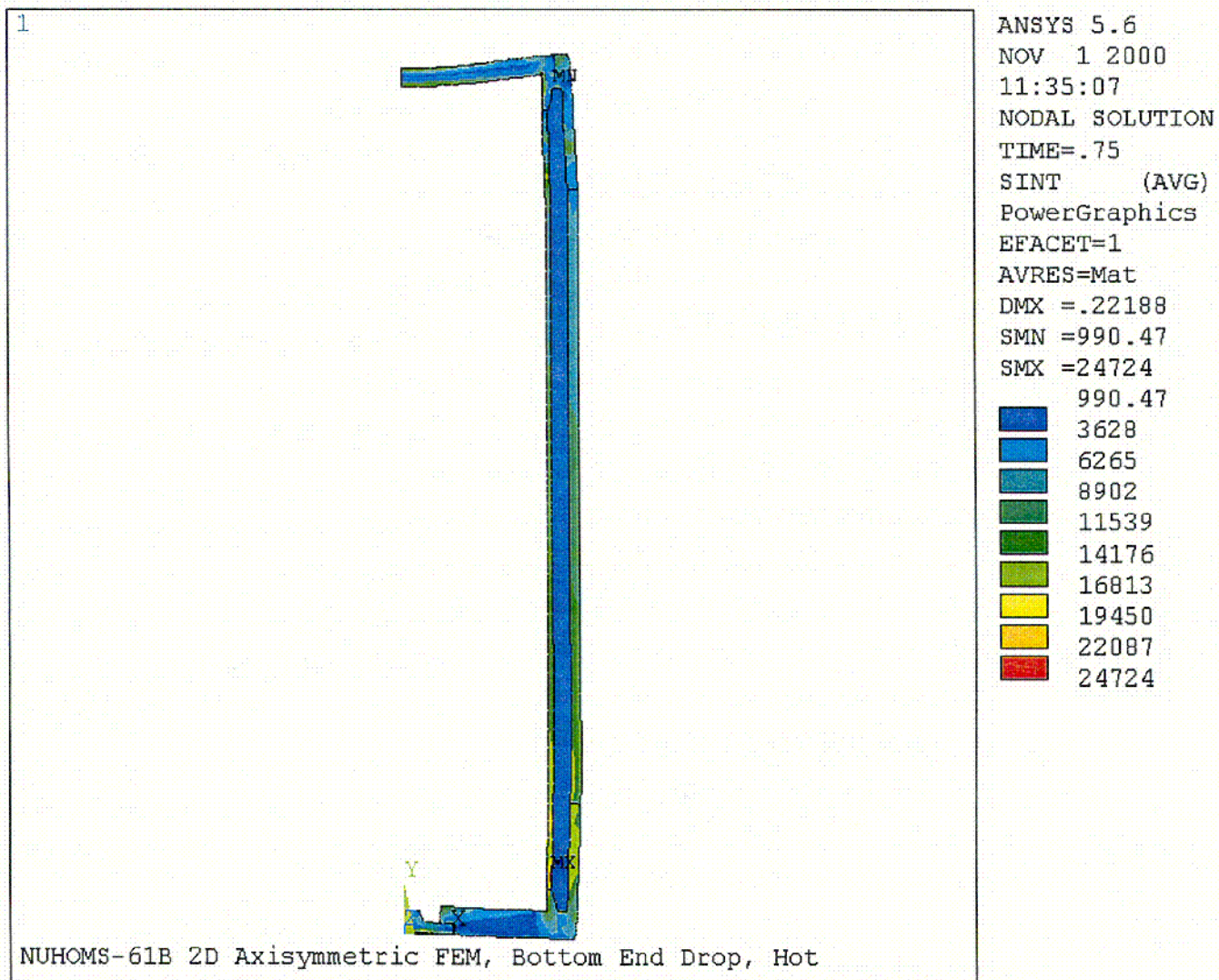
CO9

Figure 2.10.5-4
Stress Intensity – Lid End Drop, Cold Environment



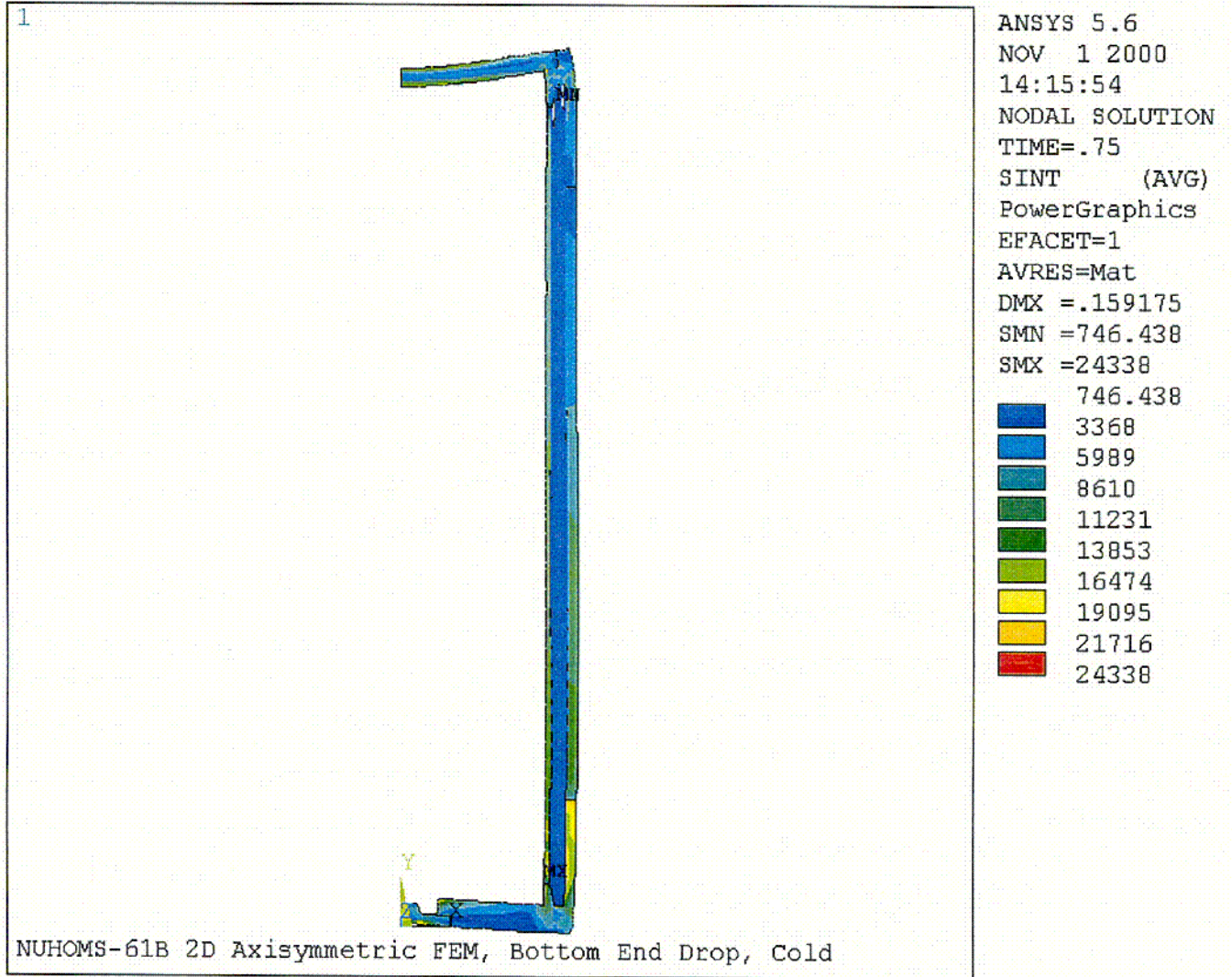
C10

Figure 2.10.5-5
Stress Intensity – Bottom End Drop, Hot Environment



CU

Figure 2.10.5-6
Stress Intensity – Bottom End Drop, Cold Environment



C12

Rev. 0 4/01

Figure 2.10.5-7
Collapse Load Determination – Lid End Drop, Hot Environment

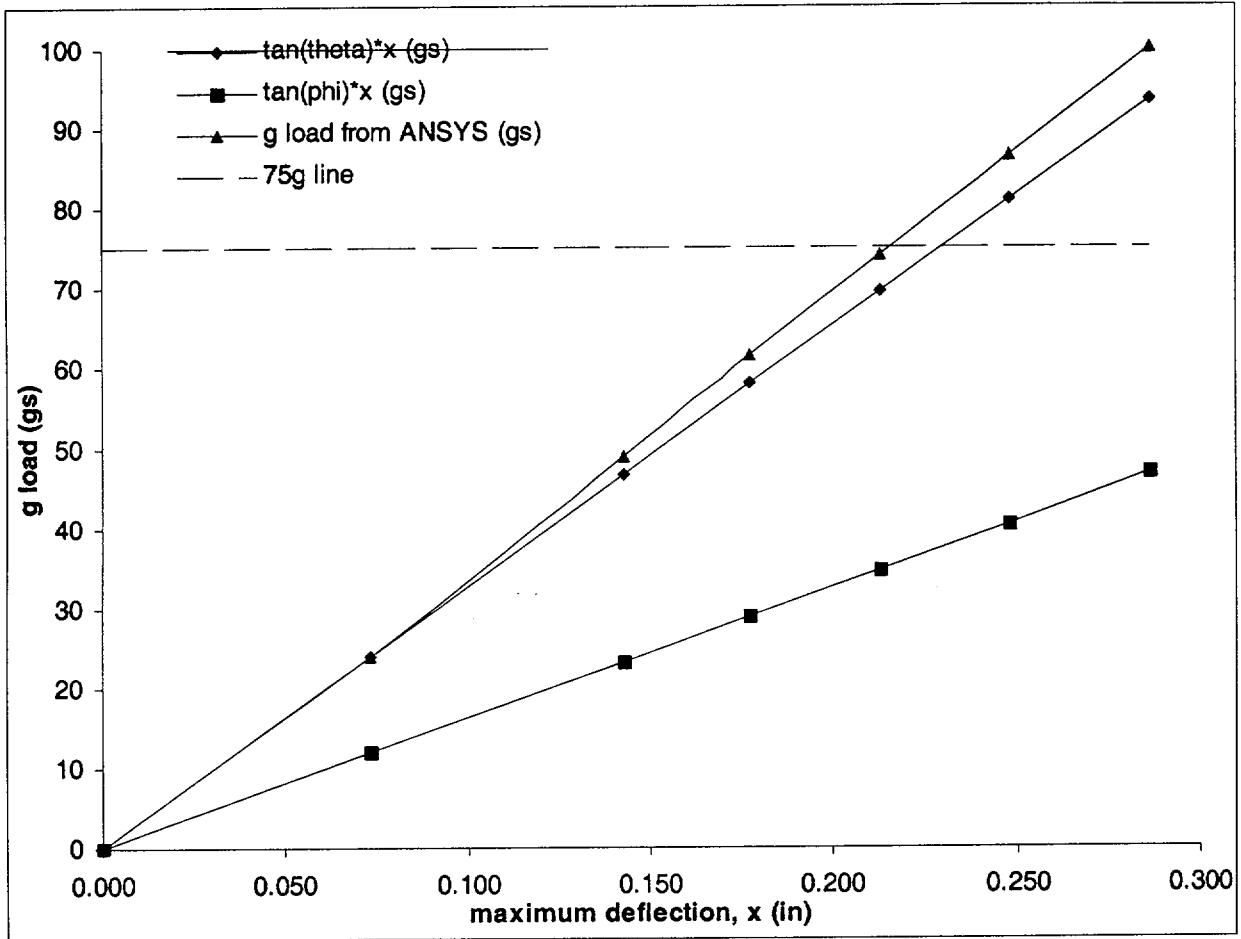


Figure 2.10.5-8
Collapse Load Determination – Lid End Drop, Cold Environment

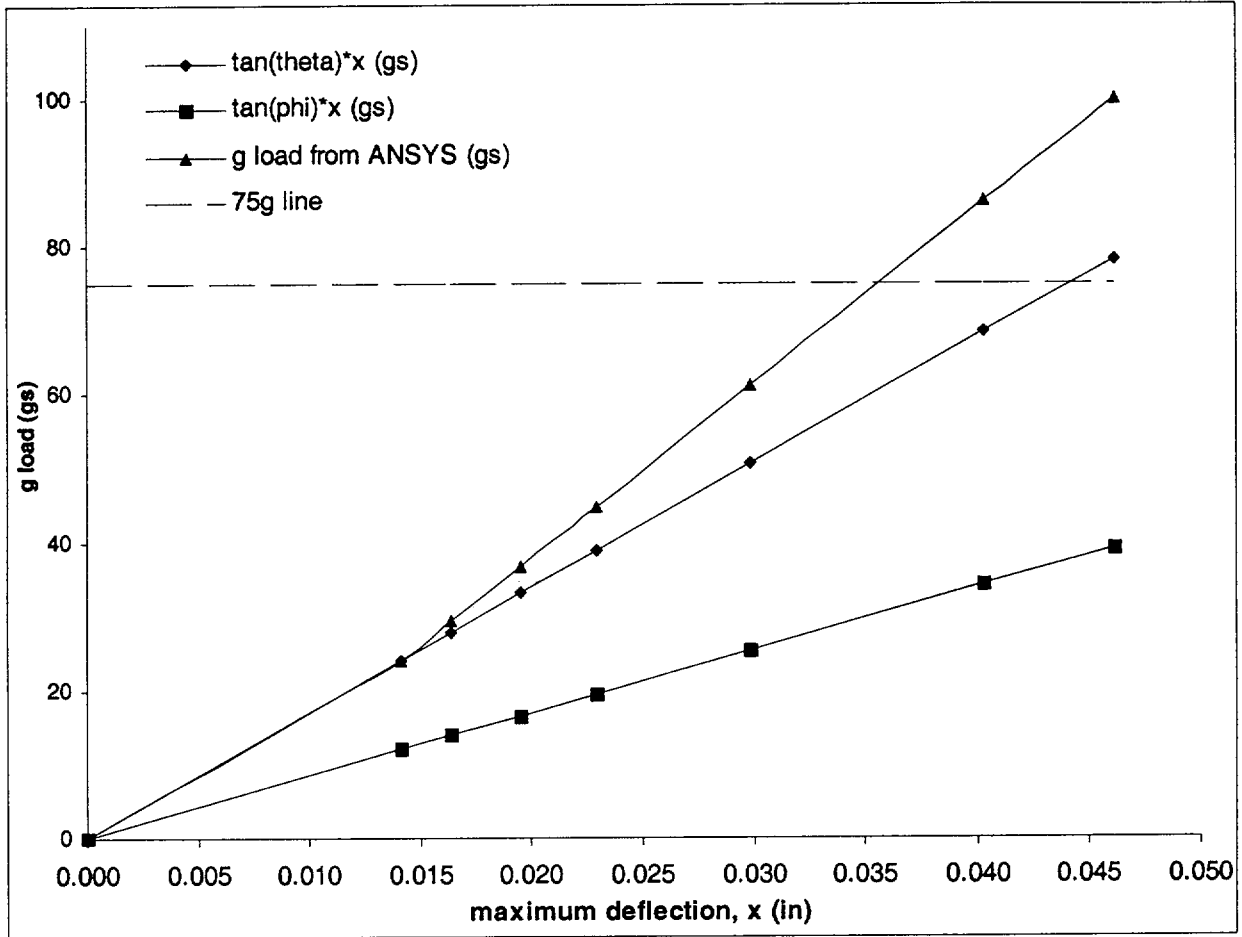


Figure 2.10.5-9
Collapse Load Determination – Bottom End Drop, Hot Environment

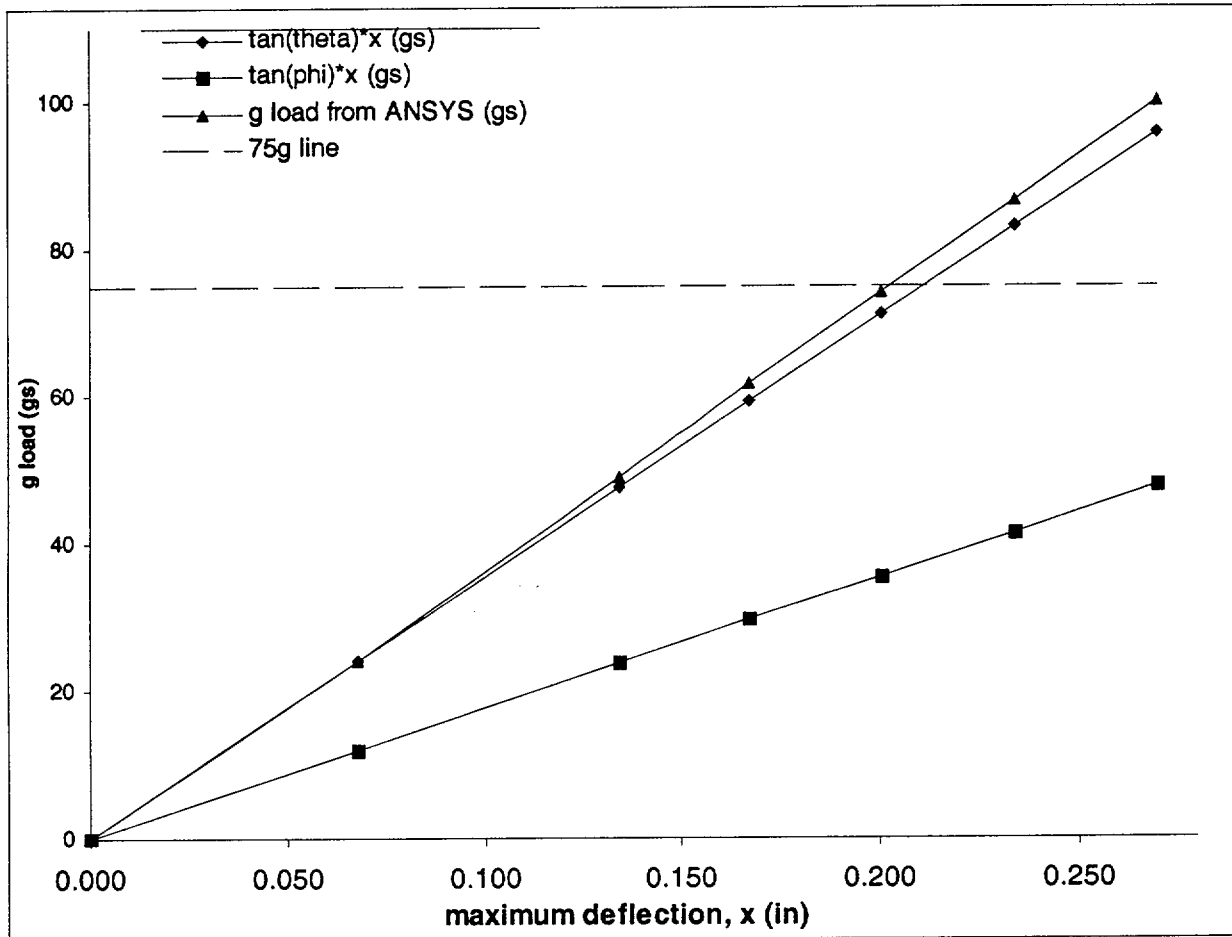
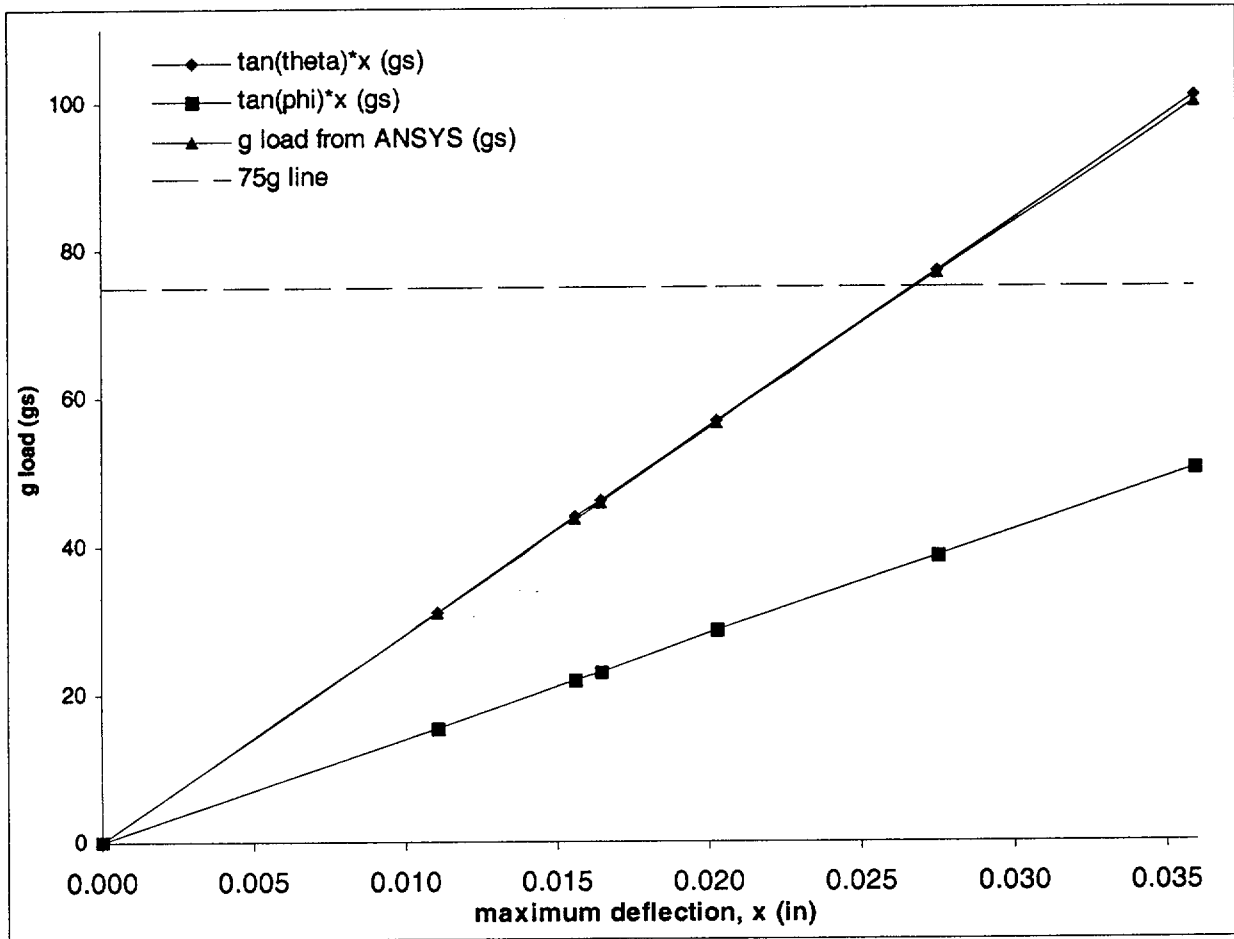


Figure 2.10.5-10
Collapse Load Determination – Bottom End Drop, Cold Environment



APPENDIX 2.10.6

TABLE OF CONTENTS

	<u>Page</u>
2.10.6 DYNAMIC AMPLIFICATION FACTOR DETERMINATION.....	2.10.6-1
2.10.6.1 Introduction	2.10.6-1
2.10.6.2 Analysis for End Drop.....	2.10.6-2
2.10.6.3 Analysis for Side Drop.....	2.10.6-4
2.10.6.4 Conclusions	2.10.6-8
2.10.6.5 References	2.10.6-9

LIST OF FIGURES

- 2.10.6-1 Dynamic Load Factor for Half Sine Wave
- 2.10.6-2 Basket Finite Element Model for Modal Analysis

APPENDIX 2.10.6

DYNAMIC AMPLIFICATION FACTOR DETERMINATION

2.10.6.1 Introduction

The purpose of the analysis presented in this appendix is to determine the dynamic amplification factor (DAF) for the NUHOMS[®]-MP197 package internals. The DAF accounts for the rigid body acceleration difference between the NUHOMS[®]-MP197 cask & NUHOMS[®]-61BT Canister and Basket during the cask drop events.

The dynamic amplification factor is taken from the results shown in Figure 2.10.6-1, which is a reproduction of figure 2.15 of NUREG/CR-3966 [1], and is a function of the ratio of the half-sine-wave impulse duration to the natural period of the structure. The dynamic amplification factor based on a half sine wave impulse is conservative relative to that of a triangular pulse.

The two components of the NUHOMS[®]-MP197 package internals with the longest and most significant natural periods are the Fuel Basket (with fuel assemblies) and the Canister. Each component is modeled separately. The Dynamic Amplification Factor used for the entire structure is conservatively taken to be the higher of the two individual dynamic amplification factors computed.

Two load cases will be evaluated in this analysis, one due to longitudinal loading, and one due to transverse loading. During an end drop, the fundamental natural periods of the NUHOMS[®]-61BT DSC components are taken to be that of simply supported cylindrical shells without axial constraint, under longitudinal vibration. The masses of the basket components and fuel assemblies are conservatively lumped together, so that an average density is used. During a side drop, the fundamental natural period of the NUHOMS[®]-61BT canister shell is taken to be that of a cylinder in an ovaling mode and a simply supported cylindrical shell without axial constraint.

Notation

The notation used in this analysis are taken from Blevins [2], and are as follows.

- E , Modulus of Elasticity, (psi).
- f_1, f_{11} , Fundamental natural frequency, (Hz.).
- I , Moment of inertia of the beam, (in.⁴).
- L , Length of beam or cylindrical shell, (in.).
- m , Mass per unit length of the beam, (lbm.in.⁻¹).
- μ , Mass density, (lbm.in.⁻³).
- ν , Poisson's ratio.
- R , Outer radius of the cylindrical shell, (in.).

2.10.6.2 Analysis for End Drop

The fundamental natural frequency of a simply supported cylindrical shell under axial vibration simplifies to that of a uniform beam, free axially at both ends. The fundamental natural frequency of a uniform beam free at both ends, under longitudinal vibration is as follows. ([2], p. 183, Table 8-16, frame 1)

$$f_1 = \frac{\lambda_1}{2\pi L} \left(\frac{E}{\mu} \right)^{1/2}$$

Where $\lambda_1 = \pi$.

2.10.6.2.1 Basket with Fuel Assemblies

The maximum normal conditions of transport fuel basket temperature is 578° F (Chapter 3). However, the basket material properties are taken at the average temperature of the basket, which is roughly 500° F. The modulus of elasticity is taken to be that of SA-240 Type 304 stainless steel at 500° F, or 25.8×10^6 psi. [3], since the stainless steel tubes and plates comprise the majority of the basket structure. The length of the basket is 164.00 inches.

Based on a stainless steel density of $0.29 \text{ lb. in.}^{-3}$ and an aluminum density of 0.1 lb. in.^{-3} and the following component weights (Section 2.2), the average mass density, μ , is calculated in the following way.

Steel Components	Weights (lb.)
61 fuel compartment tubes	9,402
4 Outer 2 × 2 boxes	1,038
5 Outer 3 × 3 boxes	1,966
type 1 Support Rails	3,320
type 2 Support Rails	2,031
Hold Down Ring	940
Inserts	98
Total Weight	18,795

$$\text{Steel Volume} = 18,795 / 0.29 = 64,810 \text{ in}^3$$

Aluminum Components	Weights lb.
Aluminum Plates	859
Poison Plates	3,264
Total Weight	4,123

$$\text{Aluminum Volume} = 4,123 / 0.1 = 41,230 \text{ in}^3$$

$$\text{Average Weight Density} = 18,795 + 4,123 / (64,810 + 41,230) = 0.216 \text{ lb.in}^{-3}$$

$$\text{Average mass density, } \mu = \frac{0.216}{386.4} = 0.000559 \text{ lbm. in.}^{-3}$$

Therefore,

$$f_1 = \frac{\pi}{2\pi(164)} \left(\frac{25.8 \times 10^6}{0.000559} \right)^{1/2} = 655 \text{ Hz.}$$

The natural period of the fuel compartments is then $1/f_1$ or $T = 0.00153 \text{ s}$.

2.10.6.2.2 Canister Shell

The maximum normal conditions of transport canister temperature is 388° F (Chapter 3). However, the basket material properties are conservatively taken at 400° F. The canister shell is constructed from SA-240 Type 304, which has a modulus of elasticity of 26.5×10^6 psi. at 400° F [3]. The length of the canister is 195.92 inches.

The average mass density, μ , is calculated in the following way.

Weight of the entire Canister = 22,467 lb. (Section 2.2)

Volume of equivalent cylinder = $(\pi/4)(67.25^2 - 66.25^2)(195.92) = 20,542 \text{ in.}^3$

$$\text{Average mass density, } \mu = \frac{22,467}{(386.4)(20,542)} = 0.00283 \text{ lbm. in.}^{-3}$$

Therefore,

$$f_1 = \frac{\pi}{2\pi(195.92)} \left(\frac{26.5 \times 10^6}{0.00283} \right)^{1/2} = 247 \text{ Hz.}$$

The natural period of the container shell is then $1/f_1$ or $T = 0.004 \text{ s}$.

2.10.6.2.3 End Drop Dynamic Amplification Factor Determination

From the impact limiter analysis performed in Appendix 2.10.8, the duration of an end drop impact, t_1 , is in the range of 0.037 seconds to 0.047 seconds, depending on the impact limiter wood properties. The minimum value of impact duration, $t_1 = 0.037$ seconds is used in DAF evaluation which is conservative. Therefore the ratio t_1/T is $0.037/0.004$ or 9.25. Consequently, the DAF for the basket and canister for end drop event, based on figure 2.10.6-1, is conservatively taken to be 1.10.

2.10.6.3 Analysis for Side Drop

2.10.6.3.1 Basket with Fuel Assemblies

ANSYS Modal Analysis

A finite element modal analysis is performed in order to compute the natural frequency of the NUHOMS®-61BT basket when subjected to transverse loads. The ANSYS finite element model described in Appendix 2.10.2 is used to perform the analysis. However, the canister shell and gap elements are removed from the model and the boundary conditions are applied directly to the rails. The canister shell is removed from the model, because the coupling of shell nodes to rail nodes would result in a stiffer structure and higher natural frequencies, which is less conservative.

The material properties used are based on an average basket temperature of 500° F. Weight densities are changed to mass densities ($\rho_m = \rho_w / 386.4$). The weight of the fuel assemblies and poison plates is accounted for by increasing the density of the stainless steel basket plates.

The basket is supported radially at the periphery, over a 180° section. Since an ANSYS modal analysis requires a linear model, all gap elements are replaced by couplings in the appropriate direction. The basket finite element model, including boundary conditions and couplings, is shown on Figure 2.10.6-2.

Modal Analysis Results

The natural frequencies resulting from the first 4 harmonics, computed by ANSYS, are tabulated below.

Mode	Frequency (Hz.)
1	125.53
2	139.95
3	142.11
4	142.40

Analytical Verification of Results

As an order of magnitude check, the frequency of the fundamental mode of vibration for the basket is calculated below and compared to the frequency of the first mode computed by ANSYS. The deformed shape of the first basket mode can be simplified to that of a single basket plate acting as a simply support beam under a uniform load. Roark [5], page 369, case 6, provides an equation for the natural frequency of a simply support beam with uniform W .

$$f = \frac{3.55}{\sqrt{\frac{5WL^3}{384EI}}}$$

Where, W is the uniform load applied the beam, 4.299 lbs. [705 lb. per assembly / 164 in. per unit length of the basket], L is the span of the basket plate, 6.22 in., E is the modulus of elasticity of the beam, 25.8×10^6 psi., and I is the beam moment of inertia, 0.000288 in^4 . [$2 \times (1 \times 0.12^3 / 12)$]. Therefore,

$$f = \frac{3.55}{\sqrt{\frac{5(4.299)(6.22)^3}{384(25.8 \times 10^6)(0.000864)}}} = 84 \text{ Hz.}$$

This value is somewhat lower than the value computed by ANSYS for the basket. The actual support conditions for the basket plate are somewhere in between simple-simple and fixed-fixed. A fixed-fixed beam's fundamental frequency is approximately double ($\sqrt{5} \times 84 = 188 \text{ Hz.}$) that of a simple-simple supported beam. The ANSYS solution of 126 Hz. is somewhere between the solutions to the simple-simple and fixed-fixed analytical equations.

Conclusions

The finite element modal analysis reveals that the fundamental natural frequency of the NUHOMS[®]-61BT basket (with fuel) when subjected to a side drop acceleration $f_1 = 125.5 \text{ Hz.}$ The natural period of the basket is then $1/f_1$ or $T = 0.00797 \text{ s.}$

2.10.6.3.2 Canister Shell

Two natural frequencies, each associated with a distinct mode of vibration, are evaluated for the canister. These two modes are the canister shell ovaling and bending modes

Canister Shell Ovaling Mode

The fundamental natural frequency of the canister shell ovaling (Radial-Axial) mode is determined assuming the cylindrical shell is simply supported without axial constraint. The natural frequency of the cylindrical shell ovaling mode is given by the following ([3], p. 305, Table 12-2, Frame 5).

$$f_{ij} = \frac{\lambda_{ij}}{2\pi R} \left(\frac{E}{\mu(1-\nu^2)} \right)^{1/2}$$

Where L is taken to be the length between the top and bottom shield plugs, which is roughly 180 in, $E = 26.5 \times 10^6$ psi. (for SA-240 Type 304 stainless steel at 400° F [3]), R is the average shell

radius, 33.375 in., ν is Poisson's ratio, which is 0.305 for stainless steel ([6], p. 5-6), and $\mu = 0.29/386.4 = 0.000751 \text{ lbm. in}^{-3}$.

$$\lambda_{ij} = \frac{\left\{ (1-\nu^2)(j\pi R/L)^4 + (h^2/12R^2) \left[i^2 + (j\pi R/L)^2 \right]^4 \right\}^{1/2}}{(j\pi R/L)^2 + i^2}$$

For the fundamental mode, $i = 2$ and $j = 1$.

$$\lambda_{ij} = \frac{\left\{ (1-0.305^2)(\pi \times 33.375/180)^4 + (0.5^2/12 \times 33.375^2) \left[2^2 + (\pi \times 33.375/180)^2 \right]^4 \right\}^{1/2}}{(\pi \times 33.375/180)^2 + 2^2} = 0.07679$$

$$f_{21} = \frac{0.07679}{2\pi \times 33.375} \left(\frac{26.5 \times 10^6}{0.000751(1-0.305^2)} \right)^{1/2} = 72.2 \text{ Hz}$$

The natural period of the canister is then $1/f_{21}$ or $T = 0.0138 \text{ s}$.

Canister Beam Bending Mode

The bending mode of the canister shell is taken to be most significant vibration mode of during a side drop event. The fundamental natural frequency of the bending mode of the canister is taken to be that of a simply supported cylindrical shell without axial constraint. This natural frequency is computed with and without the basket and fuel weights included.

Canister Beam without basket weight:

Since $L/(jR) = 180/(1 \times 33.375) = 5.39 < 8.00$, simple beam theory applies [2]. The fundamental natural frequency of the bending mode of a uniform beam pinned at both ends is as follows ([2], p. 108, Table 8-1, Frame 5).

$$f_1 = \frac{\lambda_1^2}{2\pi L^2} \left(\frac{EI}{m} \right)^{1/2}$$

Where, $E = 26.5 \times 10^6 \text{ psi.}$, $\lambda_1 = \pi$, and

$$I = \frac{\pi}{64} (d_o^4 - d_i^4) = \frac{\pi}{64} [67.25^4 - 66.25^4] = 58,399 \text{ in.}^4$$

The mass, m , of the canister is $0.323 \text{ lbm. in}^{-1}$ ($22,467 \text{ lb.} / 180 \text{ in.} / 386.4 \text{ in.s}^{-2}$, Section 2.2). Therefore,

$$f_1 = \frac{\pi^2}{2\pi \times 180^2} \left(\frac{26.5 \times 10^6 \times 58,399}{0.323} \right)^{1/2} = 106.1 \text{ Hz}$$

The natural period of the canister is then $1/f_1$ or $T = 0.0094$ s.

Canister Beam with basket weight:

Since the basket structure is stiffer ($f = 125.5$ Hz) than the canister ($f = 106.1$ Hz), during a side drop, the basket will, deflect less than the canister. This will result in a two-point contact between the basket and canister (at the basket ends). As a result, one-half of the weight of the basket and fuel will act at each contact point. One contact point is close to the end of the canister and will have no effect on the canister's behavior. The second point will be at a location roughly 16 inches from the top end of the canister. The fundamental natural frequency of the bending mode of a beam pinned at both ends and with an off-center mass is as follows ([2], p. 159, Table 8-8, Frame 5).

$$f_1 = \frac{1}{2\pi} \left\{ \frac{3EI(a+b)}{a^2b^2[M + (\alpha + \beta)M_b]} \right\}^{1/2}$$

where,

$$\alpha = \frac{a}{a+b} \left[\frac{(2b+a)^2}{12b^2} + \frac{a^2}{28b^2} - \frac{a(2b+a)}{10b^2} \right],$$

$$\beta = \frac{b}{a+b} \left[\frac{(2a+b)^2}{12a^2} + \frac{b^2}{28a^2} - \frac{b(2a+b)}{10a^2} \right],$$

and a and b are 16.0 inches and 164.0 inches respectively. The mass of the canister, M_b , is $22,467 \text{ lb.} / 386.4 \text{ in. s.}^{-1} = 58.14 \text{ lbm.}$, and the mass of $1/2$ of the basket and fuel, M , is $1/2(22,918 \text{ lb.} + 43,005 \text{ lb.}) / 386.4 \text{ in. s.}^{-1} = 85.30 \text{ lbm.}$

$$\alpha = \frac{16}{16+164} \left[\frac{(2 \times 164 + 16)^2}{12(164)^2} + \frac{16^2}{28(164)^2} - \frac{16(2 \times 164 + 16)}{10(164)^2} \right] = 0.0308$$

$$\beta = \frac{164}{16+164} \left[\frac{(2 \times 16 + 164)^2}{12(16)^2} + \frac{164^2}{28(16)^2} - \frac{164(2 \times 16 + 164)}{10(16)^2} \right] = 3.3721$$

$$f_1 = \frac{1}{2\pi} \left(\frac{3 \times 26.5 \times 10^6 \times 58,399(16+164)}{16^2 \times 164^2 [85.30 + (0.0308 + 3.3721)58.14]} \right)^{1/2} = 104.2 \text{ Hz}$$

The natural period of the canister is then $1/f_1$ or $T = 0.0096$ s.

2.10.6.3.3 Side Drop Dynamic Load Factor Determination

From the impact limiter analysis performed in Appendix 2.10.8, the duration of impact during a side drop, t_1 , is in the range of 0.032 seconds to 0.038 seconds, depending on the impact limiter wood properties. It is conservative to take t_1 to be 0.032 seconds. The ovalling mode of the canister shell is the vibration mode with the highest natural period (0.0138 s.). Therefore the minimum ratio t_1/T is 0.032/0.0138, or 2.32. Consequently, the DAF for canister during a side drop event, based on figure 2.10.6-1, is conservatively taken to be 1.10.

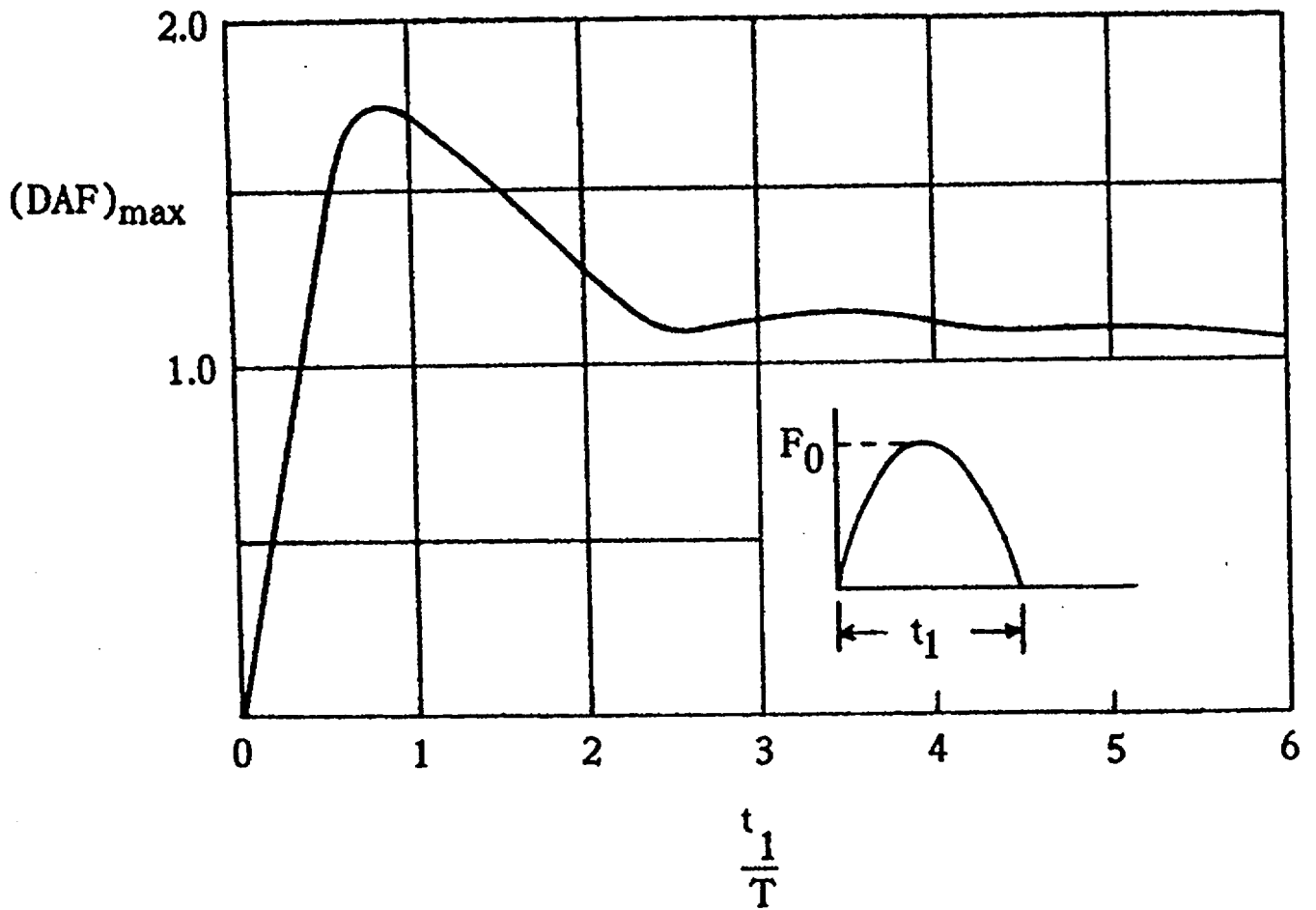
2.10.6.4 Conclusions

Conservatively taking the maximum dynamic amplification factor computed for each component under both longitudinal and transverse vibration, the overall dynamic amplification factor for the NUHOMS[®]-MP197 package internals is taken to be 1.10.

2.10.6.5 References

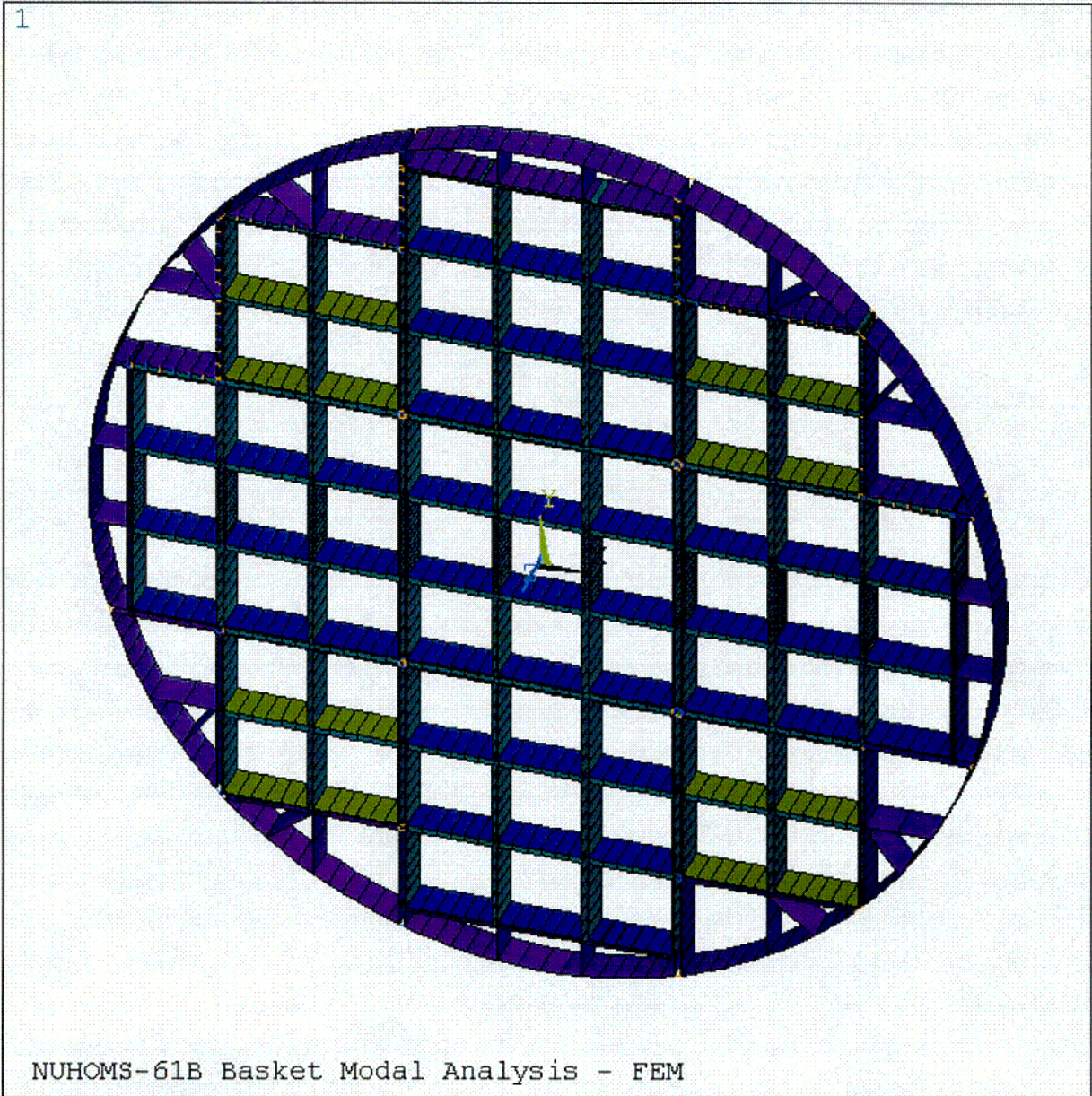
1. *Methods for Impact Analysis of Shipping Containers*, NUREG/CR-3966, UCID-20639, LLNL, 1987.
2. Blevins, *Formulas for Natural Frequency and Mode Shape*, Krieger Publishing Company, 1995.
3. American Society of Mechanical Engineers, ASME Boiler and Pressure Vessel Code, Section II, Part D, 1998, including 1999 Addendum.
4. ANSYS User's Manual, Rev 5.6.
5. Roark, Raymond J., *Formulas for Stress and Strain*, Fourth Edition, McGraw-Hill Book Company.
6. Baumeister, T., Marks, L. S., *Standard Handbook for Mechanical Engineers*, 7th Edition, McGraw-Hill, 1967.

FIGURE 2.10.6-1
DYNAMIC LOAD FACTOR FOR HALF SINE WAVE



(T = Natural period of structure)

FIGURE 2.10.6-2
BASKET FINITE ELEMENT MODEL FOR MODAL ANALYSIS



C13

APPENDIX 2.10.7

TABLE OF CONTENTS

	<u>Page</u>
2.10.7 EVALUATION OF FUEL ASSEMBLY UNDER ACCIDENT IMPACTS	2.10.7-1
2.10.7.1 Introduction	2.10.7-1
2.10.7.2 Material Properties	2.10.7-1
2.10.7.3 30 Foot Side Drop	2.10.7-2
2.10.7.4 Bottom End Drop	2.10.7-2
2.10.7.5 Brittle Fracture Evaluation	2.10.7-3
2.10.7.6 References	2.10.7-5

LIST OF TABLES

2.10.7-1	Tipover / Side Drop Impact Stress Calculations
2.10.7-2	Fuel Rod Buckling Loads for End drop Impact

LIST OF FIGURES

2.10.7-1	Tube and Fuel Finite Element Model - Buckling Analysis
2.10.7-2	Allowable Buckling Load for G9 8 × 8 Fuel Assembly

APPENDIX 2.10.7

EVALUATION OF FUEL ASSEMBLY UNDER ACCIDENT IMPACTS

2.10.7.1 Introduction

This appendix evaluates the effect of NUHOMS[®]-MP197 cask impact (30 foot side drop or end drop) on the integrity of fuel rod cladding. The material properties of irradiated zircalloy cladding and the rod impact stress analysis approach are based on LLNL Report UCID-21246 [1]. The fracture analysis of the fuel rod cladding is based on the ASME Code, Section XI [2]. The irradiated zircalloy fracture toughness data is obtained from ASTM Special Technical Publication 551 [3]. Presented below are the analyses and results that are used to conclude that the fuel rod cladding will remain intact and retain the fuel pellets during all accident scenarios.

2.10.7.2 Material Properties

This section establishes the basis for assuming particular material properties. The values of some of the parameters used in the analysis are temperature dependent. The maximum temperature during the normal conditions of transport will not exceed 598° F. However, material properties are conservatively taken at 638° F, with the expectation that the ability of the zircalloy to absorb impact loads, without rupture, will increase as the temperature decreases with time.

Weight Density

The weight density of both Zircalloy-2 and Zircalloy-4 is very close to the weight density of Zirconium itself. From Reference 1,

$$\rho_{tube} = 0.234 \text{ lb/in}^3$$

Young's Modulus

The Young's modulus for typical Zircalloy cladding is illustrated in Table 5 of Reference 1. Thus, at 638° F,

$$E_{tube} = 11.0 \times 10^6 \text{ psi}$$

$$E_{fuel} = 13.7 \times 10^6 \text{ psi (conservatively assume a lower value)}$$

Yield Strength

The yield strength for typical Zircalloy cladding is illustrated in Table 5 of Reference 1. Thus, at 638° F,

$$S_{yield-tube} = 83,710 \text{ psi}$$

2.10.7.3 30 Foot Side Drop

The fuel rod side impact stresses are computed by idealizing fuel rods as continuous beams supported at each spacer grid. Continuous beam theory is used to determine the maximum bending moments and corresponding stresses in the cladding tube. The methodology used in performing the analysis is based on work done at Lawrence Livermore National Labs [1]. The fuel gas internal pressure is assumed to be present and the resulting axial tensile stress is added to the bending tensile stress due to 75g load (Appendix 2.10.8). The stresses for different General Electric fuel assemblies are computed in Table 2.10.7-1. It is seen that the 35,393 psi is the highest stress and occurs in the GE9-8x8 fuel assembly. This stress is lower than the yield strength of zircalloy (83,710 psi). It is, therefore, concluded that the fuel tube will not fail and will withstand the side drop load without excessive plastic deformations. The grid supports (spacers) are expected to crush before the 75g load is developed and the actual tube stresses will be much lower than the above noted stress.

2.10.7.4 Bottom End Drop

In case of an end drop, the inertial forces load the rod as a column having intermediate supports at each grid support (spacer). The tube load limit is that at which the fuel rod segments between the supports become unstable.

An elastic-plastic stress analysis was performed using the ANSYS Finite Element Program [4]. A three-dimensional finite element model of the active fuel tube length was constructed using plastic PIPE20 element for cladding tube and elastic PIPE16 element for fuel. The hinge supports were modeled at each support location. The finite element model and support conditions for a typical tube model are shown in Figure 2.10.7-1. The tube and fuel nodes were coupled in x, y and z directions. The following material properties (at 638° F) were input as a bilinear kinematic stress-strain curve for Zircalloy cladding tube. These properties are taken from Reference 1.

Yield Strength = 83,710 psi

Ultimate Strength = 94,000 psi

Modulus of elasticity = 11.0×10^6 psi

Elongation = 1.75%

Max. elastic strain = $83,710 / 11.0 \times 10^6 = 0.0076$ in/in

Tangent Modulus = $(94,000 - 83,710) / (.0175 - .0076) = 1.04 \times 10^6$ psi

For fuel elements, a modulus of elasticity = 13.7×10^6 psi is conservatively used for analysis. The tube and fuel densities were modified to compensate for the extra tube length and the components which were not modeled. The calculations of equivalent tube and fuel densities are shown in Table 2.10.7-2.

In order to calculate the tube-buckling load, the large displacement option of ANSYS was used. The maximum inertia force of 200g was applied to the model. This load was applied gradually in a number of sub-steps. A small lateral load (0.001 lb.) was applied at the middle of the lowest segment to introduce an initial deflection and bending. The analysis stopped at the load sub-step

where the tube model became unstable and did not converge. In each case, the lowest segment became unstable as it was supporting the entire tube and fuel weights. The last converged load sub-step was taken as the plastic instability load.

The above analysis was repeated for one fuel rod of each fuel subassembly. All the input data and the resulting plastic instability loads are summarized in Table 2.10.7-2. It is seen from the above table, that GE9 8×8 fuel assembly drop is the critical as it results in the lowest plastic instability load of 128g. The allowable collapse load is calculated by using paragraph F-1340 of Reference 5.

As per paragraph F-1340 [5], the acceptability of a component may be demonstrated by collapse load analysis. The allowable collapse load shall not exceed 100% of plastic analysis collapse load ([5], F-1341.3). The plastic analysis collapse load is defined as that determined by plastic analysis according to the criteria given in Appendix II-1430 ([5], F-1321.6(c)).

Using the methodology described in Appendix II-1430 ([5], F-1321.6(c)) (see Figure 2.10.7-2), the allowable collapse loads has been determined for GE9 8×8 fuel assembly drop which is 128g. The allowable collapse loads for other fuel assemblies will be equal or higher than this load.

Since the internal pressure produces tensile stresses in the cladding, it will reduce the compressive stresses caused by the end drop impact. The pressure is therefore conservatively neglected in this analysis.

From the results in Table 2.10.7-2, it is seen that the lowest allowable tube-buckling load of 128g occurs for the fuel assemblies. It may be noted that the axial stresses in fuel rods are also quite small ($128 \times 6.11 / (\pi/4)(0.400)^2 = 6,224$ psi). The actual end drop impact load is less than 75g. It is, therefore, concluded that the fuel cladding tubes will not be damaged during an end drop.

2.10.7.5 Brittle Fracture Evaluation

The stress intensity factor K_1 is calculated from tube maximum stresses under pressure and impact loads. A conservative flaw configuration is assumed in the cladding tube. Stress intensity factor for the flaw model is calculated, using the methodology given in Section XI, Article A-3000 [2]. The calculated Stress intensity factor for the flaw size should satisfy the code faulted condition criteria (Section XI, para. IWB-3612 [2]):

$$K_1 < \frac{K_{1c}}{\sqrt{2}}$$

Where, K_1 is the maximum applied stress intensity factor for the flaw size in faulted condition, and K_{1c} is critical fracture toughness based on fracture initiation for the corresponding crack tip temperature.

The stress intensity factor K_1 is calculated using the following equation (Section XI, A-3300 [2]):

$$K_1 = S_m M_m \sqrt{\frac{\pi a}{Q}} + S_b M_b \sqrt{\frac{\pi a}{Q}}$$

Where, S_m and S_b are the membrane and bending stresses respectively, a is the flaw depth for a surface flaw, Q is the flaw shape parameter ([2], Fig. A-3300-1), M_m is the correction factor for membrane stress ([2], Fig. A-3300-3), and M_b is the correction factor for bending stress ([2], Fig. A-3300-5).

It is seen from Table 2.10.7-1, that the combined tensile stress of 35,393 psi, in the GE9- 8x8 fuel assembly tube, is the highest. This tube is therefore selected for a fracture evaluation. It is conservatively assumed that all the stresses are membrane stresses.

Reference 6 gives a guideline of pinhole as "included cracks of maximum width about 100 μm (0.004") but whose length could be any where between 200 -300 μm (0.008" - 0.012") and several mm". For conservatism, the following flaw size is used in the fracture evaluation:

$$a = \text{crack depth} = 0.006 \text{ in.}$$

$$l = \text{crack length} = 4 \text{ mm} = 0.16 \text{ in.}$$

$$t = \text{tube thickness} = 0.030 \text{ in.}$$

$$a/t = 0.006/0.030 = 0.2$$

$$a/l = 0.006/0.16 = 0.0375$$

$$\text{Zircaloy yield strength, } S_y = 83,710 \text{ psi}$$

$$(S_m + S_b) / S_y = (35,393) / 83,710 = 0.42$$

$$\text{Flaw shape parameter, } Q \text{ ([2] Fig. A-3300-1) = 0.99}$$

$$\text{Membrane stress factor, } M_m, \text{ ([2] Fig. A-3300-3) = 1.25}$$

$$K_1 = (35,393)(1.25) \sqrt{\frac{\pi(0.006)}{0.99}} = 6,593 \text{ psi.in.}^{\frac{1}{2}} = 6.1 \text{ ksi.in.}^{\frac{1}{2}}$$

$$K_{ic} \text{ at } 200^\circ \text{ F} = 30.0 \text{ ksi.in.}^{\frac{1}{2}} \text{ ([7], Figure 3)}$$

$$\text{Allowable fracture toughness} = \frac{30}{\sqrt{2}} = 21.2 \text{ ksi.in.}^{\frac{1}{2}}$$

Based on the above evaluations, it is concluded that the fracture toughness of the irradiated zircalloy cladding is sufficiently high to preclude a brittle fracture failure during accident conditions. Therefore, the fuel cladding tube will remain intact and retain the fuel pellets during accident conditions.

2.10.7.6 References

1. LLNL Report UCID-21246, Dynamic Impact Effects on Spent Fuel Assemblies, 10/1987.
2. ASME Boiler and Pressure Vessel Code, Section XI, 1998, including 1999 Addendum.
3. ASTM Special Technical Publication 551, Variation of Zircalloy Fracture Toughness in Irradiation, Walker and Kass, 8/1973.
4. ANSYS Engineering Analysis System User's Manual, Rev. 5.6.
5. American Society of Mechanical Engineers, ASME Boiler and Pressure Vessel Code, Section III, along with Appendices, 1998 including 1999 Addendum.
6. EPRI TR-103949, "Temperature Limit Determination for the inert Dry Storage of Spent Nuclear Fuel".
7. ASTM STP 551, 1974, "Variation of Zircalloy Fracture Toughness in Radiation", Walker and Kass.

Table 2.10.7-1
Side Drop Impact Stress Calculations

Tube Arrays	7 × 7	8 × 8	8 × 8	8 × 8	8 × 8	9 × 9	10 × 10
GE Designation	GE2, GE3	GE4	GE5	GE8	G9, G10	GE11, GE13	G12
MTU/Fuel Assy.	0.1977	0.1880	0.1856	0.1825	0.1834	0.1766	0.1867
No. of fuel rods	49	63	62	60	60	74	92
Max. active fuel length (in)	144	146	150	150	150	146	150
Fuel rod OD ⁽⁵⁾ (in)	0.559	0.489	0.479	0.479	0.479	0.436	0.400
Clad thick. ⁽⁶⁾ (in)	0.030	0.032	0.030	0.030	0.030	0.026	0.024
Fuel rod ID (in)	0.499	0.425	0.419	0.419	0.419	0.384	0.352
S_y (psi)	83,710	83,710	83,710	83,710	83,710	83,710	83,710
No. of Spacers, n	7	7	7	7	7	8	8
$L = \text{length}/n-1$	24	24.3	25	25	25	20.9	21.4
Tube, E_1 (psi)	11.0×10^6						
Tube, I_1 (in ⁴)	.00175	.001205	.001071	.001071	.001071	.000707	.000503
Fuel, I_2 (in ⁴)	.003044	.001602	.001513	.001513	.001513	.001067	.000754
Tube Wt, W_1 ⁽¹⁾	1.85	1.70	1.55	1.55	1.55	1.22	1.04
Fuel Wt, W_2 ⁽²⁾	10.09	7.46	7.49	7.61	7.64	5.97	5.07
Total Weight (lb)	11.94	9.16	9.04	9.16	9.19	7.19	6.11
W , (lb/in)	.0829	.0627	.0603	.0611	.0613	.0492	.0407
$M = .1058wl^2, 7\text{supp}$ $M = .1056wl^2, 8\text{supp}$	5.053	3.920	3.987	4.038	4.053	2.269	1.970
S_b for $1g = MC/I$ (psi)	294.6	341.4	369.5	374.2	375.7	278.8	313.4
S_b for $75g$ (psi)	22,095	25,605	27,713	28,065	28,178	20,910	23,505
Pressure at 0° C, p_0	670	642	856	870	863	822	825
Pressure ⁽³⁾ at 337° C, p (psi)	1497	1435	1913	1944	1928	1837	1843
$S_{press.}$ (psi.) ⁽⁴⁾	6599	5121	7134	7273	7215	7241	7221
$S = S_b 75g + S_{press.}$ (psi)	28,694	30,726	34,847	35,338	35,393	28,151	30,726

Notes:

- (1) $W_1 = \text{Area} \times 0.234 \text{ lb/in}^3 \times 158'' \text{ length}$
- (2) $W_2 (\text{UO}_2) = [\text{MTU} \times 1000 (\text{kg/MTU}) \times 2.2046 (\text{lb/kg}) \times 270 (\text{M.W of UO}_2)/238 (\text{M.W of U})] / \text{No. of Tubes} = [2501 \times \text{MTU}] / \text{No. of Tubes}$
- (3) The max. rod temp. is 638° F, the max. rod pressure is 870 psia at 0° C. The pressure at 638° F (337° C) is $p = (337 + 273) / (0 + 273) \times p_0$
- (4) $S_{press.}$ axial stress = $p \times D_{avg} / 4t$
- (5) Includes 0.004 in. reduction in cladding OD to account for water side cladding corrosion [11].
- (6) Thickness is reduced by 0.002 in. to account for corrosion [11].

Table 2.10.7-2
Fuel Rod Buckling Loads for End drop Impact

Tube Arrays (No. of Tubes)	7 × 7 (49)	8 × 8 (63)	8 × 8 (62)	8 × 8 (60)	8 × 8 (60)	9 × 9 (74)	10 × 10 (92)
GE Designation	GE2, GE3	GE4	GE5	GE8	G9, G10	GE11, GE13	G12
Tube Length (in.)	158	158	158	158	158	158	158
Tube Active Length (in)	144	146	150	150	150	146	150
No. of Spacers	7	7	7	7	7	8	8
Length between spacers, L (in.)	24	24.3	25	25	25	20.9	21.4
Cladding tube OD (in)	0.559	0.489	0.479	0.479	0.479	0.436	0.400
Cladding tube thickness (in)	0.030	0.032	0.030	0.030	0.030	0.026	0.024
Cladding Tube ID (in)	0.499	0.425	0.419	0.419	0.419	0.384	0.352
Tube Area, A (in ²)	0.050	0.046	0.042	0.042	0.042	0.033	0.028
Fuel area, (in. ²)	0.196	0.142	0.138	0.138	0.138	0.116	0.097
Tube weight = Ax Density ⁽³⁾ × 158 (lb)	1.85	1.70	1.55	1.55	1.55	1.22	1.04
Fuel Weight (lb)	10.09	7.46	7.49	7.61	7.64	5.97	5.07
Tube + Fuel Weight, (lb)	11.94	9.16	9.04	9.16	9.19	7.19	6.11
Eqv. Density Tube ⁽¹⁾	0.257	0.253	0.246	0.246	0.246	0.253	0.247
Eqv. Density Fuel ⁽²⁾	0.357	0.360	0.362	0.368	0.369	0.352	0.347
ANSYS Plastic Instability Load (g)	176	146	131	128	128	151	128
Allowable Buckling g Load (Fig2.10.7-2)	*	*	*	*	128	*	*

* The allowable buckling g load for these assemblies will be higher or equal to 128g.

Notes:

- (1) Eqv. Density Tube = $(0.234 \times \text{Actual tube length}) / \text{Active tube length modeled}$
- (2) Eqv. Density Fuel = $\text{Fuel Weight} / (\text{Fuel area} \times \text{Active tube length modeled})$
- (3) Zircaloy Density = 0.234 lb/in.^3

Figure 2.10.7-1

Tube and Fuel Finite Element Model - Buckling Analysis

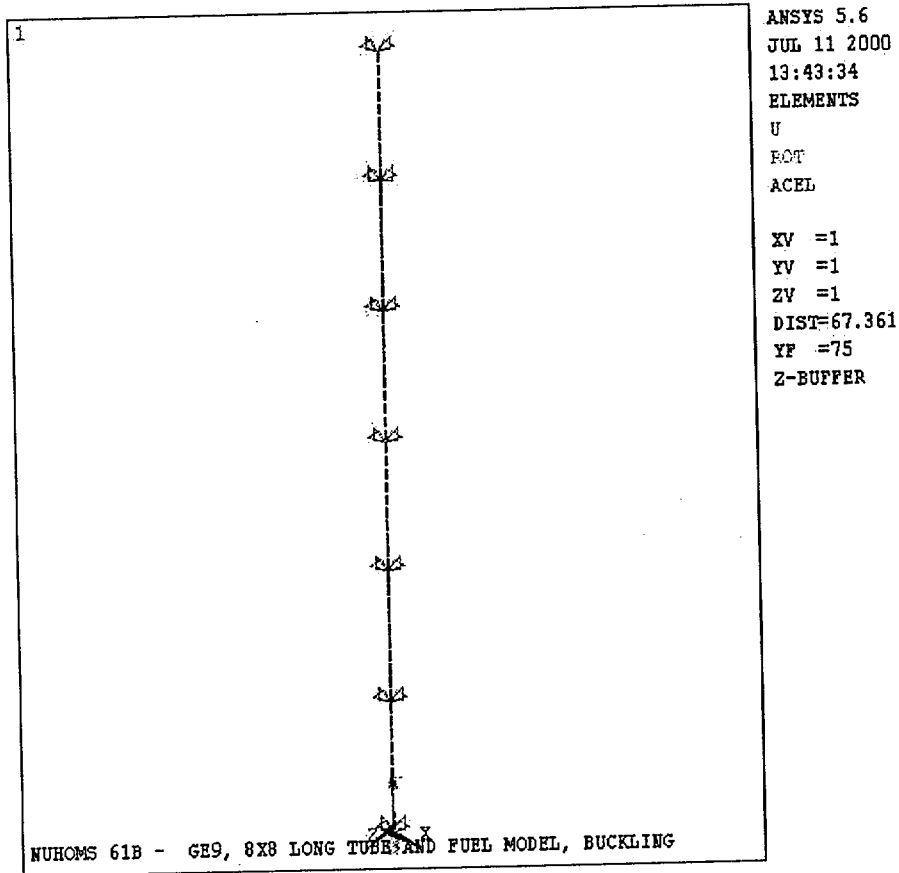
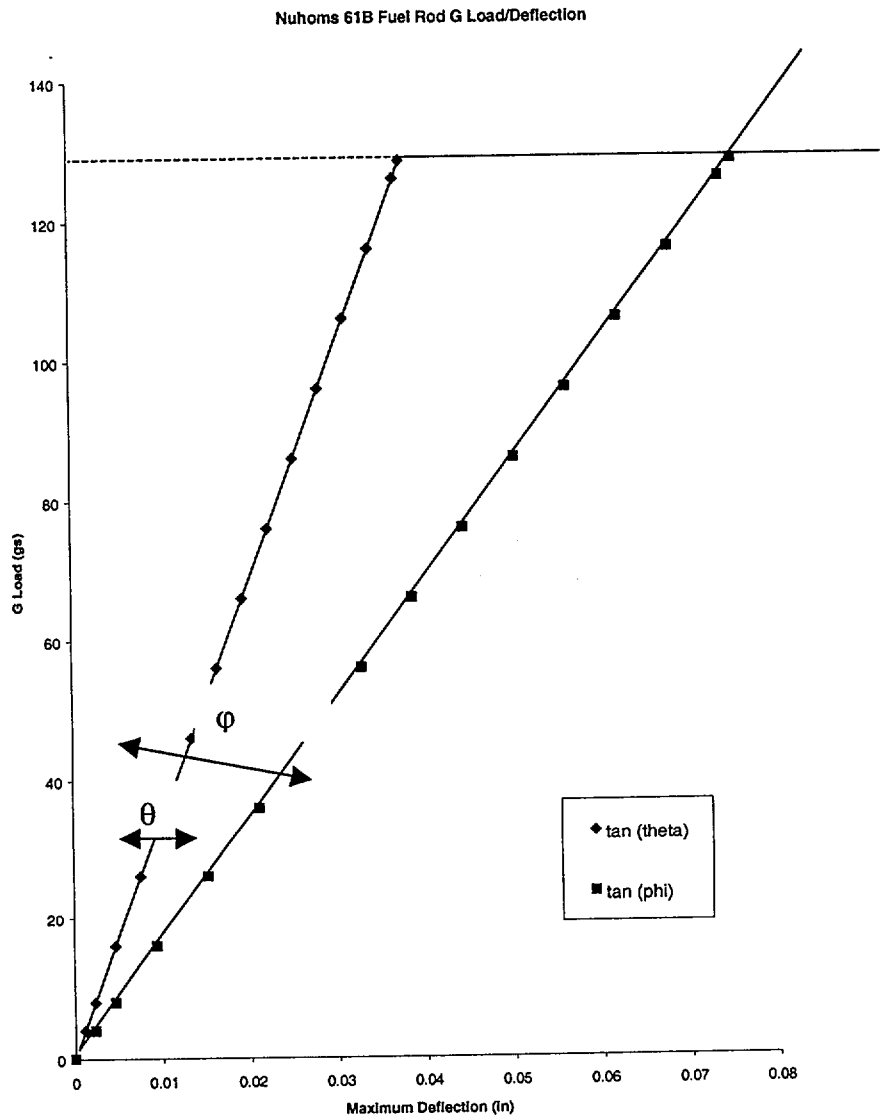


Figure 2.10.7-2

Allowable Buckling Load for G9 8 × 8 Fuel Assembly



APPENDIX 2.10.8

TABLE OF CONTENTS

	<u>Page</u>
2.10.8 STRUCTURAL EVALUATION OF THE NUHOMS®-MP197 PACKAGE IMPACT LIMITERS.....	2.10.8-1
2.10.8.1 Introduction.....	2.10.8-1
2.10.8.2 Design Description.....	2.10.8-2
2.10.8.3 Design Criteria.....	2.10.8-3
2.10.8.4 Analysis for 30 Foot Free Drop Accident Conditions.....	2.10.8-4
2.10.8.5 Analysis for One Foot Drop Normal Conditions.....	2.10.8-6
2.10.8.6 Impact Limiter Attachment Analysis.....	2.10.8-6
2.10.8.7 Summary of ADOC Results Used for Structural Analysis.....	2.10.8-13
2.10.8.8 Summary Description of ADOC Computer Code.....	2.10.8-14
2.10.8.9 References.....	2.10.8-25

LIST OF TABLES

2.10.8-1	Mechanical Properties of Wood and Adhesive
2.10.8-2	Typical Wood Material Properties
2.10.8-3	First Impact Maximum Inertia <i>g</i> Load versus Initial Angle of Impact for 30 Foot Drop using Maximum Wood Crush Stress Properties
2.10.8-4	Second Impact Maximum Inertia <i>g</i> Load versus Initial Angle of Impact for 30 Foot Drop using Maximum Wood Crush Stress Properties
2.10.8-5	First Impact Maximum Inertia <i>g</i> Load versus Initial Angle of Impact for 30 Foot Drop using Minimum Wood Crush Stress Properties
2.10.8-6	Second Impact Maximum Inertia <i>g</i> Load versus Initial Angle of Impact for 30 Foot Drop using Minimum Wood Crush Stress Properties
2.10.8-7	Depth of Crush versus Crush Force, 20° Impact Angle
2.10.8-8	Depth of Crush versus Crush Force, 20° Impact Angle
2.10.8-9	Depth of Crush versus Crush Force, 45° Impact Angle
2.10.8-10	Depth of Crush versus Crush Force, 60° Impact Angle
2.10.8-11	Depth of Crush versus Crush Force, 80° Impact Angle
2.10.8-12	Depth of Crush versus Crush Force, 90° Impact Angle
2.10.8-13	Maximum Inertial <i>g</i> Load During One Foot Drop
2.10.8-14	Loading Used in Cask Body and Cask Internals Analysis versus Maximum <i>g</i> Load Predicted by ADOC Program

LIST OF FIGURES

- 2.10.8-1 Impact Limiter Geometry
- 2.10.8-1A Sample Force/Deflection Curve for Balsa
- 2.10.8-1B Sample Force/Deflection Curve for Redwood
- 2.10.8-2 ADOC Computer Model for NUHOMS[®]-MP197 Transport Package
- 2.10.8-3 Geometry of Package
- 2.10.8-4 Package at Time, t
- 2.10.8-5 Geometry of Impact Limiter Parameters
- 2.10.8-6 Definition of Limiter Deformation
- 2.10.8-7 Crush Pattern in Impact Limiter
- 2.10.8-8 Impact Limiter Segments
- 2.10.8-9 Strain Computation for Crush Pattern I
- 2.10.8-10 Strain Computation for Crush Pattern II
- 2.10.8-11 Strain Computation for Crush Pattern III
- 2.10.8-12 Wood Stress-Strain Curve
- 2.10.8-13 Impact Limiter Free Body Diagram during 20° Slap Down

APPENDIX 2.10.8

STRUCTURAL EVALUATION OF THE NUHOMS[®]-MP197 PACKAGE IMPACT LIMITERS

2.10.8.1 Introduction

This appendix presents the details of the structural analysis of the NUHOMS[®]-MP197 impact limiters. The impact limiters are designed to absorb the kinetic energy resulting from the one (1) foot and thirty (30) foot normal conditions of transport and hypothetical accident conditions free drop events specified by 10 CFR 71. Redwood and balsa wood are used as the primary energy absorption material(s) in the impact limiters. A sketch of the impact limiter is shown in Figure 2.10.8-1. A functional description of the impact limiters is given in Section 2.10.8.2. The impact limiter design criteria are described in Section 2.10.8.3.

A computer model of the NUHOMS[®]-MP197 Transport Packaging was developed to perform system dynamic analyses during impacts of 30 foot accident and 1 foot normal condition drops. The model was developed for use with the ADOC (Acceleration Due To Drop On Covers) computer code described in detail in Section 2.10.8.8 which determines the deformation of the impact limiters, the forces on the packaging and the packaging deceleration due to impact on an unyielding surface. Numerous cases were run to determine the effects of the wood properties and the initial drop angle. A description of the computer model, input data, analysis results and conclusions for the 30 foot accident condition and one foot normal condition free drops are given in Sections 2.10.8.4 and 2.10.8.5 respectively. The analysis of the impact limiter attachments is described in Section 2.10.8.6. A summary of results for all drop orientations is provided in Section 2.10.8.7. The forces and decelerations used in the cask body and basket structural analysis, presented in detail in Appendix 2.10.1 and Appendix 2.10.5, are given in Table 2.10.8-12 (loading values calculated in this appendix are increased for conservatism). The testing program for the NUHOMS[®]-MP197 wood filled limiters is discussed in Appendix 2.10.9. Test results indicate that ADOC predicts higher deceleration values, crush forces and crush depths than measured test results.

2.10.8.2 Design Description

The impact limiters absorb energy during impact events by crushing of balsa and redwood. The size, location and orientation of each wood block is selected to provide protection for the cask during all normal and hypothetical accident conditions of transport.

The top and bottom impact limiters are identical. Each has an outside diameter of 122 inches and a height of 60.75 inches. The inner and outer shells are Type 304 stainless steel joined by radial gussets of the same material. The gussets limit the stresses in the 0.25 in. thick steel outer cylinder and end plates due to pressure differentials caused by elevation and temperature changes during normal transport and provide wood confinement during impact. The metal structure positions, supports, confines and protects the wood energy absorption material. The metal structure does contribute to the energy absorbing capability of the impact limiter. However, the contribution to a side drop or oblique angles is negligible because contact starts at a single point with the unyielding surface (target) and initiates buckling of a single gusset. After the drop event is complete, relatively few gussets are buckled.

The materials and grain orientations are selected to provide acceptably low deceleration to prevent excessively high stresses in the cask during impact after the thirty foot end drop. A 2.50 inch layer of balsa wood with the grain parallel to the end of the cylindrical cask is provided on the outer face of the impact limiter to minimize decelerations after a one foot end drop.

A 18.0 inch wide ring of redwood and a 6.75 inch wide ring of balsa wood (consisting of 12 segments or blocks of wood) is located in the sides of the pie shaped compartments which surround the end of the cylindrical surface of the cask with the grain direction oriented radially. This ring of wood absorbs most of the kinetic energy during a side drop. Wood for this portion of the impact limiter was selected to absorb a large amount of energy in a relatively short crush distance.

The corners of the pie shaped compartments are filled with redwood. The primary function of the redwood block in this region is energy absorption during a 30 foot corner drop.

All wood blocks used in the impact limiters are composed of individual boards glued together with a Phenol Resorcinol Adhesive or equivalent. This adhesive is selected for its superior strength and moisture resistance. The wood blocks are assembled and glued together in accordance with an approved QA procedure. Minimum properties of the adhesive are listed in Table 2.10.8-1. Ranges of shear and tensile strengths of each type of wood are also listed. The adhesive is significantly stronger than any of the wood used in the limiter in terms of shear and tensile strength. Therefore the boards or blocks of wood will not fail along the glue joints.

The other mechanical properties of the wood used in the analysis are shown in Table 2.10.8-2. The crush strength properties used cover the range of expected values for the density and moisture content specified in the procurement specification. During procurement, wood samples are tested for density, moisture content and crush strength in accordance with an approved

sampling plan. If the density, moisture content, and crush strength are not within the specified range, the wood blocks from which samples are taken would be rejected.

During the end drop, all of the wood in the central part of the impact limiter that is directly "backed-up" by the cask body will crush. The wood in the corner and side of the limiter will tend to slide around the side of the cask since it is not supported or backed-up by the body and it will not crush or absorb energy as effectively as the wood that is backed-up. During the side or oblique drop the wood backed up by the cask will crush, while the wood beyond the end of the cask body will have a tendency to slide around the end of the cask. The analyses assume that the effectiveness of the portion of the wood that is not backed-up is 20%. Effectiveness is defined as the actual crush force developed at the target by this material divided by the theoretical force required to deflect the material. The analysis also assumes a range of wood crush strengths. When determining maximum deceleration, the maximum crush strengths are used. When determining crush depth, the minimum wood crush strengths are used.

The impact limiters are attached to the cask by twelve attachment bolts each. The attachment bolts have been sized to withstand the loads transmitted during a low angle drop slap down. This analysis is described in Section 2.10.8.6 of this Appendix.

2.10.8.3 Design Criteria

The outside dimensions of the impact limiter are sized to be within federal and state highway height and width restrictions. The balsa and redwood distribution and densities have been selected to limit the maximum cask body inertia loads due to the one foot normal condition drop and the thirty foot hypothetical accident drop so that the design criteria specified for the cask and basket (See Section 2.1) are met.

The welded stainless steel structure of the impact limiter is designed so that the wood is maintained in position and is confined during crushing of the impact limiters. The outer shell and gussets are designed to buckle and crush during impact. Local failure of the shell is allowed during impact limiter crushing. The welded stainless steel shell and its internal gussets are designed to withstand pressure differences and normal handling and transport loads with stresses limited to the material yield strength.

The impact limiters are designed to remain attached to the cask body during all normal and hypothetical accident conditions.

2.10.8.4 Analysis of 30 Foot Free Drop Accident Conditions

2.10.8.4.1 Approach

The kinetic energy due to the hypothetical 30 ft drop accident is absorbed by crushing of the impact limiters on the ends of the packaging. The limiters contain materials, i.e. balsa and redwood, which provide controlled deceleration of the packaging by crushing between the target surface and the cask body.

The applicable regulation, 10CFR71.73, requires that the packaging be oriented for the drop so that it strikes the target in a position for which maximum damage is expected. Dynamic impact analyses were performed for various packaging orientations using the ADOC computer code described in Section 2.10.8.8. This computer code has been validated by comparing its dynamic results with those from hand calculations for relatively simple problems, comparing its calculated force-deflection curves with those obtained from static crush tests, and by correlating dynamic results with actual measured cask behavior on other programs.

2.10.8.4.2 Assumptions and Boundary Conditions

The assumptions and boundary conditions are as follows:

1. The cask body is assumed to be rigid and absorb no energy. This assumption is realistic since the design criteria of Section 2.1.2 limit metal deformations to small values. All of the impact energy is therefore assumed to be absorbed by the impact limiters.
2. The crushable material is one or several anisotropic materials. The different wood regions are modeled individually.
3. The crush strengths of the wood sections are obtained from the properties parallel to and perpendicular to the grain based on the orientation of the cask at impact.
4. Each wood region is modeled as a one dimensional elastic, perfectly plastic material up to a specific locking strain. After reaching the locking strain, the stress increases linearly with the additional strain. The wood properties (modulus of elasticity, average crush strength, locking modulus, and locking strain) are taken from force-deflection curves of sample blocks of wood. Typical force-deflection curves for balsa and redwood are shown in Figures 2.10.8-1A and 2.10.8-1B. Since the locking strain varies from sample to sample, conservatively low locking strains of 80% for balsa and 60% for redwood are used.
5. The crush properties of the wood are varied with the initial angle of impact and do not change during the drop event being evaluated.
6. The cask and impact limiters are axisymmetric bodies.

7. The crushing resistance of the impact limiter shell and gussets have a negligible effect on the crush strength of the limiter and, therefore, a negligible effect on the impact forces and inertial loads.

2.10.8.4.3 Packaging Dynamic Computer Model

Figure 2.10.8-2 illustrates the computer model used for all packaging orientations. Regions I, II, and III in the model are used to delineate regions where different impact limiter materials are used. It should be noted that the properties of the three regions have been designed by choosing wood types and orientations to accommodate the crush requirements of the drop orientations. The crushable materials of Regions I, II, and III are selected to control the decelerations resulting from end, corner, and side drop orientations, respectively. Table 2.10.8-2 tabulates the wood properties that were used to describe the wood stress-strain behavior in the analysis.

A portion of the impact limiter crushable material is backed up by the cask body as it crushes against the impact surface. The remaining material overhangs the cask body and is not backed up. Backed up regions project vertically from the target footprint to the cask body, while unbacked regions do not project vertically to the cask. The effectiveness of the energy absorbing crushable material varies depending on whether it is "backed up" by the cask or is unsupported. Two cases are analyzed to bound impact limiter performance. In one case, the non-backed up material is assumed to be 20% effective and maximum wood crush strength is used (maximum of the possible range based on specified density). In the other case, the non-backed up material is also assumed to be 20% effective but the minimum wood strength is used. Evaluating impact limiter performance in this way results in a range of deceleration values, crush forces and crush depths. This, in combination with close control of wood properties during procurement, assures that the effects of wood property variations (including temperature effects) are bounded by the analyses.

2.10.8.4.4 Analysis Results Predicted by ADOC

The peak inertia loadings or cask body decelerations (in terms of gs) versus initial angle of impact are presented in Tables 2.10.8-3 through 2.10.8-6 for the 30 foot drop. The 30 foot drop is measured from the impact surface to the bottom of the impact limiter; the center of gravity (CG) of the cask is much higher than 30 feet. The values of crush depth vs. impact force are shown in Tables 2.10.8-7 to 2.10.8-12. Since the packaging CG is within ½ inch of the packaging center and the impact limiters are identical, these tables are valid for impacts on either end.

Based on the crush depths for the side drop from Table 2.10.8-7, the neutron shield shell will not hit the impact surface. Using maximum wood properties, the clearance after the limiters crush would be approximately 10.2 inches. Using minimum wood properties, the clearance after the limiter crush would be 9.2 inches. It is expected that the crush depth would be somewhere between the two bounding cases.

2.10.8.5 Analysis for One Foot Drop Normal Condition

This section describes the analysis of the NUHOMS[®]-MP197 for the one foot normal conditions of transport drop. The NUHOMS[®]-MP197 in the transport configuration is lifted and transported horizontally. Therefore, the side drop orientation is considered the only credible normal condition drop event. The accident condition analysis in Section 2.10.8.4 bound any possible accident condition drops. However, a 1 foot end drop and a 60° CG over corner drop are also evaluated for completeness. The results from the one foot, 60° corner drop are only used to compute the maximum NUHOMS[®]-MP197 lid bolt stress caused by a normal condition impact event.

The packaging kinetic energy is absorbed by crushing of the impact limiters. The dynamic system model of Section 2.10.8.4 was used to perform the side drop (0°) analysis using the ADOC computer program described in Section 2.10.8.9. The end drop analysis was performed assuming that the energy would be absorbed by the soft balsa wood (oriented in the weak direction) in the outer end of the limiter. This is an accurate way to determine g loads on an end drop since the g values can be calculated by the expression $F = Ma$ where F is the crush stress times the area and M is the package weight divided by the acceleration of gravity g .

The inertial load results of these one foot drop analyses are presented in Table 2.10.8-13. Again, two extreme cases are considered. The upper bound stiffness case assumes maximum wood crush strength and the lower bound stiffness case assumes minimum wood strength. Stress analyses in Section 2.10.1 are conservatively performed for the case(s) with maximum inertia loads resulting from upper bound stiffness cases.

2.10.8.6 Impact Limiter Attachment Analysis

2.10.8.6.1 Approach

The impact limiter attachments are designed to keep the impact limiters attached to the cask body during all normal and hypothetical accident conditions. The loading that has the highest potential for detaching the impact limiter is the slap down or secondary impact after a shallow angle 30 foot drop. During this impact, the crushing force on the portion of the impact limiter beyond the cask body (the non backed-up area) tends to pull the limiter away from the cask. The end and corner drops are not critical cases for the impact limiter attachments since the impact force tends to push the impact limiter onto the cask in these orientations.

For the impact limiter attachment bolt analysis, maximum wood crush strengths of 2010 psi for balsa and 6500 psi for redwood are assumed. The maximum wood properties produce the highest overturning moment on the limiter. Based on the dynamic analysis performed using the ADOC code, the most severe slap down impact occurs after a shallow angle oblique impact. The calculated peak contact forces at the end of the cask body subjected to secondary impact (slap down) for the orientations analyzed are as follows.

Drop Orientation	Impact Force (lb.×1000)
5°	10,200
10°	10,116
15°	10,222
20°	12,343

Therefore, the 20° slap down impact will result in the most severe overturning moment. The peak impact force that is applied to the impact limiter is conservatively increased by roughly 33% to 16,500,000 lb. for the structural analysis of the attachment bolts.

The maximum moment applied to the impact limiter attachments is conservatively determined ignoring the mass of the impact limiter which tends to reduce the attachment forces. The resultant of the external impact force on the limiter is offset 1.42 in. from the resultant of the cask reaction force. Therefore, the net moment applied to the limiter is $16.500 \times 10^6 \times 1.42$ or 2.343×10^7 in lb. There is also a frictional force that acts to pull the impact limiter away from the cask. Assuming a frictional coefficient of 0.12 between the cask and limiter and between the limiter and impact surface, the magnitude of this force is

$$F_f = \mu R = .12(16,500,000) = 1.980 \times 10^6 \text{ lbs.}$$

The crush depth on the side is 10.03 inches. The resultant moment due to friction is

$$M_f = (1,980,000)(10.03) = 1.986 \times 10^7 \text{ in lbs.}$$

The total moment is therefore 4.329×10^7 in lbs. This moment is reacted by the twelve impact limiter attachment bolts. A free body diagram of the impact limiter is shown in Figure 2.10.8-13. It is conservatively assumed that the impact limiter pivots about the edge of the cask. The attachment bolt forces vary linearly with distance from the pivot point, so that the maximum force, F_{max} , occurs in the bolt farthest from the pivot point. The worst case angular orientation occurs when any one of the attachment bolts is oriented closest to the point of impact.

The attachment bolts counteract the moment applied to the impact limiter in the following way.

$$M = 84.38F_{\max} + 2\frac{(78.64^2)}{84.38}F_{\max} + 2\frac{(62.94^2)}{84.38}F_{\max} + 2\frac{(41.50^2)}{84.38}F_{\max} \\ + 2\frac{(20.06^2)}{84.38}F_{\max} + 2\frac{(4.36^2)}{84.38}F_{\max} = 375.65F_{\max}$$

Where M is the moment applied to the impact limiter and F_{\max} is the maximum attachment bolt force, which is applied to the attachment bolt farthest from the pivot point. Therefore,

$$F_{\max} = \frac{4.329 \times 10^7}{375.65} = 115,240 \text{ lbs.}$$

The stress limits for the impact limiter attachments during the accident condition free drop are taken to be S_u and $0.42S_u$ for membrane plus bending and shear stresses respectively. For stress analysis, all material properties are taken at 300° F.

2.10.8.6.2 Attachment Bolt Stress

The critical tensile area of the 1.072 inch diameter attachment bolt is in the bolt shank, since the threads are 1¼-7UNC. The tensile area of the bolt is $(\pi/4)(1.072^2) = 0.903 \text{ in}^2$. The maximum allowable stress is taken to be S_u of SA-540, Grade B24 at 300° F, or 165 ksi. [4]. So the maximum attachment bolt tensile stress is $115,240/0.903/1000 = 127.7 \text{ ksi}$, which is less than 165 ksi.

2.10.8.6.3 Stress in Bolt Tunnel

The allowable stress for the bolt tunnel is the ultimate strength of SA-240, Type 304 at 300°F, or 66.2 ksi. [4]. The tensile force in the attachment bolt is reacted in the impact limiter shell by both the outer and inner bolt tunnels. A compressive stress is generated in the inner bolt tunnel, while a tensile stress is generated in the outer bolt tunnel. The critical cross sectional area in the outer bolt tunnel is that of the weld between the outer tunnel and the tunnel shelf. Therefore, the cross sectional area available to react the bolt force, A_{bt} , is that of the weld between the outer tunnel and the tunnel shelf plus the cross sectional area of the inner bolt tunnel.

$$A_{bt} = (\pi/4) \times (2.00^2 - 1.50^2) \text{ in.}^2 \text{ (inner tunnel)} + \pi \times 2.50 \times 0.19 \times \sin(45^\circ) \text{ in.}^2 \text{ (outer tunnel)} \\ = 2.430 \text{ in.}^2$$

The stress generated in the inner and outer bolt tunnels, σ_{bt} , is,

$$\sigma_{bt} = 115,240 \text{ lb.} / 2.430 \text{ in.}^2 = 47,431 \text{ psi.} < 66,200 \text{ psi.}$$

2.10.8.6.4 Stress in Bolt Tunnel Weld

The bolt tunnel assembly is attached to the impact limiter shell by a weld at both ends of the bolt tunnel assembly plus a weld between the inner bolt tunnel and the inner shell. The cross sectional area of the weld available to react the bolt force, A_{bt} , is,

$$A_{bt} = \pi \times 2.00 \times 0.25 \times \sin(45^\circ) \text{ in.}^2 \text{ (inner tunnel)} + \pi \times 3.00 \times 0.25 \times \sin(45^\circ) \text{ in.}^2 \text{ (outer tunnel)} \\ + 2 \times 24.75 \times 0.19 \times \sin(45^\circ) = 9.427 \text{ in.}^2$$

The stress generated in the inner and outer bolt tunnels, σ_{bt} , is,

$$\sigma_{bt} = 115,240 \text{ lb.} / 9.427 \text{ in.}^2 = 12,224 \text{ psi.} < 66,200 \text{ psi.}$$

2.10.8.6.5 Attachment Block Analysis

The impact limiter attachment bolts thread into attachment block that are welded to the outer shell of the NUHOMS[®]-MP197 cask. The material used for the attachment bolt blocks is SA-240 Type 304 with $S_u = 66.2$ ksi. at 300° F. [4]. The allowable shear stress is $0.42S_u = 27.8$ ksi., and the allowable primary plus bending stress is $S_u = 66.2$ ksi.

Attachment bolt block / cask shell weld

There is a 1/2 inch groove weld on all four sides of the of the attachment block between the block and the cask shell.

$$\text{Weld area, } A_{weld} = (4.81 \times 4.50) - (3.81 \times 3.50) = 8.31 \text{ in.}^2$$

$$\text{Weld moment of inertia, } I_{weld} = \frac{bh^3}{12} = \frac{(4.81)(4.50^3)}{12} - \frac{(3.81)(3.50^3)}{12} = 22.91 \text{ in.}^2$$

$$\text{Max. moment applied to block weld, } M_{weld} = 115,240 \text{ lb.} \times 1.88 \text{ in.} = 216,650 \text{ in.} \cdot \text{lb.}$$

$$\text{Bending stress, } \sigma_b = \frac{M_{weld} c}{I_{weld}} = \frac{(216,650)(4.50/2)}{22.91} = 21,277 \text{ psi.}$$

$$\text{Shear stress, } \tau = F_{max} / A_{weld} = 115,240 / 8.31 = 13,868 \text{ psi.} < 31,500 \text{ psi.}$$

$$\text{Stress intensity, } S.I. = \sqrt{\sigma_b^2 + 4\tau^2} = \sqrt{(21,277)^2 + 4(13,868)^2} = 34,957 \text{ psi.} < 66,200 \text{ psi.}$$

Minimum Engagement Length for Attachment Bolt and Block

The bolt material is SA-540, Grade B24, Class 1, with

$$S_u = 165 \text{ ksi.}, \text{ and} \\ S_y = 150 \text{ ksi at room temperature [4].}$$

The bolt block material is SA-240 Type 304 or SA-182 F304, with

$$S_u = 75 \text{ ksi.}, \text{ and} \\ S_y = 30 \text{ ksi. at room temperature [4].}$$

The minimum engagement length, L_e , for the bolt and flange is ([5], Page 1149),

$$L_e = \frac{2A_t}{3.146K_{n\max} \left[\frac{1}{2} + .57735n(E_{s\min} - K_{n\max}) \right]}$$

For a 1¼ - 7UNC 2A bolt,

$$A_t = \text{tensile stress area} = 0.969 \text{ in.}^2, \\ n = \text{number of threads per inch} = 7, \\ K_{n\max} = \text{maximum minor diameter of internal threads} = 1.123 \text{ in.}, ([5], \text{ p. 1290}). \\ E_{s\min} = \text{minimum pitch diameter of external threads} = 1.1476 \text{ in.}, ([5], \text{ p. 1290}).$$

Substituting the values given above,

$$L_e = \frac{2(0.969)}{(3.146)1.123 \left[\frac{1}{2} + .57735(7)(1.1476 - 1.123) \right]} = 0.915 \text{ in.}$$

$$J = \frac{A_s \times S_{ue}}{A_n \times S_{ui}} \quad [5]$$

Where, J is a factor for the relative strength of the external and internal threads, S_{ue} is the tensile strength of external thread material, and S_{ui} is the tensile strength of internal thread material.

$$A_s = \text{shear area of external threads} = 3.1416 nL_e K_{n\max} [1/(2n) + .57735 (E_{s\min} - K_{n\max})]$$

$$A_n = \text{shear area of internal threads} = 3.1416 nL_e D_{s\min} [1/(2n) + .57735(D_{s\min} - E_{n\max})]$$

For a 1¼ - 7UNC 2A bolt,

$$D_{s \min} = \text{minimum major diameter of external threads} = 1.2314 \text{ in. ([5], p. 1290)}$$

$$E_{n \max} = \text{maximum pitch diameter of internal threads} = 1.1668 \text{ in. ([5], p. 1290).}$$

Therefore,

$$A_s = 3.1416(7)(0.915)(1.123)[1/(2 \times 7) + .57735 (1.1476 - 1.123)] = 1.935 \text{ in.}^2$$

$$A_n = 3.1416(7)(0.915)(1.2314)[1/(2 \times 7) + .57735 (1.2314 - 1.1668)] = 2.694 \text{ in.}^2$$

So,

$$J = \frac{1.935(165.0)}{2.694(75.0)} = 1.580$$

The required length of engagement, Q , to prevent stripping of the internal threads is,

$$Q = L_e J = (0.915)(1.580) = 1.446 \text{ in.}$$

The actual minimum engagement length = 3.50 in. > 1.446 in.

2.10.8.6.6 Attachment Bolt Torque

Assume a bolt tensile stress of 15,000 psi.

$$F_a = 15,000 \times 0.969 = 14,535 \text{ lb.}$$

$$Q = K D_b F_a = 0.1 \times 1.25 \times 14,535 = 1,817 \text{ in. lb.} = 151 \text{ ft. lb.}$$

Where F_a is the bolt force, Q is the applied torque, K is the nut factor (0.1 with lubrication), and D_b is the nominal bolt diameter at the threads (0.969 in. [5], p. 1266).

Specify a bolt torque of 140 to 160 ft. lb.

For a bolt torque of 140 ft. lb.,

$$F_a = \frac{Q}{K D_b} = \frac{140 \times 12}{0.1 \times 1.25} = 13,440 \text{ lb.}$$

For a bolt torque of 160 ft. lb.,

$$F_a = \frac{Q}{K D_b} = \frac{160 \times 12}{0.1 \times 1.25} = 15,360 \text{ lb.}$$

Therefore, the maximum tensile stress in the bolt is $15,360/0.903 = 17,010$ psi. Which is much less than the yield strength of the bolt material at 300° F., 138,600 psi. [4].

2.10.8.7 Summary of ADOC Results Used for Structural Analysis

2.10.8.7.1 Cask Structural Analysis - g Load and Drop Orientation

In order to determine the cask stresses, the maximum g loads from ADOC runs are converted to forces and applied as quasistatic loadings on the cask body. A detailed ANSYS finite element model of the NUHOMS[®]-MP197 cask is used to perform this analysis.

Only the loads corresponding to the most critical normal and accident condition free drop orientations are used in the cask body analysis in Section 2.10.1. For the 30 foot accident condition drops, g loads corresponding to four different angles are evaluated, and for the 1 foot normal condition drops, g loads corresponding to two different angles are evaluated. The orientations evaluated in Section 2.10.1 are as follows.

Drop Height (Normal / Accident)	Orientation Analyzed
30 Foot Accident Condition Drop	0° Side Drop
	20° Slap Down
	60° C.G. Over Corner Drop
	90° End Drop
1 Foot Normal Condition Drop	0° Side Drop
	90° End Drop

The g loads corresponding to these drop orientations are provided in Tables 2.10.8-3 through 2.10.8-6, and 2.10.8-13.

The thirty foot side drop is evaluated because it produces the highest normal transverse g load. The 20°, thirty foot slap down is analyzed because it produces a high normal as well as rotational g load at the ends of the cask (second impact). Stresses in the cask and lid bolts are most sensitive to g loads applied in the 60° (CG over corner) direction. Consequently, the thirty foot CG over corner drop is evaluated. The highest axial g load occurs during a 90°, thirty foot end drop, and is therefore also evaluated.

For the normal conditions of transport one foot drops, the 0° side drop, and the 90° end drop are bounding, since they produce the highest normal g loads in the transverse and axial directions respectively. The 60° CG over corner drop acceleration is only used in the transport cask lid bolt analysis, since the 60° drop is the bounding orientation for the lid bolt impact load case.

When the g loads are applied to the cask model in Section 2.10.1, the g loads predicted by ADOC are increased in order to bound all drop angles, and to create conservatism. The g loads predicted by ADOC as well as the increased g loads used in the cask body analysis are shown in Figure 2.10.8-14.

Basket Structural Analysis - g Load and Drop Orientation

The loading conditions considered in the evaluation of the fuel basket consist of inertial loads resulting from normal handling (1 foot drop) and hypothetical accident (30 foot) drops. The inertial loads of significance for the basket analysis are those that act transverse to the cask and basket structural longitudinal axes, so that the loading from the fuel assemblies is applied normal to the basket plates and is transferred to the cask wall by the basket. The side drop will generate the highest stress in the basket, because of the inertial load caused by the fuel assemblies impacting the basket plates. For example, the maximum transverse g load resulting from a 0° side drop is 60 gs, and the maximum transverse g load resulting from a 5° slap down second impact is 53 gs. The rotational g loads from slap down impact will have a very small effect on the basket because the cask stiffness is much greater than the basket stiffness and the basket is enveloped by the cask. Consequently, any rotational bending affect will be absorbed by the cask body. Therefore, the basket structure is analyzed for 1 foot and 30 foot side drops. The basket structure is also analyzed for 1 foot and 30 foot end drops despite a large margin of safety. Table 2.10.8-14 lists the g loads used for the basket structural analysis.

2.10.8.8 Summary Description of ADOC Computer Code

One of the accident conditions which must be evaluated in the design of transport packagings to be used for the shipment of radioactive material is a free drop from a thirty-foot height onto an unyielding surface (10CFR71). The packaging must be dropped at an orientation that results in the most severe damage. Impact limiters are usually provided on the packaging to cushion the effects of such impact on the containment portion of the packaging. The limiters are usually hollow cylindrical cups which encase each end of the containment and are filled with an energy absorbing material such as wood or foam.

A computer code, ADOC (Acceleration due to Drop On Covers), has been written to determine the response of a packaging during impact. The analysis upon which this code is based is discussed in this section. The overall analysis of the packaging response is discussed in Section 2.10.8.8.1, and the methods used to compute the forces in the limiters as they crush are presented in Section 2.10.8.8.2.

2.10.8.8.1 General Formulation

The general formulation used to compute the response of the packaging as it impacts with a rigid target is discussed in this section. The assumptions upon which the analysis is based are first presented followed by a detailed development of the equations of motion used to calculate the packaging dynamic behavior. This is followed by a discussion of the numerical methods and the computer code used to implement the analysis. A significant part of the development is concerned with the prediction of forces developed in the impact limiters as the impact occurs. This aspect of the evaluation is discussed in Section 2.10.8.8.2.

Assumptions

The cask body is assumed to be rigid and axisymmetric. Therefore, all of the energy absorption occurs in the impact limiters which are also assumed to have an axisymmetric geometry. Several assumptions are made in calculating the forces which develop in the limiters as they crush. These are discussed in Section 2.10.8.8.2. Since the packaging is axisymmetric, its motion during impact will be planar. The vertical, horizontal, and rotational components of the motion of the packaging center of gravity (CG) are used to describe this planar motion.

Equations of Motion

A sketch of the packaging at the moment of impact is shown on Figure 2.10.8-3. The packaging is dropped from a height (H), measured from the lowest point on the packaging to the target. The packaging is oriented during the drop, and at impact, so that the centerline is at an angle (τ) with respect to the horizontal. At the instant of impact, the packaging has a vertical velocity of

$$V_0 = \sqrt{2GH} . \quad (1)$$

Where G is the gravitational constant.

At some time, t , after first impact, the packaging has undergone vertical, u , horizontal, x , and rotational, ρ , displacements. The location of the packaging at this time is shown on Figure 2.10.8-4. One or both of the limiters have been crushed as shown. The resulting deformations (and strains) in the limiters result in forces which the limiters exert on the packaging, thereby decelerating it. These forces, and their points of application on the packaging, are shown on Figure 2.10.8-4 as F_{v1} , F_{v2} , and F_h . The method used to calculate these forces and the points of application are provided in Section 2.10.8.8.2, below.

The three equations of motion of the cask are

$$M\ddot{u} + F_{v1} + F_{v2} - W = 0 , \quad (2)$$

$$M\ddot{x} - F_h = 0 , \text{ and} \quad (3)$$

$$J\ddot{\rho} - F_{v1}x_{v1} + F_{v2}x_{v2} + F_h Y_h = 0 . \quad (4)$$

Where, M is the mass of packaging, J is the polar moment of inertia of the packaging about its CG, W is the packaging weight, and $\ddot{}$ denotes acceleration. At impact ($t = 0$), all of the initial conditions are zero except that $u =$ the vertical velocity.

Computer Solution

The computer code is written to compute the motion of the packaging during impact. The solution is obtained by numerically integrating the equations of motion (equations 2, 3, and 4) from the time of impact, $t = 0$, to a specified maximum time, t_{max} . The integrations are carried forward in time at a specified time increment, Δt . Parametric studies indicate that a time increment of 1 msec is sufficiently small so that further reduction of the time increment does not affect the results. Solutions are usually carried out to about 150 msec for the near horizontal drops and to about 50 msec for the near vertical drops. The significant motions of the packaging normally occur within these time periods.

A standard fourth order Runge Kutta numerical integration method is used to perform the numerical integrations. The following procedure is used to carry the solution from time t_i to time t_{i+1} . Note that at time t_i the displacements and velocities of the three degrees of freedom describing the motion of the CG of the packaging are known.

1. Calculate the deformation of each of the limiters based on the packaging geometry and the motion of the packaging's CG (see Section 2.10.8.8.2).
2. Calculate the forces which the limiters exert on the packaging body using the deformation of the limiters and their stress-strain characteristics (see Section 2.10.8.8.2).
3. Use Equations 2, 3, and 4 to calculate the accelerations during the time interval. Use the Runge Kutta equations to calculate the location and velocity of the cask CG at time t_{i+1} .
4. Go to step (1) to repeat the process until time t_{max} .
5. Generate the output.

Output from the code consists of:

- Problem title, packaging geometry, drop conditions, and integration data.
- Limiter geometric and material property data.
- History of packaging CG motion and amount of crushing in each of the limiters.
- Force history data.
- Plot of acceleration histories.
- Plot of maximum limiter deformations.

2.10.8.8.2 Forces in Limiters

The methods used to calculate the forces F_{v1} , F_{v2} , and F_h in the limiter at a given crush depth are discussed in this section. These calculations are used to perform steps (1) and (2) above. The limiter geometry and material specification is discussed first. The general methodology used to calculate the forces are then presented which is followed with a detailed development of the equations used to calculate the force-displacement relationships.

Limiter Geometry

A sketch of the model of a limiter is shown on Figure 2.10.8-5. Regions I, II and III are used to delineate regions where different materials are used. It should be noted that the properties of the three regions are designed to accommodate the crush requirements of the three significant drop orientations. The properties of regions I, II and III are selected to control the decelerations resulting from vertical, corner, and shallow drop orientations, respectively. The properties used to describe the stress-strain behavior of each of the three materials are discussed below. The dimensions A and B may vary for the limiters at each end of the packaging, but R_0 and R_i are taken to be the same for both limiters. The same material properties are used for each of the limiters.

General Approach

The ideal energy absorbing material is one that has a stress-strain curve that has a large strain region where the stress is constant. Such a material absorbs the maximum energy while minimizing force (which determines the magnitude of the deceleration). Wood, foam, and honeycomb materials exhibit such behavior and are prime candidates for impact limiter crushable material. If the constant stress region of the stress-strain curve is of primary interest, the forces may be calculated as the crush stress times the area of the surface defined by the intersection of the target and the impact limiter. This approach assumes that the crush stress, which acts normal to the crush surface, is not influenced by stresses acting in directions parallel to the crush surface (i.e., the confining stresses). This assumption is made in the computer code. The crush stress used as input to the code is selected to represent that value which is consistent with the degree of confinement afforded by the impact limiter geometry for the drop orientation considered.

Therefore, the crushable material is modeled in the code with a one dimensional (oriented normal to the crush surface) stress-strain law. The properties of the stress-strain law are selected to represent the degree of confinement provided by stresses acting in the other two dimensions. The properties of the crushable material are not modified as the packaging rotates but are selected to represent the material properties for the initial crush direction of the material.

A portion of the "crushed" area of the limiter is often not backed up by the packaging body (*i.e.*, a projection of a point in this non backed up area normal to the target (impact surface) does not intersect the cask body). The user must specify the percentage of these forces which are to be included in the calculation. The confinement provided by the overall construction of the limiter will determine the extent to which these non backed up forces are actually effective. The computer code does not perform any computations which would allow the user to judge the adequacy of the selected percentage of non backed up forces which are counted.

The evaluation of the impact area and its centroid (required to locate the impact forces) is computationally complicated because of the many variations possible in the manner in which the target intersects the limiter. This problem is resolved by dividing the surface of the limiter into many small segments. The segment is located relative to the target at each computation. If the segment's original location is below the target, then it has crushed and it contributes a force equal to the stress times its area projected on the target. The location of this force is also known. The strain at the segment may also be evaluated so that the peak strains may be determined and stresses may be evaluated for strains which fall outside of the constant crush stress region of the stress-strain law.

The forces must be calculated at each time that the solution for the packaging response is computed. The problem, therefore, is to determine the forces acting on the limiters given the current location of the packaging center of gravity. The solution for the location of the packaging center of gravity is discussed in Section 2.10.8.8.1. The procedure used to perform these computations is as follows (each of the steps is detailed below).

1. Define the location of the target relative to the limiters from the current location of the packaging center of gravity relative to the target.
2. Divide the surface of the limiter into segments and calculate the strain in a one-dimensional element spanning the distance between the center of the segment and the packaging body.
3. Compute the stress in the element from the stress-strain relationship. Multiply the stress by the area of the element projected onto the target.
4. After all of the segments on the limiter are evaluated, sum the segment forces and moments of the forces to find the total force and moment acting on the packaging.
5. Calculate the horizontal force and moment of the horizontal force.
6. Use equations 2, 3, and 4 to extend the solution to the next time step. The new solution consists of the location of the packaging CG at the new time. The above steps are then repeated. This process is continued until the specified maximum time is reached.

Details of Force Computations

Details of each of the six steps outlined above are given in this section. Note that the location of the packaging CG is known at the beginning of this computational sequence.

Deformation of the Limiter

The first step in the computation is to evaluate the location of the limiters relative to the target given the location of the packaging CG relative to the target. The limiter position relative to the target is defined by the six variables, D_1 through D_6 , as shown on Figure 2.10.8-6. The location of the cask at first contact is shown on Figure 2.10.8-6a with the subscript 0 added to the D 's indicating initial values. The initial values of these parameters (when the lowest corner of the packaging first contacts) are found from the following geometric considerations.

$$\begin{aligned}D_{10} &= 2R_0 \cos \theta, \\D_{20} &= 0, \\D_{30} &= B_1 \sin \theta, \\D_{40} &= D_{30} + D_{10} + L \sin \theta + B_2 \sin \theta, \\D_{50} &= D_{40} - D_{10}, \\D_{60} &= D_{30} + L \sin \theta,\end{aligned}\tag{5}$$

At a given time, t , the packaging CG has displaced vertically, u , horizontally, x , and has rotated, ρ , and reached the position shown in Figure 2.10.8-6b. Each of the six points have then fallen by an amount:

$$\Delta D = u + l [\sin \theta - \sin(\theta - \rho)] + r [\cos \theta - \cos(\theta - \rho)]\tag{6}$$

Where l is the axial distance CG to point (+CG to top), and r is the radial distance CG to point (+CG to impact).

Then the corner deformation, D_2 , at time, $t + 1$, becomes

$$D_{2(t+1)} = D_{2t} + \Delta D_2.$$

Where

$$\begin{aligned}l_1 &= l_2 = -yL^* - B_1, \\l_3 &= -yL^* \\l_4 &= l_5 = (l - y)L^* + B_2, \\l_6 &= (l - y)L^*, \\r_1 &= r_4 = -R_0, \text{ and} \\r_2 &= r_3 = r_5 = r_6 = R_0.\end{aligned}$$

To facilitate the computation of strains in the limiter, the position of the limiter relative to the impact surface is classified as shown in Figure 2.10.8-7. There are three possible locations of the impact surface relative to the limiter. The task is therefore to define which of the three patterns apply, and to determine the parameters ϕ and Δ in terms of the variables D_1 through D_6 , just determined.

These deformations are next related to the three types of crush patterns for the bottom limiter shown on Figure 2.10.8-7. Crush pattern I applies when

$$D_1 < 0; D_2 < 0; D_3 > 0. \quad (8)$$

Then,

$$\Delta = -\frac{D_2}{\cos \phi}, \text{ and} \quad (9)$$

$$\phi = \cos^{-1} \frac{D_3 - D_2}{B_1}.$$

Crush pattern II applies when

$$D_1 > 0; D_2 < 0; D_3 > 0. \quad (10)$$

Then,

$$\Delta = -\frac{D_2}{\cos \phi}, \text{ and} \quad (11)$$

$$\phi = \cos^{-1} \frac{D_3 - D_2}{B_1}.$$

Crush pattern III applies when:

$$D_1 > 0; D_2 < 0; D_3 < 0. \quad (12)$$

Then,

$$\Delta = \frac{D_2}{\sin \phi}, \text{ and} \quad (13)$$

$$\phi = \sin^{-1} \frac{D_1 - D_2}{2R_0}.$$

The same set of equations applies to the top limiter if $D_1, D_2, D_3,$ and B_1 are replaced with $D_4, D_5, D_6,$ and B_2 in equations (8) through (13).

Strains in Limiters

The next step in the computation is to calculate strains in the limiters given the deformation defined above. The limiters are first divided into segments as shown in Figure 2.10.8-8. The number of segments used for the bottom, $NB,$ and the sides, $NS,$ are input by the user. Locations on the surface of the limiters are described in terms of the (R, Z, β) coordinate systems shown on the figure. Strains in the segments along the sides of the limiters are calculated based on the location of the center of the segment $(R_0, Z, \beta).$ The segments at the bottom are divided into two pieces: one for $R < R_i$ (i.e. in Region 1) and the second for $R > R_i.$ A strain is calculated for each of these two pieces for each segment along the bottom surface.

The strains, $\epsilon,$ are calculated as the deformation of the point normal to the crush surface, $\delta,$ divided by the undeformed distance of the point from the surface of the limiter to the outer container (q), again measured normal to the crush surface. Therefore:

$$\epsilon = \delta / q \quad (14)$$

Different equations govern each of these parameters for each of the three crush patterns as shown on Figure 2.10.8-7.

The geometry for crush pattern I is shown on Figure 2.10.8-9. Forces resulting from deformation of the side elements are neglected for this crush pattern. It may be shown that the deformation is

$$\delta = \Delta \cos \phi + (R \cos \beta - R_0) \sin \phi \quad (15)$$

The undeformed length of the element is taken measured to the plane of the packaging bottom so that

$$q = A_1 \cos \phi \quad (16)$$

The geometry for crush pattern II is shown on Figure 2.10.8-10. The deformation of the points on the bottom (a) and along the side (b) may be represented with the same equation

$$\delta = \Delta \cos \phi + (R \cos \beta - R_0) \sin \phi - Z / \cos \phi \quad (17)$$

The original length of the element depends on the intersection of the projection of the point on the impact surface with the outline of the limiter. Four points are identified as shown on Figure 2.10.8-10. The lengths are

$$\begin{aligned}
 q_1 &= \frac{A-Z}{\cos \phi}, \\
 q_2 &= \frac{X}{\sin \phi}, \\
 q_3 &= \frac{B-Z}{\cos \phi}, \text{ and} \\
 q_4 &= \left[(R_0^2 - R^2 \sin^2 \beta)^{1/2} + R \cos \beta \right] \sin \phi.
 \end{aligned}
 \tag{18}$$

Where $X = R \cos \beta + (R^2 \cos^2 \beta - R^2 + R_1^2)^{1/2}$.

The deformation for crush pattern III is shown on Figure 2.10.8-11. Deformations of points on the bottom of the limiter are neglected for this crush pattern. The deformation is

$$\delta = \frac{\Delta - Z / \tan \phi - R_0 (1 - \cos \beta)}{\sin \phi}$$

The original length is measured to, R_i , so that

$$q = \frac{R_0 - R_i}{\sin \phi}.
 \tag{20}$$

Segment Stress

The stresses in the elements are calculated from the above strains. As mentioned above, three sets of stress-strain laws are input to the code, one for each of the regions defined in Figure 2.10.8-5.

The location of the center of the segment on the surface of the limiter is used to determine which of the three stress-strain laws is to be used. The model may be viewed as a set of one dimensional rods which run from the center of the segment, normal to the target, to another boundary of the limiter. The entire rod is given the properties which the limiter material has at the beginning point of the rod (i.e., the intersection with the target).

The stress-strain law used for the materials is shown on Figure 2.10.8-12. Each of the seven parameters shown on the figure is input to the code for each of the three regions of the limiter. The arrows on the figure indicate the load-unload paths used in the model. The step in the crush strength is built into the stress-strain law so that two crushable materials in series may be modeled. The two crush strengths should be specified as the actual crush strengths of the two materials. The first locking strain, ϵ_i , should be specified as the locking strain of the weaker material times the length of the weaker material divided by the total specimen length. The higher locking strain, ϵ_L , should be specified as the first locking strain plus the locking strain of the stronger material times its length and divided by the specimen length.

As stated above, the properties of the limiter material are not varied as the limiter crushes and the packaging rotates. Limiter materials such as wood exhibit anisotropic material properties. This must be accounted for when the properties are input to the code based on the anticipated direction of crushing. Most of the anisotropic wood data is based on tests performed in the elastic range. The following relationship has been used to represent wood properties for a loading which is applied at an angle (α) with respect to the wood grain:

$$P = \frac{P_1 \cos^4 \alpha + P_2 \sin^4 \alpha}{\cos^4 \alpha + \sin^4 \alpha} \quad (21)$$

Where P is the property of interest at angle α , and P_1 and P_2 are properties parallel and perpendicular to grain.

Evaluation of Forces

The stresses determined above are multiplied by the area of the segment projected onto the crush surface. The areas of the sidewall segments are (see Figure 2.10.8-8):

$$A_s = \frac{2R_0 B \cos(\theta - \rho)}{(NB)(NS) \tan \beta} \quad (22)$$

The area of the bottom segments is divided into two parts, one in region I and the other in region II. These areas are

$$A_b = \frac{4R_0 L_b \sin(\theta - \rho)}{NB} \quad (23)$$

Where, $L_b = (R_i^2 - R_c^2)^{1/2}$ for region 1, and $L_b = (R_0^2 - R_c^2)^{1/2} - (R_i^2 - R_c^2)^{1/2}$ for region II.

These forces are summed for all of the elements to determine the total force acting on the packaging. The forces are also multiplied by their moment arms about the packaging CG to calculate the total moment acting on the packaging. The point on the segment is first projected, normal to the target, to evaluate whether or not it intersects the packaging body. If the projection does not intersect the packaging body, only a percentage of the force is included in the summation. The user specifies the percentage to be used.

Horizontal Force

A horizontal force develops at the limiter/target interface. This force is only considered for the bottom limiter (i.e., the first to impact) since the packaging is always close to horizontal when the top impact limiter is in contact.

The horizontal force, F_h , is first calculated as that required to restrain horizontal motion of the tip of the limiter.

The horizontal acceleration, $\ddot{\Delta}_H$, at the tip of the bottom limiter (point 2 on Figure 2.10.8-6) may be related to the CG motion of the packaging by

$$\ddot{\Delta}_H = \ddot{x} - \ddot{\rho} \left[(\gamma L^* + B_1) \cos \phi + R_0 \sin \phi \right] \quad (24)$$

Where $\phi = \frac{\pi}{2} - \theta + \rho$.

Equating Δ_H to zero would result in no acceleration of the tip in the horizontal direction and provides the solution for x in terms of ρ .

Substituting this solution for x into Equation (3) results in an expression for the horizontal force, F_h , required to restrict horizontal acceleration of the tip, in terms of the rotational acceleration, ρ . Finally, equation 4 is used to eliminate ρ with the following result.

$$F_h = \frac{M_v W \left[(\gamma L^* + B_1) \cos \phi + R_0 \sin \phi \right]}{J_g + W \left[(\gamma L^* + B_1) \cos \phi + R_0 \sin \phi \right]^2} \quad (25)$$

Where M_v is the moment due to vertical forces, which is equal to $F_{v1}x_{v1} - F_{v2}x_{v2}$, and W is the packaging weight.

This force is restricted to

$$F_h < \mu F_{v1} \quad (26)$$

Where μ is the coefficient of friction specified by user.

2.10.8.9 References

1. Federal Specification MMM-A-188b.
2. Dreisback, J.F., *Balsa Wood and Its Properties*, Columbia Graphs, Columbia, CT 1952.
3. Baumeister, T., Marks, L. S., *Standard Handbook for Mechanical Engineers*, 8th Edition, McGraw-Hill, pg. 6-124.
4. American Society of Mechanical Engineers, ASME Boiler and Pressure Vessel Code, Section II, Part D, 1998, including 1999 Addenda.
5. *Machinery Handbook*, 21st Edition, Industrial Press, 1979.

Table 2.10.8 -1
Mechanical Properties of Wood and Wood Adhesive

Minimum Properties of Adhesive	
Shear Strength by Compression Loading	2,800 lb in ⁻² [1]
Shear Strength by Tension Loading	340 lb in ⁻² [1]
Properties of Heavy Balsa (10-12 lb ft ⁻³)	
Shear Strength Parallel to Grain	315-385 psi max. [2]
Tensile Strength Perpendicular to Grain	140-160 psi [2]
Properties of Redwood	
Shear Strength Parallel to Grain	940 psi [3]
Tensile Strength Perpendicular to Grain	240 psi [3]

Table 2.10.8-2
Typical Wood Material Properties

Property	High Density Balsa	Redwood
Density	10-12 lb ft ⁻³	18.7-27.5 lb ft ⁻³
Parallel to Grain		
Crush Stress	1560-2010 psi	5000-6500 psi
Locking Strain	0.8	0.6
Unloading Modulus	32,000 psi	1,247,000 psi
Locking Modulus	10 × (max. crush stress)	10 × (max. crush stress)
Perpendicular to Grain		
Crush Stress	300-420 psi	750-975 psi
Locking Strain	0.8	0.6
Unloading Modulus	32,000 psi	1,247,000 psi
Locking Modulus	10 × (max. crush stress)	10 × (max. crush stress)

Table 2.10.8-3
 First Impact Maximum Inertia g Load versus Initial Angle of Impact
 for 30 Foot Drop,
 using Maximum Wood Crush Stress Properties

Impact Angle, 30 Foot Drop	Maximum g Load During First Impact, Maximum Wood Properties			
	Axial	Transverse		
	CG	Top	Bottom	CG
0°	3	60	59	59
5°	9	19*	$G_{nor} = 31$ $G_{rot} = 50$	31
10°	14	21*	$G_{nor} = 36$ $G_{rot} = 57$	36
15°	21	24*	$G_{nor} = 43$ $G_{rot} = 66$	43
20°	31	28*	$G_{nor} = 53$ $G_{rot} = 80$	53
30°	10	12	$G_{nor} = 12$ $G_{rot} = 25$	12
40°	17	9	$G_{nor} = 14$ $G_{rot} = 24$	14
45°	24	7	$G_{nor} = 17$ $G_{rot} = 24$	17
50°	26	4	$G_{nor} = 15$ $G_{rot} = 18$	15
60°	34	4	$G_{nor} = 12$ $G_{rot} = 10$	12
70°	43	4	13	9
80°	46	3	7	5
90°	44	2	0	1

* Maximum acceleration occurred during second impact.

Table 2.10.8-4
 Second Impact Maximum Inertia g Load versus Initial Angle of Impact
 for 30 Foot Drop,
 using Maximum Wood Crush Stress Properties

Impact Angle, 30 Foot Drop	Maximum g Load During Second Impact (Top), Maximum Wood Properties					
	Axial	Transverse				
	CG	Top			Bottom	CG
		Normal	Rotational	Impact Force (lb.×1000)		
5°	1	37	71	10,200	33	37
10°	1	37	69	10,116	32	37
15°	3	37	70	10,222	33	37
20°	9	44	83	12,343	37	44

Table 2.10.8-5
 First Impact Maximum Inertia g Load versus Initial Angle of Impact
 For 30 Foot Drop,
 Using Minimum Wood Crush Stress Properties

Impact Angle, 30 Foot Drop	Maximum g Load During First Impact (Bottom), Minimum Wood Properties			
	Axial	Transverse		
	CG	Top	Bottom	CG
0°	4	53	53	53
5°	7	16*	$G_{nor} = 24$ $G_{rot} = 41$	24
10°	11	19*	$G_{nor} = 29$ $G_{rot} = 48$	29
15°	16	20*	$G_{nor} = 34$ $G_{rot} = 53$	34
20°	24	22*	$G_{nor} = 40$ $G_{rot} = 62$	40
30°	27	14	$G_{nor} = 34$ $G_{rot} = 48$	34
40°	15	8	$G_{nor} = 13$ $G_{rot} = 21$	13
45°	21	7	$G_{nor} = 15$ $G_{rot} = 22$	15
50°	23	4	$G_{nor} = 14$ $G_{rot} = 17$	14
60°	32	4	$G_{nor} = 11$ $G_{rot} = 8$	11
70°	41	4	13	8
80°	50	5	8	6
90°	34	2	0	1

* Maximum acceleration occurred during second impact

Table 2.10.8-6
 Second Impact Maximum Inertia g Load versus Initial Angle of Impact
 for 30 Foot Drop,
 using Minimum Wood Crush Stress Properties

Impact Angle 30 Foot Drop	Maximum g Load During Second Impact (Top), Minimum Wood Properties					
	Axial	Transverse				
	C.G.	Top			Bottom	C.G.
		Normal	Rotational	Impact Force (lb.×1000)		
5°	1	35	69	9,659	34	35
10°	1	32	64	8,916	31	32
15°	3	32	61	8,755	29	32
20°	7	36	69	10,154	32	36

Table 2.10.8-7
Depth of Crush versus Crush Force, 0° Impact Angle

Maximum wood properties		Minimum wood Properties	
Crush Depth Δ (in.)	Force (Kips)	Crush Depth Δ (in.)	Force (Kips)
2.62	4,081	2.62	3,006
5.00	6,346	5.08	4,674
7.01	6,346	7.25	4,674
8.55	8,027	9.07	4,599
9.54	8,027	10.50	5,912
10.01	5,504	11.50	6,912
		12.11	5,632

Table 2.10.8-8
Depth of Crush versus Crush Force, 20° Impact Angle

First Impact			
Maximum wood properties		Minimum wood Properties	
Crush Depth Δ (in.)	Force (Kips)	Crush Depth Δ (in.)	Force (Kips)
5.28	218	5.29	167
10.51	598	10.54	454
15.56	669	15.66	528
20.32	13,568	20.51	10,645
22.41	15,386	22.84	12,050
Second Impact			
Maximum wood Properties		Minimum wood Properties	
Crush Depth Δ (in.)	Force (Kips)	Crush Depth Δ (in.)	Force (Kips)
0.47	0	0.16	0
9.68	6,071	8.51	4,238
16.22	10,757	15.86	7,719
18.15	6,573	19.95	5,946

Table 2.10.8-9
Depth of Crush versus Crush Force, 45° Impact Angle

First Impact			
Maximum wood properties		Minimum wood Properties	
Crush Depth Δ (in.)	Force (Kips)	Crush Depth Δ (in.)	Force (Kips)
5.29	259	5.29	199
10.55	899	10.57	688
15.68	2,023	15.76	1,551
20.41	4,536	20.64	3,502
24.35	6,184	24.91	5,365
27.08	7,523	28.20	6,583
28.16	7,292	30.64	6,110

Table 2.10.8-10
Depth of Crush versus Crush Force, 60° Impact Angle

First Impact			
Maximum wood properties		Minimum wood Properties	
Crush Depth Δ (in.)	Force (Kips)	Crush Depth Δ (in.)	Force (Kips)
5.29	224	5.29	164
10.58	930	10.59	691
15.75	2,675	15.81	2,040
20.56	5,055	20.77	3,871
24.73	6,418	25.22	5,294
27.99	7,745	28.97	6,669
30.13	9,445	31.79	8,559
30.92	6,490	33.81	5,077

Table 2.10.8-11
 Depth of Crush versus Crush Force, 80° Impact Angle

First Impact			
Maximum wood properties		Minimum wood Properties	
Crush Depth Δ (in.)	Force (Kips)	Crush Depth Δ (in.)	Force (Kips)
5.29	1,194	5.29	897
10.41	5,269	10.46	4,106
14.83	9,153	15.11	7,103
18.06	10,243	18.83	8,504
19.90	12,570	21.41	12,705
20.23	7,981	22.46	6,695

Table 2.10.8-12
 Depth of Crush versus Crush Force, 90° Impact Angle

First Impact			
Maximum wood properties		Minimum wood Properties	
Crush Depth Δ (in.)	Force (Kips)	Crush Depth Δ (in.)	Force (Kips)
2.59	11,291	2.60	8,656
6.82	11,291	7.10	8,656
9.48	11,957	10.42	9,196
10.54	6,006	12.53	9,196
		13.44	8,012

Table 2.10.8-13
Maximum Inertial g Load During One Foot Drop

Impact Angle, 1 foot Drop	Maximum g Load During First Impact, Maximum Wood Properties			
	Axial	Transverse		
	CG	Top	Bottom	CG
90°	10	0	0	0
60°	5	1	3	2
0°	0	24	24	24

Impact Angle, 1 foot Drop	Maximum g Load During First Impact, Minimum Wood Properties			
	Axial	Transverse		
	CG	Top	Bottom	CG
90°	7	0	0	0
60°	5	1	2	2
0°	1	18	17	17

Table 2.10.8-14
 Loading Used in Cask Body and Cask Internals Analysis
 (Appendices 2.10.1, 2.10.3, and 2.10.4)
 versus
 Maximum g Load Predicted by ADOC Program

Accident Conditions (30 Foot Drops)		
Drop Orientation	Max. g Load from ADOC	Input Loading Used in Analysis
End Drop on Lid and Bottom	50g Axial	75g Axial
Side Drop	60g Transverse	75g Transverse
CG over Corner Drop on Lid And Bottom	34g Axial	45g Axial
	12g Transverse	16g Transverse
		48g Resultant Vertical
Low Angle Slap Down on Top Impact Limiter	31g Axial	35g Axial
	53g Normal	60g Normal

Normal Conditions (1 Foot Drops)		
Drop Orientation	Max. g Load from ADOC	Input Loading Used in Analysis
90° End Drop on Lid and Bottom	10g Axial	30g Axial
0° Side Drop	24g Transverse	30g Transverse

Figure 2.10.8-1
Impact Limiter Geometry

**FIGURE WITHHELD AS SENSITIVE
UNCLASSIFIED INFORMATION**

Figure 2.10.8-1A
Sample Force/Deflection Curve for Balsa

SAMPLE SIZE : 2.0"DIA × 2.0" HT.
WOOD DENSITY : 6.03 LBS/FT³

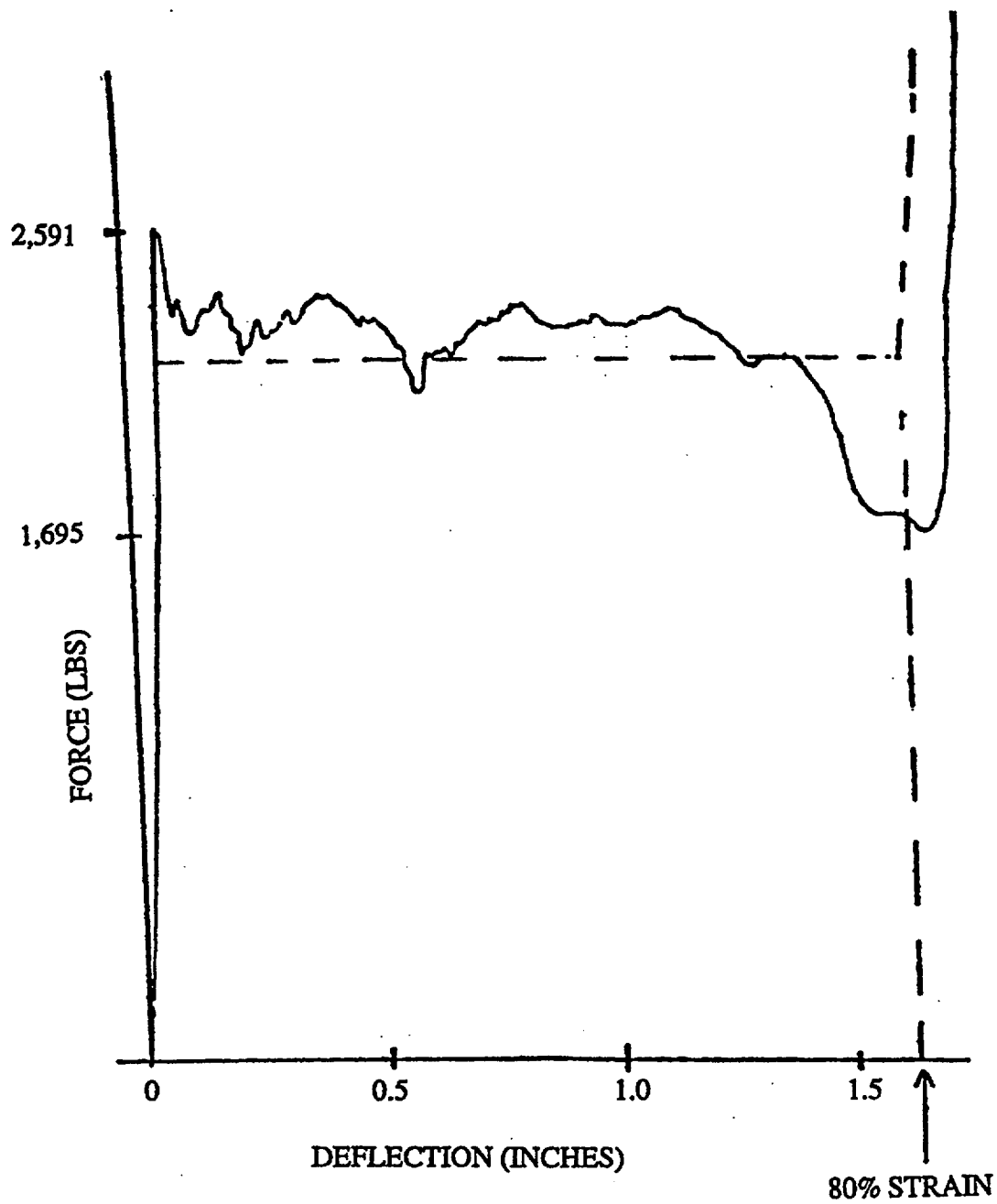


Figure 2.10.8-1B
Sample Force/Deflection Curve for Redwood

NOTE : NOMINAL SAMPLE 1.625" DIA x 1.625" HT.

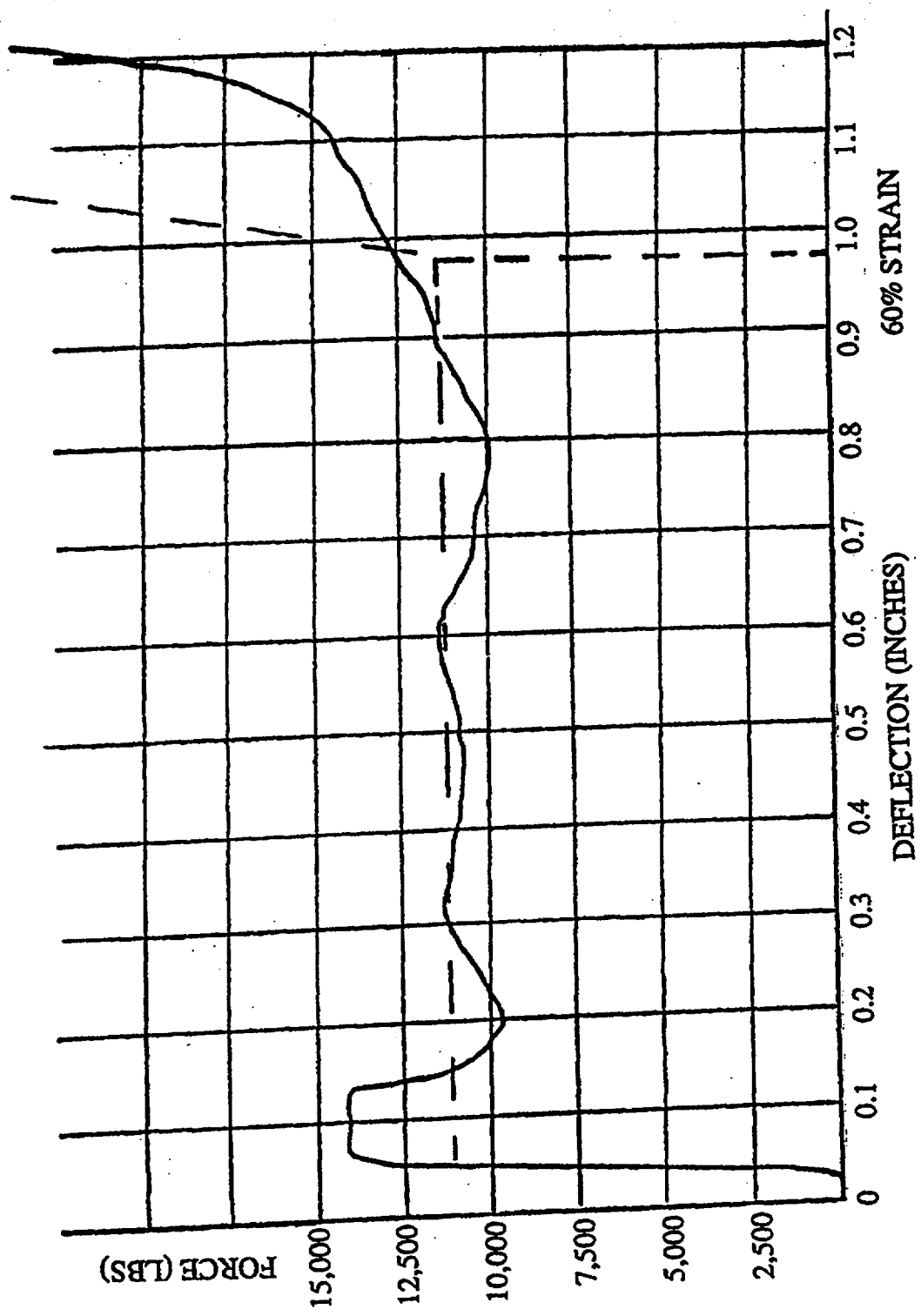


Figure 2.10.8-2
ADOC Computer Model for NUHOMS®-MP197 Transport Package

**FIGURE WITHHELD AS SENSITIVE
UNCLASSIFIED INFORMATION**

Figure 2.10.8-3
Geometry of Packaging

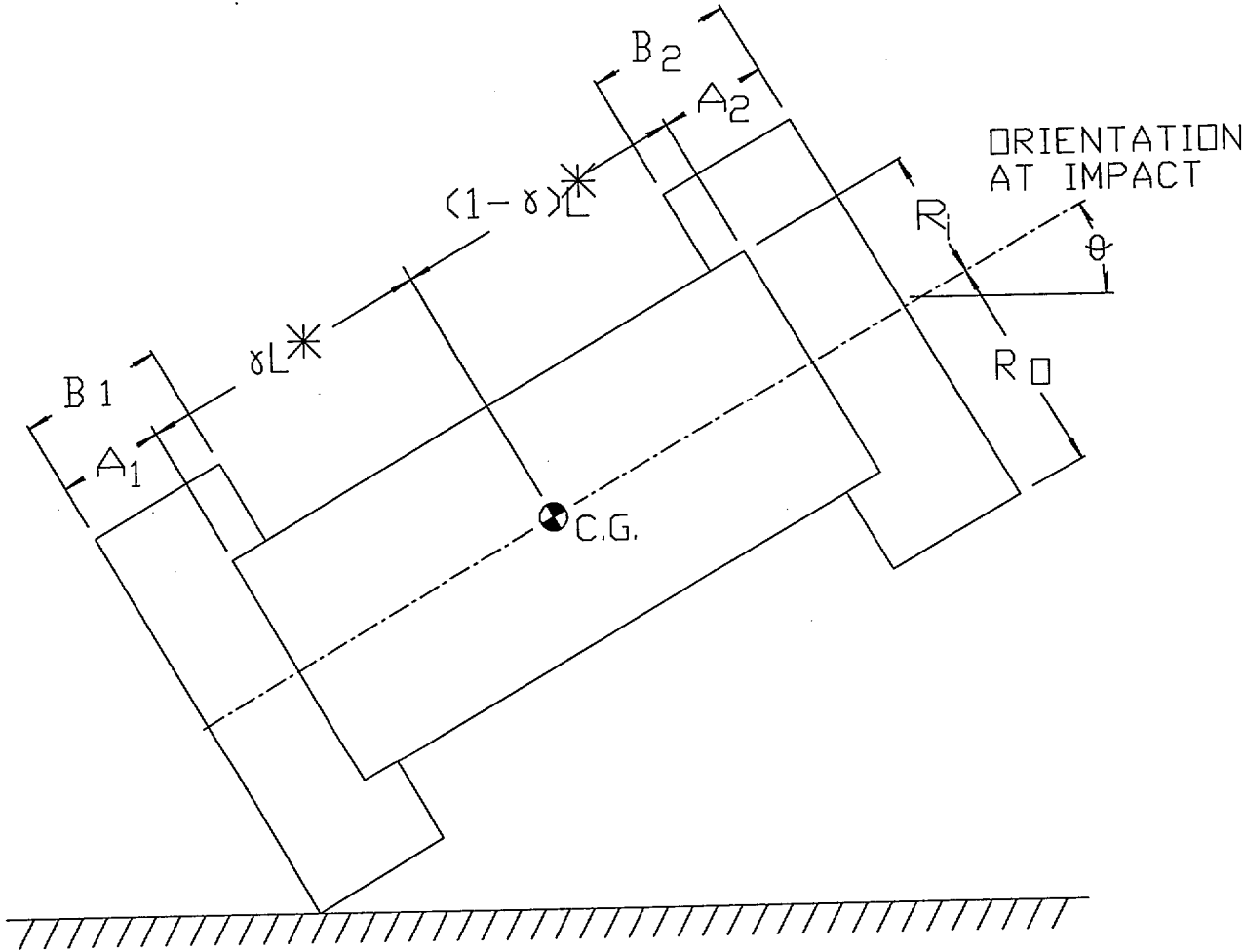


Figure 2.10.8-4
Packaging at Time, t

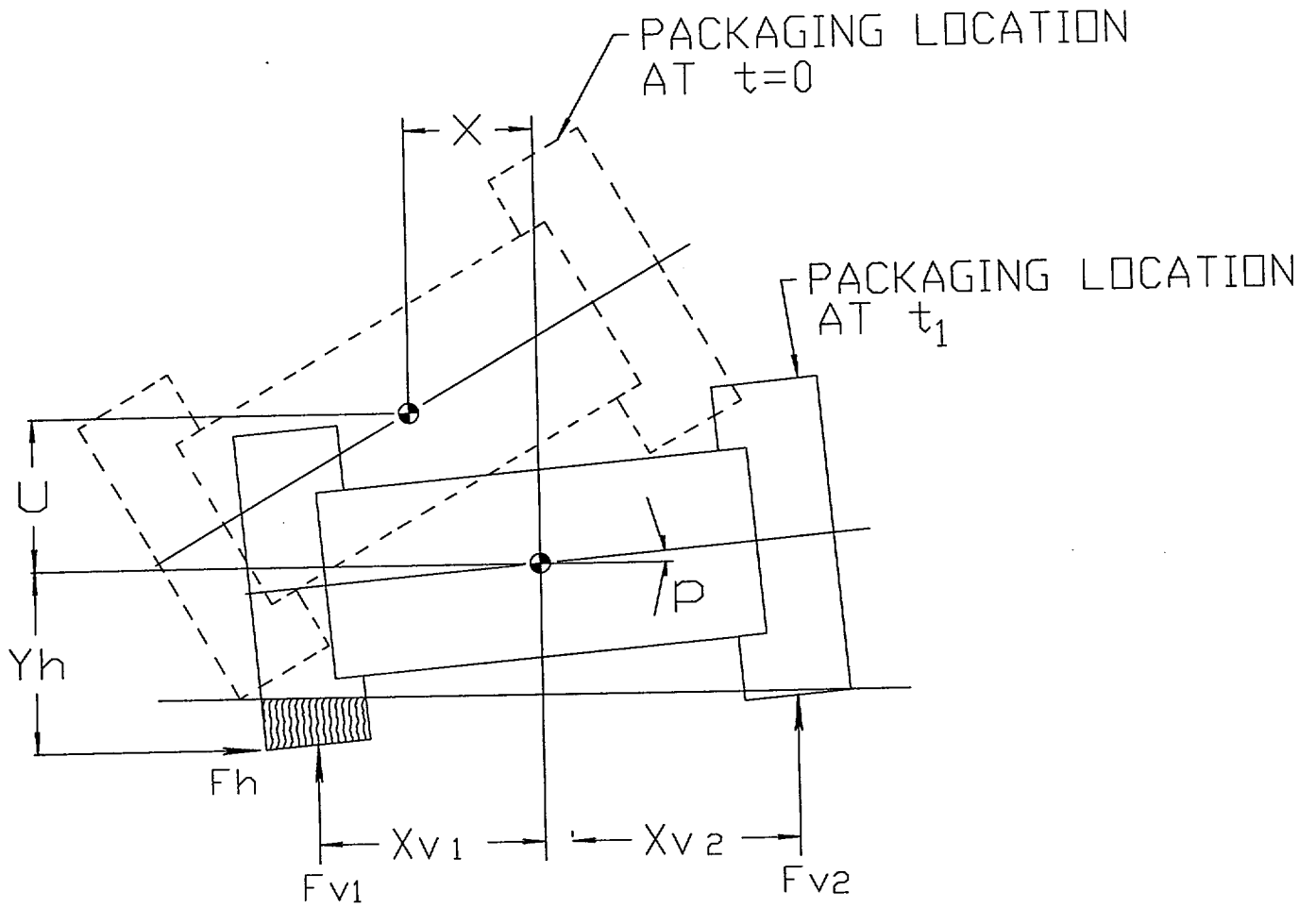


Figure 2.10.8-5
Geometry of Impact Limiter Parameters

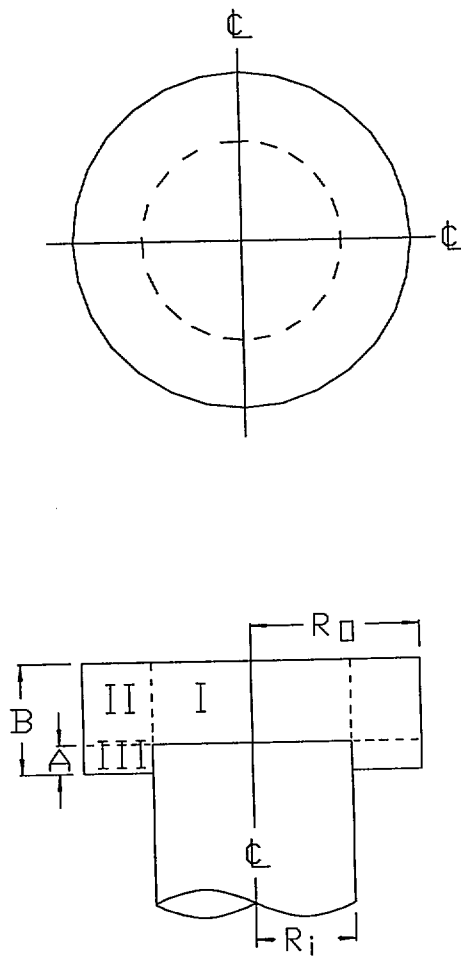
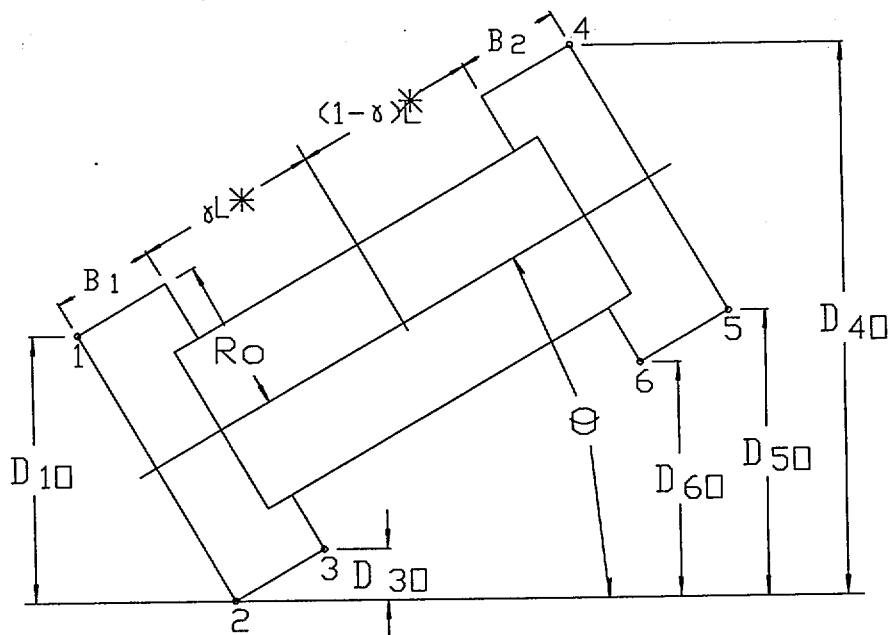
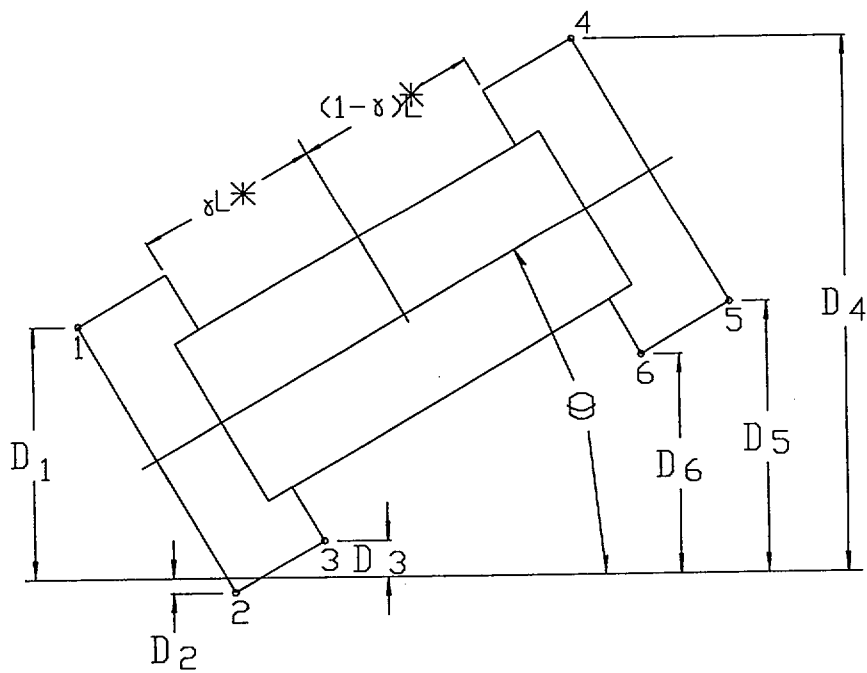


Figure 2.10.8-6
 Definition of Limiter Deformation

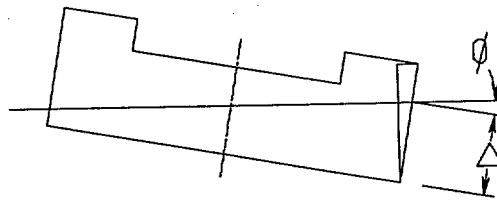


a) IMPACT LIMITER PARAMETERS AT FIRST IMPACT

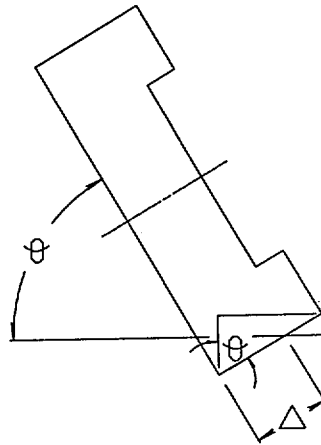


b) IMPACT LIMITER PARAMETER - GENERAL

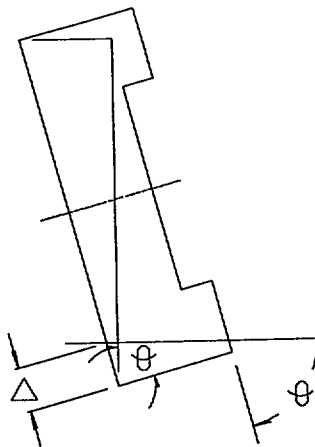
Figure 2.10.8-7
Crush Pattern in Impact Limiter



a) CRUSH PATTERN I



b) CRUSH PATTERN II



c) CRUSH PATTERN III

Figure 2.10.8-8
Impact Limiter Segments

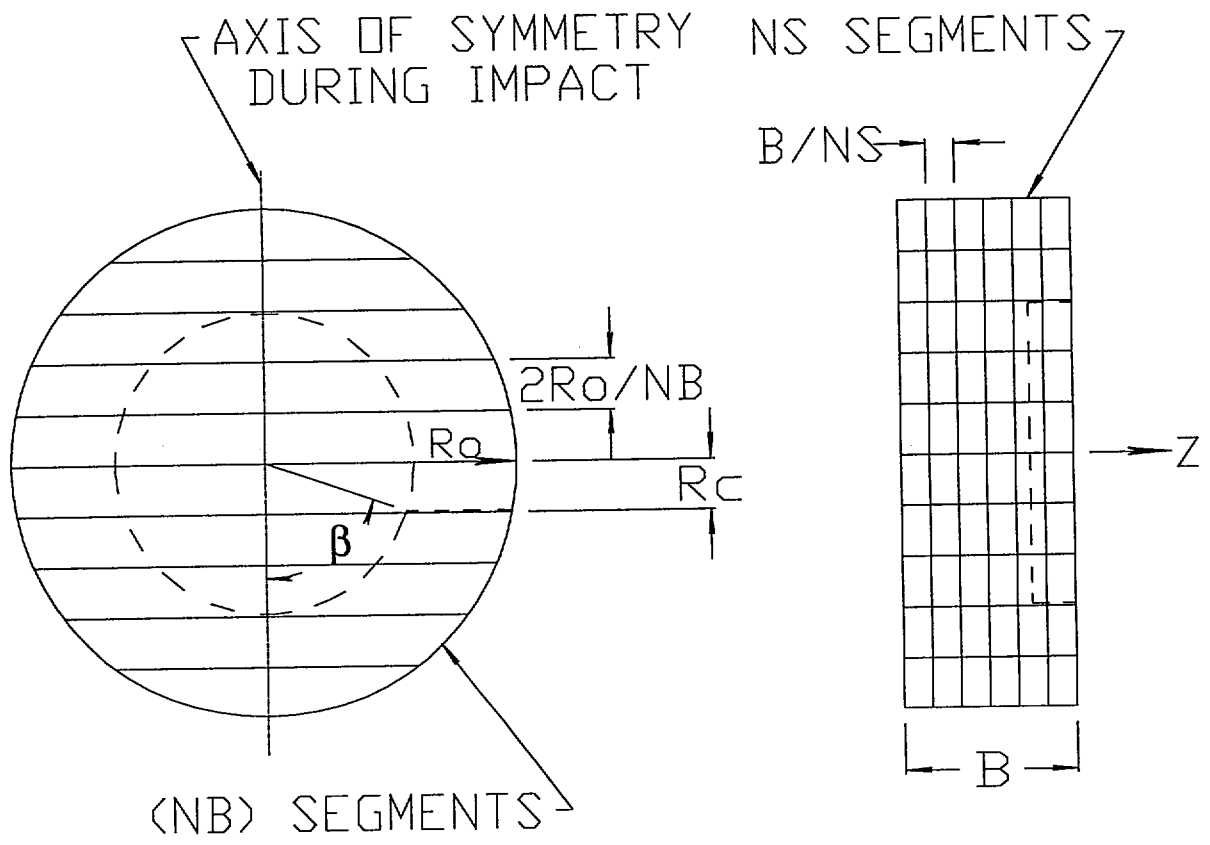


Figure 2.10.8-9
Strain Computation for Crush Pattern I

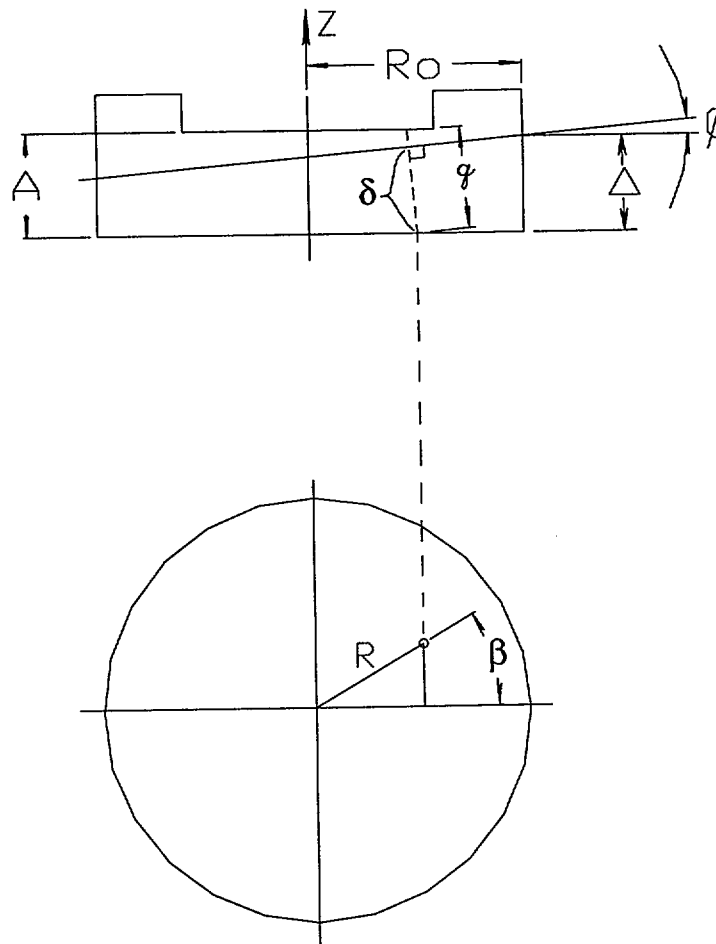


Figure 2.10.8-10
Strain Computation for Crush Pattern II

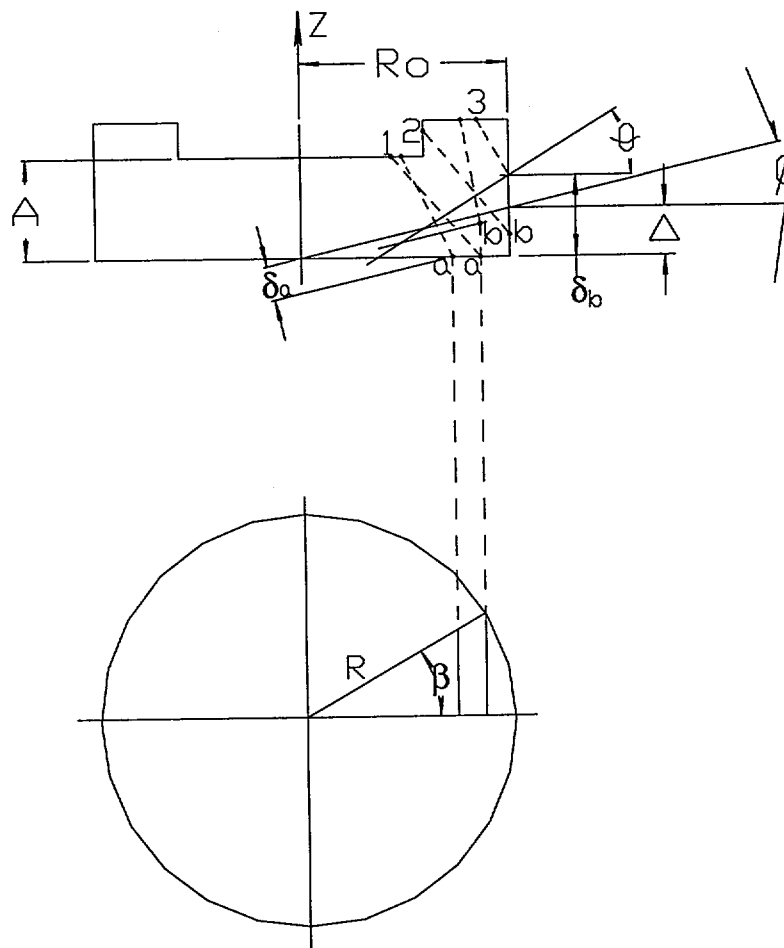


Figure 2.10.8-11
Strain Computation for Crush Pattern III

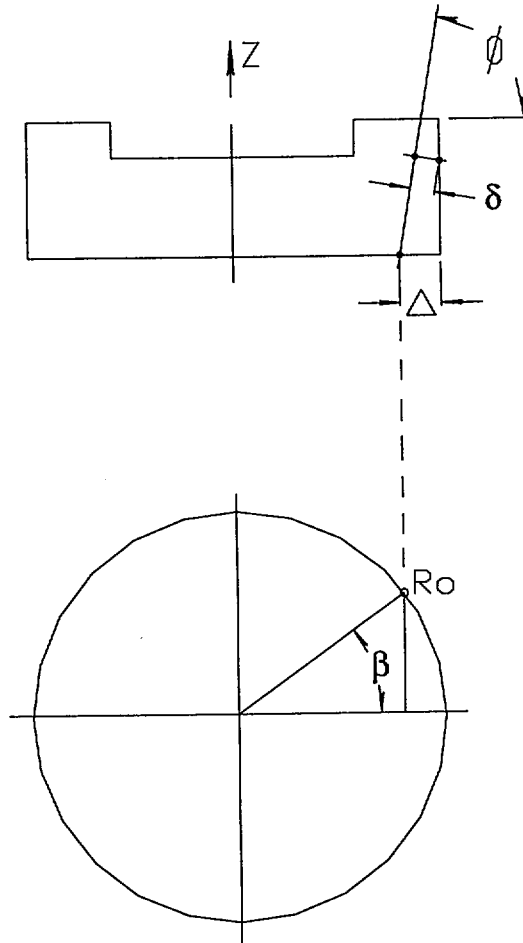


Figure 2.10.8-12
Wood Stress-Strain Curve

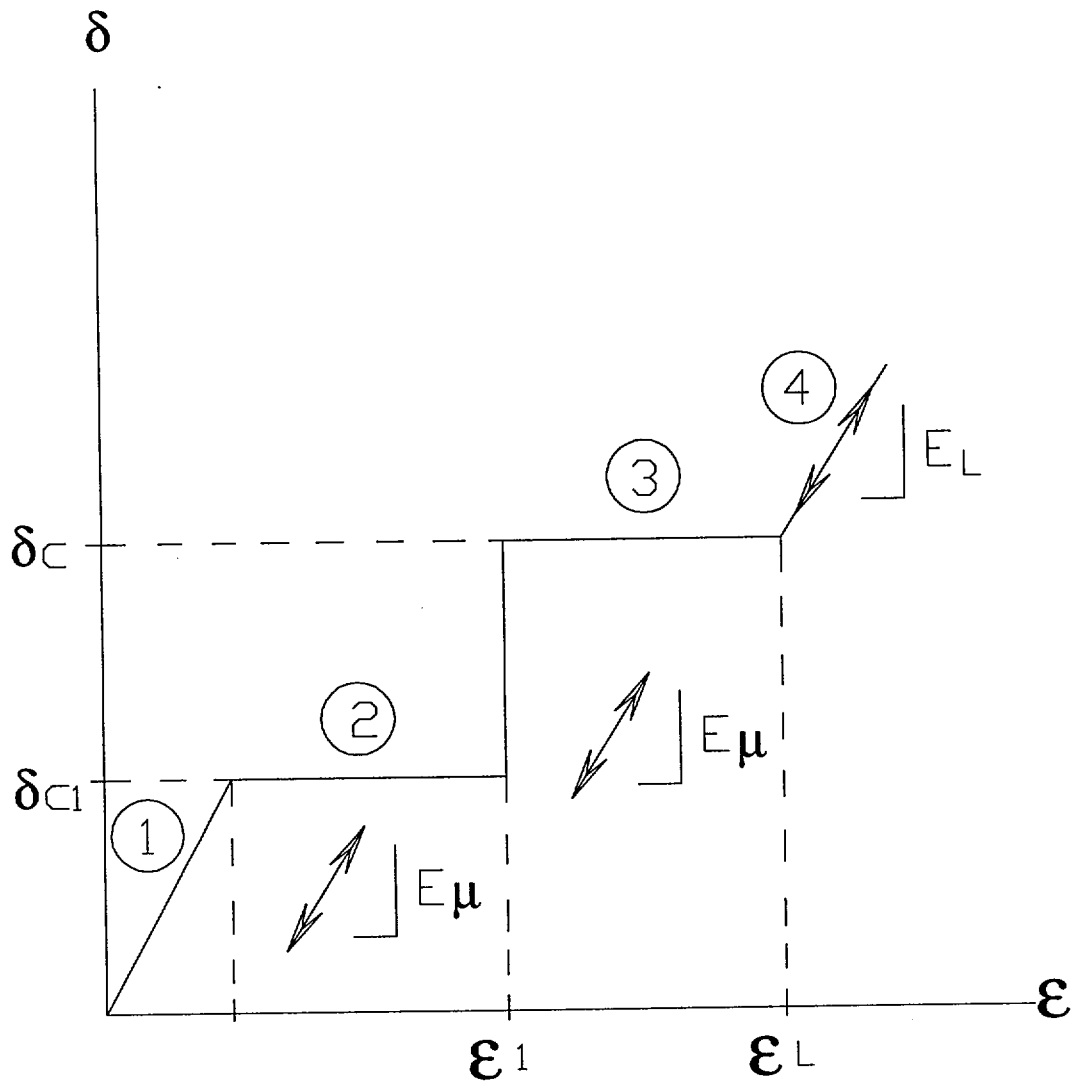
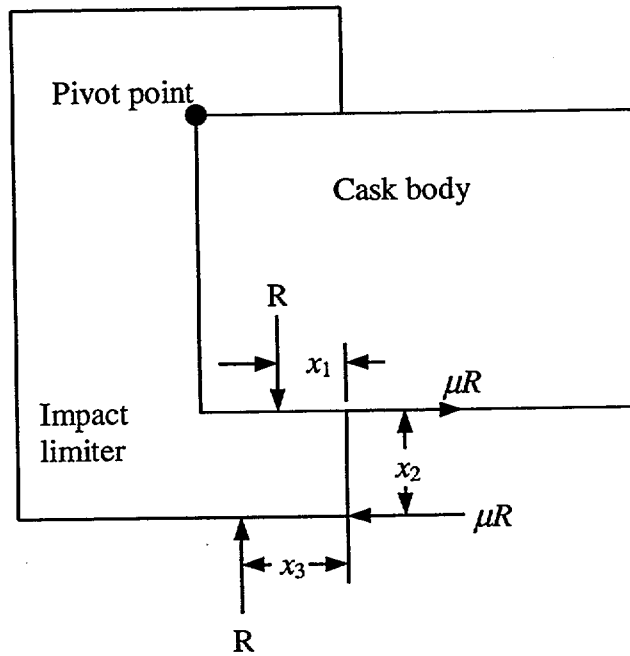


Figure 2.10.8-13
Impact Limiter Free Body Diagram during 20° Slap Down



Where:

R = reaction force, 16,500 kips.

μ = friction coefficient, 0.12

$x_1 = 25.00/2 = 12.50$ in.

$x_2 = (\text{I.L. od} - \text{I.L. id})/2 - \text{crush depth} = (122 - 83.00)/2 - 9.47 = 10.03$ in.

$x_3 = 25.00 - (209.75 - 104.60 - 94.07) = 13.92$ in.